INFORMATION TO USERS

This manuscript has been reproduced from the microfilm master. UMI films the text directly from the original or copy submitted. Thus, some thesis and dissertation copies are in typewriter face, while others may be from any type of computer printer.

The quality of this reproduction is dependent upon the quality of the copy submitted. Broken or indistinct print, colored or poor quality illustrations and photographs, print bleedthrough, substandard margins, and improper alignment can adversely affect reproduction.

In the unlikely event that the author did not send UMI a complete manuscript and there are missing pages, these will be noted. Also, if unauthorized copyright material had to be removed, a note will indicate the deletion.

Oversize materials (e.g., maps, drawings, charts) are reproduced by sectioning the original, beginning at the upper left-hand corner and continuing from left to right in equal sections with small overlaps.

Photographs included in the original manuscript have been reproduced xerographically in this copy. Higher quality 6" x 9" black and white photographic prints are available for any photographs or illustrations appearing in this copy for an additional charge. Contact UMI directly to order.

ProQuest Information and Learning
300 North Zeeb Road, Ann Arbor, MI 48106-1346 USA
800-521-0600

Carrier Phase and Frequency Estimation for Burst-Mode Communications

Yan Zhang

A Thesis

in

The Department

of

Electrical and Computer Engineering

Presented in Partial Fulfillment of the Requirements

for the Degree of Master of Applied Science at

Concordia University

Montréal, Québec, Canada

March 2001

© Yan Zhang, 2001

National Library of Canada
Acquisitions and Bibliographic Services
395 Wellington Street
Ottawa ON K1A 0N4
Canada

Bibliothèque nationale du Canada
Acquisitions et services bibliographiques
395, rue Wellington
Ottawa ON K1A 0N4
Canada

Your file Votre référence

Our file Notre référence

The author has granted a non-exclusive licence allowing the National Library of Canada to reproduce, loan, distribute or sell copies of this thesis in microform, paper or electronic formats.

L'auteur a accordé une licence non exclusive permettant à la Bibliothèque nationale du Canada de reproduire, prêter, distribuer ou vendre des copies de cette thèse sous la forme de microfiche/film, de reproduction sur papier ou sur format électronique.

The author retains ownership of the copyright in this thesis. Neither the thesis nor substantial extracts from it may be printed or otherwise reproduced without the author's permission.

L'auteur conserve la propriété du droit d'auteur qui protège cette thèse. Ni la thèse ni des extraits substantiels de celle-ci ne doivent être imprimés ou autrement reproduits sans son autorisation.

0-612-59311-8

Canada

ABSTRACT

Carrier Phase and Frequency Estimation for Burst-Mode Communications

Yan Zhang

It is necessary for coherent communication systems to apply synchronization of carrier phase and frequency for proper demodulation of data. These synchronizers play an even greater role when transmission is in burst mode. It is because that the receiver always asks for relock for separated burst, which transmits information from different users. Therefore, fast and efficient carrier synchronization schemes are highly needed. In the thesis, we studied various algorithms that are all fallen into the Maximum Likelihood estimation, and chose the proper ones that are suitable to burst-mode transmission. The chosen algorithms employ different recovery methods, from non-data-aided method to data-aided method, and from feedforward topology to feedback topology. The performances of the chosen algorithms are studied by both theoretical analysis and computer simulation. Their advantage and disadvantage are summarized and compared, such that the improved schemes are proposed to compensate their disadvantages, make use of their advantages, and obtain better performance.

Dedicated to my father and mother .....

ACKNOWLEDGEMENTS

It is with the utmost sincerity that I would like to express my thanks to my thesis supervisor, Dr. M. R. Soleymani, for his constant guidance and stimulating suggestions through the various stages of the thesis developement. I would also like to thank all the professors with whom I have interacted during my studies at Concordia University. Last but not least, I would like to thank my family and friends. Their love, trust and support accompany with me throughout all these years. I am grateful to all of you.

TABLE OF CONTENTS

LIST OF TABLES

LIST OF FIGURES

LIST OF ABBREVIATIONS AND SYMBOLS

a	All unknowns of the transmitted signal data symbol
a_k	Transmitted signal data symbol, corresponding to the symbol data phase θ_k
a_k^*	Conjugate of a_k
$\hat{a}_k$	Detected signal data symbol
e_k	Error signal
D	Decimation factor of a D-step decimation filter
E_k	Energy per symbol
f_{CF}	Carrier frequency
f_{LF}	Local reference frequency
J	Fisher's Information Matrix
K	Number of symbols in observation window
l	Start point of an observation window
$L(\ )$	Objective function
M	Number of signaling elements for MPSK
$n(t)$	Random process representing AWGN
n_k	Discrete time, delta-correlated complex Gaussian noise process, with zero mean and variance $\sigma^2 = \frac{N_o}{2}$
n_k'	Corresponding result of n_k after non-linear transform
n_k^I	In-phase part of n_k
n_k^Q	Quadrature-phase part of n_k
P_E	Bit error probability
P_f	Period of frequency offset
$P_r[X]$	Probability of random variable X

$p(X)$	Probability density function of random variable X
$r(t)$	Pass-band signal received at the receiver end
r_k	Integrate-and-dump sample in a symbol period T_s of received signal
	$r_k = x_k + jy_k$
$r_k^{\cdot}$	Corresponding result of r_k after non-linear transform
$s(t)$	Low-pass of signal being transmitted at the transmitter end
s_k	Integrate-and-dump sample corresponding to $s(t)$
T_s	Symbol period
x_k	Random variable denoting in-phase component of r_k
y_k	Random variable denoting quadrature component of r_k
τ	Time discrepancy between the oscillators of transmitter and receiver
$\lvert r_k \rvert$	Amplitude of the received symbol
φ_k	Summation of ϑ_k and ε_k
ϑ_k	Estimated parameter parts, and is equal to $(2\pi\Delta fk + \Delta\theta)$
ϕ	Stand for estimated parameter, either Δf or $\Delta\theta$
$\hat{\phi}$	Estimated parameter of ϕ
ε_k	Phase noise in the received symbol introduced by channel noise
δ	Random variable denoting degradation of Viterbi & Viterbi phase estimator
Δf	Unknown normalized frequency offset
$\Delta f^{\cdot}$	Corresponding result of Δf after non-linear transform
$\Delta\tilde{f}$	Trial value of normalized frequency offset
$\Delta\hat{f}$	Estimated normalized frequency offset
$\Delta\hat{f}_1$	Coarse estimation of frequency offset
Δf_2	Remaining small frequency offset after coarse estimation
$\Delta\hat{f}_2$	Estimation of frequency offset Δf_2
$\Delta\theta_1$	Carrier phase difference between transmitter and receiver oscillators

$\Delta\theta$	Unknown carrier phase offset
$\Delta\theta^{'}$	Corresponding result of $\Delta\theta$ after non-linear transform
$\Delta\tilde{\theta}$	Trial value of carrier phase offset
$\Delta\hat{\theta}$	Trial value of carrier phase offset
θ_k	Symbol data phase
σ^2	Variance of channel noise
μ	Certain small constant
$\frac{1}{\varsigma^2}$	Define as signal-to-noise ratio $\frac{E_s}{N_o/2}$
$E[X]$	Expected value of random variable X
$Var[X]$	Variance of random variable X
$\Im[X]$	Imaginary part of complex quantity X
$\Re[X]$	Real part of complex quantity X

Chapter 1

Introduction

1.1 Background

A digital communication system involves transmission of information in digital form from one point to another through a physical channel. Corresponding to pass-band characteristics of most channels, as shown in Figure 1.1, instead of transmitting the information sequence itself, the transmitter is required to modulate the information bearing base-band signal onto a high frequency carrier. At the receiver, this signal should be demodulated to remove the effect of the carrier and down-converted back to base-band, which can permit the receiver to retrieve the source information sequence. These two stages of frequency conversion are achieved by means of oscillators operating at certain frequency and initial phase.

Ideally, the two oscillators are completely synchronized and therefore, their presence does not degrade the end-to-end performance. In practice, however, two oscillators in different locations cannot be identically synchronized. Oscillation, instability, time-varying nature of the transmission medium and relative movement between a transmitter and a receiver are sources of receiver uncertainty. Consequently, the received signal is a function of the transmitted information, the noise

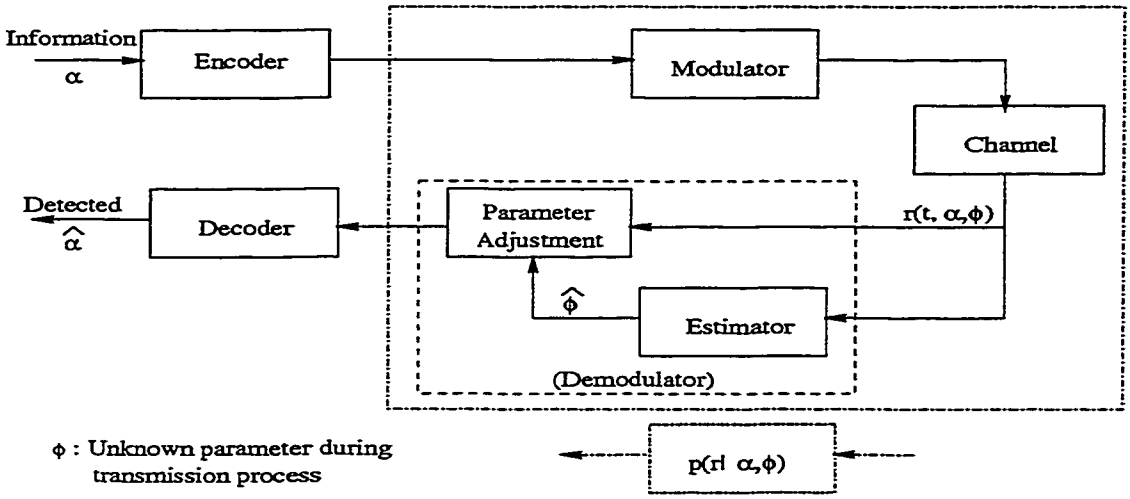

Figure 1.1: Physical Communication Model

introduced by the channel, and some unknown parameters arising from the discrepancies between the oscillators, which can be generally expressed as:

$$\begin{aligned} r(t) &= s_p(t-\tau) + n(t) \\ &= \Re\left\{s(t-\tau)e^{j[2\pi(f_{CF}+\Delta f)(t-\tau)+\Delta\theta_1]}\right\} + n(t) \\ &= \Re\left[s(t-\tau)e^{j(2\pi f_{CF}t+2\pi\Delta ft+\Delta\theta)}\right] + n(t) \\ &= \Re\left\{\left[s(t-\tau)e^{j(2\pi\Delta ft+\Delta\theta)} + v(t)\right]e^{j2\pi f_{CF}t}\right\} \end{aligned} \tag{1.1}$$

Where,

τ : time discrepancy between the oscillators arising from all the reasons mentioned above,

$s_p(t)$: pass-band signal being transmitted at the transmitter end,

$s(t)$: corresponding low-pass signal of $s_p(t)$,

$n(t)$: a sample function of white Gaussian noise, with zero mean and variance $\sigma^2 = \frac{N_o}{2}$,

$v(t)$: corresponding low-pass signal of $n(t)$,

$r(t)$: pass-band signal received at the receiver end,

f_{CF} : carrier frequency,

Δf : carrier frequency difference between transmitter and receiver oscillators,

$\Delta\theta_1$: carrier phase difference between transmitter and receiver oscillators,

$\Delta\theta$: carrier phase due to the time discrepancy, Δf, and $\Delta\theta_1$.

All of these unknown factors result in serious performance degradation which are supposed to be removed by synchronizations. The time discrepancy τ belongs to the timing estimation area. For a coherent communication system, it is required that the input samples to the receiver-data-detection unit must be independent of any phase and/or frequency errors. The purpose of this thesis is to propose and analyze some of these carrier synchronization strategies. Although there are other reference parameters may be involved in the detection process, such as word synchronization, they do not belong to this thesis.

For point-to-point applications involving communication between two users, traditional continuous-mode transmission are usually applied. Meanwhile, the receiver usually employs analog techniques for carrier synchronization, which could be categorized under two broad headings: waveform regenerators and analog trackers. The waveform regenerators pass the received random waveform through a nonlinear operation, producing a deterministic signal at the carrier frequency, or one of its harmonics. A bandpass filter or phase-locked-loop (PLL) could then be used to track this deterministic signal. The most common example of such a synchronizer is the times-M analog multiplier, applicable to M-ary phase shift keying (MPSK). Most other synchronizers can be classified under the heading of analog trackers, which inherently involve PLL, and attempt to track the carrier phase by forcing an error signal to zero. The most common of these synchronizers, such as Costas loop, has been throughly analyzed in numerous texts [6]. Apparently, all of these analog techniques could not be applied to all signaling formats. Furthermore, these kinds of PLL circuits take time to be in lock and so work slowly.

In recent years, the point-to-multi-point applications involving communication between many users are much more prevalent. In these applications, the burst-mode

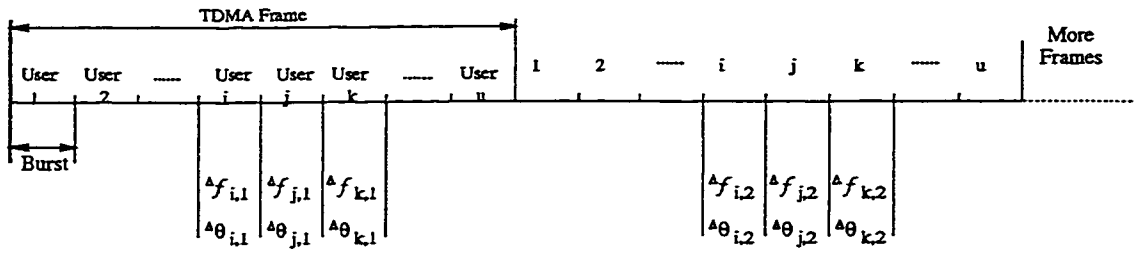

Figure 1.2: Phase and Frequency Offsets in TDMA System

transmission of digital data and voice has become commonplace, especially in satellite communications and mobile cellular radio. As an efficient channel utilization scheme, Time-Division-Multiple Accession (TDMA), as shown in Figure 1.2, is commonly chosen in communications involving many users. In such an access scheme, each burst corresponding to a different user occurs in short non-overlapping time slots and is affected by different frequency offset and phase offset. Hence fast and precise phase estimation in each successive burst becomes essential. Traditional slow synchronizers are not suitable for this application if their acquisition problem is not fixed, as the receiver should re-acquire lock within a short time for every burst.

In the past, analog circuitry was used in implementing the synchronizer and the processing was done in continuous time domain. The advent of high-speed Analog to Digital Converters (ADC) and the continuing progress in increasing the performance, speed, reliability, and the simultaneous reduction in size and cost of Application Specific Integrated Circuits (ASICs) have resulted in a strong interest in the implementation of communication systems in digital domain. There are a host of other factors that have led to the gain in significance of digital over analog strategies. A few remarkable factors are listed below:

- Memory and delays pose serious problem in analog strategies. They are easily implemented digitally.
- Complex nonlinear signal processing functions (required for estimation) are very cumbersome for implementation using analog circuits. They are easily

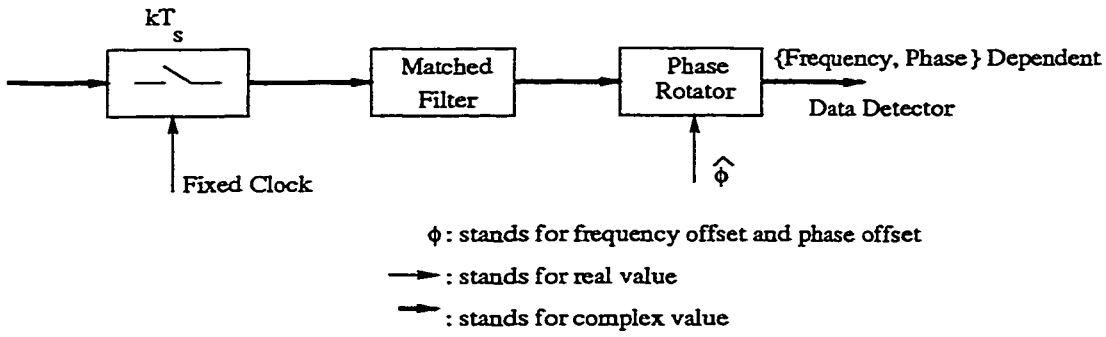

Figure 1.3: General Digital Receiver Structure

implemented using digital circuits.

- With the advances and the certainty of full digitization in communication area, one can implement an all-digital implementation of the continuous/burst-mode receiver with greatly reduced complexity owing to the sharing of operations between the synchronization and the detection process.

Clearly, all of the above features tend to enhance performance since more complex circuitry may be used to get better functional characteristics. Especially, some specific traits of digital circuits directly affect the feasibility of certain synchronization algorithms. For example, memory, which makes practicable some operations that would be complicated or even impossible in analog form.

It is believed that all the above factors substantiate the rationale behind analyzing digital synchronization techniques. A fully digital receiver has an entirely different structure from the traditional analog one. It means that we want to recover the phase and carrier frequency by operating only on signal samples taken at a suitable rate, which is in contrast with the familiar analog methods which work on continuous-time waveforms. Such a digital receiver also makes our assumption of perfect timing synchronization more reasonable because in most digital receivers timing recovery is done prior to phase recovery.

In a fully digital receiver, without taking timing synchronization into consideration, it is shown in Figure 1.3. From the first stage of the process, the received

pass-band signal with carrier $e^{j(2\pi f_{CF}t+\Delta\theta_1)}$ is down-converted by a local reference components of complex base-band signal $e^{j2\pi f_{LF}t}$ with local reference frequency f_{LF}. It is sampled by a local sampler with very precise timing synchronization, but still leaves carrier frequency offset $\Delta f = f_{LF} - f_{CF}$ and carrier phase offset $\Delta\theta$. Carrier estimate is performed after the matched filter (MF) at symbol rate $\frac{1}{T_s}$. For MPSK signaling, the integrate-and-dump samples in a symbol period T_s from MF at the receiver end are given by,

$$\begin{aligned} r_k &= \sqrt{E_k}e^{j(2\pi\Delta fT_sk+\Delta\theta+\theta_k)} + n_k \\ &= a_k e^{j(2\pi\Delta fT_sk+\Delta\theta)} + n_k \\ &= s(k;\Delta f,\Delta\theta) + n_k \\ &= s_k + n_k \end{aligned} \tag{1.2}$$

where,

n_k is a discrete time, delta-correlated complex Gaussian noise process,

ΔfT_s is the normalized frequency offset, hereafter, Δf is used to stand for ΔfT_s directly,

$\Delta\theta$ is the carrier phase offset, which is an unknown constant and is assumed to be random variable, which is uniformly distributed in $[0, 2\pi)$,

θ_k is the symbol data phase, for MPSK, $\theta_k \in \left\{\frac{2\pi m}{M}, m = 0, 1, 2, ..., M-1\right\}$,

a_k is the corresponding data symbol of θ_k,

E_k is the symbol energy of the complex sinusoidal signal.

For convenience, the above equation can also be expressed in polar form,

$$\begin{aligned} r_k &= s_k^I + js_k^Q + n_k^I + jn_k^Q \\ &= x_k + jy_k \\ &= |r_k|\, e^{-j\varphi_k} \\ &= |r_k| \exp\left[-j\left(2\pi\Delta fk + \Delta\theta + \theta_k + \varepsilon_k\right)\right] \end{aligned} \tag{1.3}$$

where,

s_k^I is the in-phase part of $s(k;\Delta f,\Delta\theta)$, and $s_k^I = s_k\cos(2\pi\Delta fk + \Delta\theta + \theta_k)$,

s_k^Q is the quadrature part of $s(k; \Delta f, \Delta\theta)$, and $s_k^Q = s_k \sin(2\pi\Delta f k + \Delta\theta + \theta_k)$,

n_k^I and n_k^Q are the in-phase and quadrature parts of n_k, with the characteristics described in Appendix,

x_k and y_k are the in-phase and quadrature parts of the received symbol,

$|r_k|$ is the amplitude of the received symbol,

ε_k is the phase noise in the received symbol introduced by the noise,

$\arg(r_k)$ is the summation of estimated parameter part $\vartheta_k = (2\pi\Delta f k + \Delta\theta)$, data phase θ_k, and phase noise ε_k.

It has been thoroughly stated that these integrate-and-dump samples cause no loss of information, they are sufficient for symbol detection and estimation [7, 11, 17].

All subsequent signal-precessing operations are performed digitally at the fixed processing rate of symbol rate or a fraction of it. Provided timing is known, one sample per symbol of the MF output is sufficient for carrier phase/frequency estimation. To obtain the fastest operation, people prefer using the maximum processing rate, which is the symbol rate itself, and such is the case in the thesis.

1.2 Outline of the Thesis

Our objective is to obtain fast and accurate carrier synchronizers for MPSK signaling, formulate, and analyze them. Corresponding to it, we analyze and study various non-data-aided or data-aided methods, feedforward or feedback structures. The whole thesis is divided into six chapters.

This chapter is the introduction and shows the importance of fast and accurate synchronization in nowadays communication systems. The general signal model, channel model, and digital receiver model that will be used in the derivation and analysis of various algorithm are given in this part. The evolution of synchronization strategies is also reviewed, which leads to the proposed algorithms in Chapter 3 and

Chapter 4.

Chapter 2 focuses on the theoretical approach to the Maximum-Likelihood (ML) estimation of phase and frequency error ($\Delta\theta$ and Δf). Since variance performance [25] is the main evaluation standard for an estimation system. The lower bound for the variance performance, namely, Cramer-Rao Lower Bound (CRLB) is also derived in Chapter 2. The classification as well as the overview corresponding to the classification of current digital estimators is included in this part.

Chapter 3 presents different steps in the development of a combined carrier frequency and phase offset estimator. This chapter presents the simulation and analysis of some carrier phase and frequency estimators - one for frequency estimation and two for phase estimation techniques. The modified version of Rife & Boorstyn algorithm (which is called NDA-FF frequency estimator later on) is chosen as the frequency estimator. The original Rife & Boorstyn is described in [8], this modified Rife & Boorstyn algorithm borrows the idea of Viterbi & Viterbi phase offset estimator algorithm to delete the data effect. The feed-forward Viterbi & Viterbi phase estimator (which is called NDA-FF phase estimator later on) and a Decision-Directed (DD) Digital Phase-Lock-Loop (DPLL) phase estimator (which is called DD-FB phase estimator later on since the PLL circuit also has the feedback structure) proposed by Takahata et al [4] are studied and compared. The NDA-FF frequency estimation algorithm and NDA-FF phase estimation algorithm are then combined to form an all feedforward NDA Carrier estimator.

Chapter 4 presents the simulation and analysis of a modified joint phase/frequency offset estimator proposed by W. Shaw Yuan & Costas N. Georghiades [22] (which is called DA-FB joint phase/frequency estimator in the thesis).

In Chapter 5 presents the comparison and improvement of the carrier synchronizers. Effort has been made on the frequency estimation part: to decrease the number of outliers - where the frequency offset estimation value is very far from the real frequency offset value, and increase the frequency estimation range.

Conclusion of the studied synchronizers and suggestions for further research are given in Chapter 6.

To investigate the general property of carrier synchronizer only, the Additive White Gaussian Noise (AWGN) channel is assumed. Numerical results for QPSK are given as illustrative examples.

1.3 Contributions of the Thesis

The major contributions of this thesis include the following:

- A systematic performance evaluation of a few estimation algorithms. Namely, a NDA-FF phase estimation algorithm, a DD-FB phase estimation algorithm, a NDA-FF frequency estimation algorithm, a combined NDA-FF phase/frequency algorithm, a DA-FB joint phase/frequency estimation algorithm.

- Proposal and performance evaluation of a combined NDA-FF frequency estimation algorithm and DA-FB algorithm in Chapter 5, which gives low threshold and broad estimation range of frequency estimation.

- Proposal of a method in Chapter 5 to decrease the outliers number of NDA-FF frequency estimator at low signal-to-noise ratio approaching its working threshold.

Chapter 2

Carrier Recovery Techniques

In general, there are two methods to estimate unknown parameters in estimation theory. First, is Maximum A Posterior (MAP) procedure, which is used for random parameters with known probability distribution functions. Second, is Maximum-Likelihood (ML) procedure, which is used for nonrandom parameters. However, these two estimate methods can be identical if the parameters to be estimated are uniformly distributed [25]. In reality, since the probability distribution functions of estimated parameters are usually unknown, they can be effectively treated as being uniformly distributed. Therefore, ML estimation procedure is prevalent. Actually, ML methods are the most efficient estimates, and offer two major advantages: they easily lead to appropriate circuit configurations, and provide optimum or nearly optimum performance under certain circumstances.

Recent literature [23,24] indicates that most of the existing synchronization algorithms have been discovered through heuristic arguments or by applications of ML estimate method. Therefore, the ML estimation technique offers a systematic and conceptually simple guide to the synchronization problems and can be treated as a general principle for us to derive various synchronization schemes.

In this chapter, we focus on the estimation of carrier parameters - frequency offset Δf and phase offset $\Delta\theta$. General ML estimation techniques for carrier recovery

will be discussed at first. Then phase and frequency estimation techniques will be discussed separately; joint phase/frequency estimation techniques will be the next issue. This classification is important. We will fit our algorithms to be studied in this framework. Finally, Cramer-Rao Lower Bound (CRLB) will be discussed as the fundamental lower limit to the variance of any unbiased estimator for performance evaluation.

In the derivation of our carrier synchronizer structures, two assumptions have been made:

1. The unknown parameters - frequency offset Δf and phase offset $\Delta\theta$ are treated as uniformly distributed random variables. It reduces the complexity of the analysis. This assumption is not only simple and effective, especially at the beginning of estimation, but also equivalent to reducing the estimation task to the estimation of unknown (constant) parameters.

2. The channel will be assumed to have infinite bandwidth, thus allowing the transmitters to use rectangular pulse shaping. More importantly, this implies that there is no inter-symbol or inter-burst interference as in finite bandwidth circumstance. Furthermore, we will assume that there is no fading. As a result only a single burst is needed to be considered.

2.1 Maximum Likelihood Estimation

ML parameter estimation requires different mathematical tools, depending on whether the observation is a continuous-time waveform or a sample sequence. Although the former looks more like the physical signal, the latter is particularly tailored for the digital receiver operation. As explained in Chapter 1, what we focus on is digital synchronizers. So, we will only concentrate on the latter one.

The ML estimate can be generally expressed as:

$$(\widehat{\phi}) = \arg\left\{\max_{\phi} p(r|a,\phi)\right\} \tag{2.1}$$

where,

$p(r|a,\phi)$ is the probability density function (pdf) of the received signal,

a is the transmitting data sequence,

ϕ is the general estimated parameters, and here stands for unknown carrier parameter to be estimated.

Thus, for carrier frequency and phase offset, the ML estimate would be expressed as:

$$(\widehat{\Delta f}, \widehat{\Delta\theta}) = \arg\left\{\max_{\widetilde{\Delta f},\widetilde{\Delta\theta}} p(r|a,\Delta f,\Delta\theta)\right\} \tag{2.2}$$

where, we use $\widetilde{\Delta f}$ and $\widetilde{\Delta\theta}$ to stand for the trail value.

From equation (2.2), the algorithms are obtained as the solution to a mathematical optimization problem. Conceptually, the systematic derivation of ML synchronizers is straight forward. The likelihood function must be averaged over the unwanted parameters. Such as:

Phase estimation:

$$p(r|\Delta\theta) = \int \left[\sum_{a} p(a)p(r|a,\Delta f,\Delta\theta)\right] d_{\Delta f} \tag{2.3}$$

Frequency estimation:

$$p(r|\Delta f) = \int \left[\sum_{a} p(a)p(r|a,\Delta f,\Delta\theta)\right] d_{\Delta\theta} \tag{2.4}$$

Joint estimation of $(\widehat{\Delta f}, \widehat{\Delta\theta})$:

$$p(r|\Delta f,\Delta\theta) = \sum_{a} p(a)p(r|a,\Delta f,\Delta\theta) \tag{2.5}$$

With the exception of a few isolated cases, it is impossible to perform these averaging operations in closed form, and we have to resort to approximation techniques. Systematically deriving the synchronization algorithms may, therefore, be

understood as the task of finding suitable approximations. The various algorithms are then the result of applying these techniques.

There are several ways to classify the synchronizers.

- From the way the data dependency is eliminated, synchronizers are classified into two main categories:

1. Class DD/DA: Decision-Directed (DD) or Data-Aided (DA)
2. Class NDA: Non-Data-Aided (NDA)

When the data sequence is known, for example a preamble is given during acquisition, DA synchronization algorithms are performed. Since an additional preamble at the beginning of each burst is needed that is just used for the synchronization, the transmission efficiency is degraded. However, it has the obvious advantage that this estimate is independent of any modulation type, and the efficiency penalty can be greatly compensated by the performance improvement. Ideally, preamble should be as short as possible. For example, current trends in satellite communication indicate that an overhead less than 10% of the burst is acceptable.

When the detected sequence is used as if it were the actual sequence, DD synchronization algorithms are performed. Its performance can approach that of DA, especially at high signal-to-noise ratio (SNR). However, all DD algorithms require an initial parameter before starting the estimation process. This is called the acquisition process. To obtain a reliable and fast estimate, a preamble may be used.

NDA algorithms can only be obtained by either exactly or approximately averaging the received signals to remove data dependence. It tends to be specific to particular modulation format, and turns out to have some performance degradations because of ignoring a reliable estimate of date, especially at low SNR. In the meantime, the estimation time will not be as short as when a preamble is used. However, it does not require a priori knowledge of the transmitted data information

as in DA, and is free of acquisition time problem as in DD. These two advantages outweigh the DD/DA algorithm and NDA algorithms become the practical interest points for fast and efficient estimation.

- From the realization structure points of view, as shown in Figure 1.3, estimation algorithms can be classified as Feed-Forward (FF) or Feedback (FB) synchronization methods.

1. FF algorithm derives the estimate from the received signal before it is corrected in the phase rotator.

2. FB algorithm derives an error signal $\widehat{e}_\vartheta = \widehat{\vartheta} - \vartheta$. It is called FB because it derives an estimate of the error and feed a corrective signal back to the phase rotator and gets a recursive estimation.

- In addition to these common classifications, we should also mention that the carrier synchronizers can also be classified by,

1. timing-directed ($D\varepsilon$), where timing ε has already been established

2. non-timing-directed ($ND\varepsilon$) method

Joint estimate of timing and carrier parameters is also practical [11], but we focus on perfect $D\varepsilon$ algorithm as what we have assumed in Chapter 1. Actually, $D\varepsilon$ is not only reasonable but also useful when the frequency offset is not excessively large. Therefore, the derived structure is suitable for normalized frequency offset $|\Delta f T_s| < 15\%$. This is not a severe restriction because the normalized frequency offset is commonly less than 10% [16].

As indicated in Chapter 1 by references [7, 11, 17], it has been indicated that the sample sequences are sufficient for ML estimation. We should further restrict the estimated parameters in such samples to be slowly varying. Such that the time scale over these parameters change is much longer than a symbol period. Thus, we can

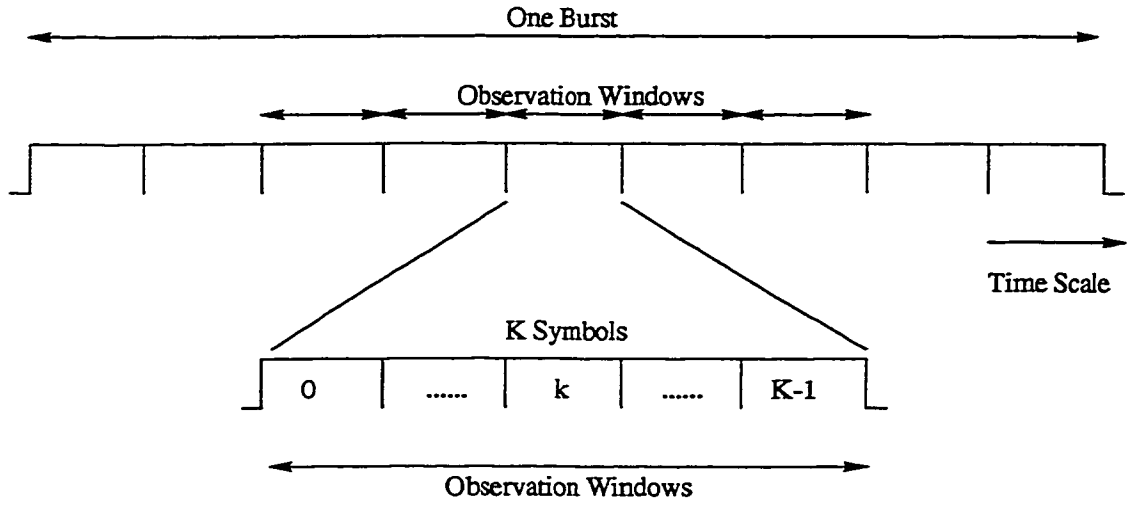

Figure 2.1: Description of Observation Windows in Single Burst

consider the synchronization parameters as approximately piecewise constant and estimate these parameters over segments of $K >> 1$ symbols as shown in Figure 2.1.

The joint probability density function of a set of K samples passing over the AWGN channel is given by:

$$p(\overrightarrow{r}|a, \Delta f, \Delta\theta) = (\pi N_o)^{-\frac{K}{2}} e^{-\frac{1}{N_o}\Sigma_{k=0}^{K-1}|r_k - s(k;\Delta f,\Delta\theta)|^2} \tag{2.6}$$

As stated earlier, synchronization algorithms can be systematically derived by finding suitable approximations to remove the "unwanted" parameters in the ML function. The result of these approximations is an objective function $L(a, \Delta f, \Delta\theta)$. Taking logarithm of both sides of (2.6), neglecting the constant part and with only the inner product part left,

$$\max\left\{\arg_{\widetilde{\Delta f},\widetilde{\Delta\theta}} \ln p(\overrightarrow{r}|a, \Delta f, \Delta\theta)\right\}$$

$$= \max\left\{\arg_{\widetilde{\Delta f},\widetilde{\Delta\theta}} \left[\ln (\pi N_o)^{-\frac{K}{2}} - \tfrac{1}{N_o}\Sigma_{k=0}^{K-1} |r_k - s(k;\Delta f, \Delta\theta)]|^2\right]\right\}$$

Omitting the constant part,

$$= \min\left\{\arg_{\widetilde{\Delta f},\widetilde{\Delta\theta}} \left[\tfrac{1}{N_o}\Sigma_{k=0}^{K-1} |r_k - s(k; f, \theta)]|^2\right]\right\}$$

$$= \min\left\{\arg_{\widetilde{\Delta f},\widetilde{\Delta\theta}}\left[\Sigma_{k=0}^{K-1}\left(|r_k|^2+|s(k;\Delta f,\Delta\theta)|^2-2\Re\left\{r_k s^*(k;\Delta f,\Delta\theta)\right\}\right)\right]\right\}$$

Omitting parts common to all,

$$= \max\left\{\arg_{\widetilde{\Delta f},\widetilde{\Delta\theta}}\left[\Sigma_{k=0}^{K-1}\Re\left(r_k s^*(k;\Delta f,\Delta\theta)\right)\right]\right\}$$

$$= \max\left\{\arg_{\widetilde{\Delta f},\widetilde{\Delta\theta}}\left[\Sigma_{k=0}^{K-1}\Re\left\{a_k^* r_k e^{-j(2\pi\Delta f k+\Delta\theta)}\right\}\right]\right\} \tag{2.7}$$

Thus, we get the objective function:

$$L(a,\Delta f,\Delta\theta)=\sum_{k=0}^{K-1}\Re\left\{a_k^* r_k e^{-j(2\pi\Delta f k+\Delta\theta)}\right\} \tag{2.8}$$

Maximizing this objective function is the same as the operation of ML estimator as in (2.6). We will mainly use (2.8) to derive various ML estimation structures. There exist a variety of algorithms for maximum search of the ML function, such as parallel search, processing, and error feedback system [7]. The choice depends mostly on the bit rate and technology available. It should be indicated that synchronization literature is so vast as to comprise over 1,000 technical papers. So, we can only discuss the main categories, which is sufficient enough for us to obtain the synchronizer principle.

As noted by Gardner [24], there are mainly three strategies to finding the maximum of ML function with respect to the estimated parameters. The first method of maximization actually reduces to a tracker. At the maximum, the derivative of the objective function reduces to zero. Therefore, an error signal is obtained and a digital closed-loop tracker is resulted, and a FB structure is needed.

The second method of maximization is by direct computation. This method also involves setting the derivation of the objective function to zero, usually making some simplifying assumption, and directly solving for the estimation. With such method, a FF structure can be obtained.

The third is using a brute force search technique. Values over the entire space of the estimated parameters are substituted into the ML function, and the estimation

is selected as the one which produces the maximum. We can foresee that this technique has very long acquisition times, owing to the number of computations which may be required to find the absolute maximum. Presentation and analysis of such technique is given in [27]. Its theory is simple, but its application is too complicated. Therefore, if we want to used this strategy, it must be modified to suit for the realization, as in [8].

Our discussion later on will be mainly based on the estimator topology - namely FF or FB, taking consideration of whether the additional knowledge is available - namely DD, DA, or NDA. The third approach of Gardner's classification is also included in FF topology when frequency offset estimator is discussed.

2.2 Phase Offset Estimation

The performance of phase estimators can be quite distinguished by the presence of carrier frequency offset. For the sake of simplicity, the theoretical approach is done by assuming that frequency recovery has already been accomplished. This is in keeping with the fact that most phase estimators can cope with moderate residual frequency error.

- FB structure

If we try to use decision direction method, it appears that the estimate can be derived directly from the objective function, and two approaches are readily available. When detector decisions are exploited in place of true data, closed-loop structures are unavoidable.

The first approach is easily obtained by replacing a by its estimation and maximizing (2.8) for one phaser, the DD estimation will be expressed directly,

$$e^{j\widehat{\Delta\theta}} = e^{j \arg \Sigma_{k=0}^{K-1} \widehat{a}_k^* r_k} \tag{2.9}$$

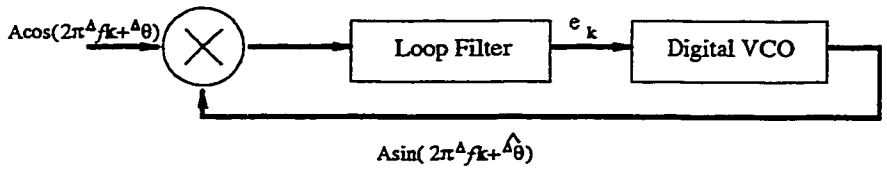

Figure 2.2: Simplified Diagram of Phase-Lock-Loop Circuit

Such phasor estimator only needs one synchronized Matched Filter (MF) output sample r_k and a detected symbol $\widehat{a}_k$.

The second approach is a recursive method to compute the zero of the derivative of the objective function (2.8). Taking the derivative of (2.8) with respect to $\Delta\theta$ and rearranging yields,

$$\frac{d}{d\Delta\theta}L\left(a,\Delta\theta\right)=\sum_{k=0}^{K-1}\Im\left\{-a_k^*r_ke^{-j\Delta\theta}\right\} \tag{2.10}$$

Where $\Im\{\}$ is the imagine part for the inside. They are easily realized by phase error feedback system, which is the famous phase-lock-loop (PLL) circuit. A digital PLL circuit is shown in Figure 2.2.

Its general principle can be easily illustrated by its analog counterpart. In analog case, we use t instead of k in the figure and all processing is realized by analog circuits. It basically consists of a multiplier, a loop filter, and a voltage-controlled oscillator (VCO). If the input to the PLL is the sinusoid $\cos\left(2\pi\Delta ft+\Delta\theta\right)$, and the output of the VCO is then be $\sin\left(2\pi\Delta ft+\widehat{\Delta\theta}\right)$. The product of these two signals is,

$$\begin{aligned} e_k &= \cos\left(2\pi\Delta ft+\Delta\theta\right)\sin\left(2\pi\Delta ft+\widehat{\Delta\theta}\right) \\ &= \tfrac{1}{2}\sin\left(\widehat{\Delta\theta}-\Delta\theta\right)+\tfrac{1}{2}\sin\left(4\pi\Delta ft+\Delta\theta+\widehat{\Delta\theta}\right) \end{aligned} \tag{2.11}$$

The loop filter is a low-pass filter that responds only to the low-frequency component $\frac{1}{2}\sin\left(\widehat{\Delta\theta}-\Delta\theta\right)$ and removes the component at high-frequency $2\Delta f$. In normal operation when the loop is tracking the phase of the incoming carrier, the

phase error $\left(\widehat{\Delta\theta} - \Delta\theta\right)$ is very small and, hence,

$$\sin\left(\widehat{\Delta\theta} - \Delta\theta\right) \approx \widehat{\Delta\theta} - \Delta\theta \tag{2.12}$$

With the error signal e_k being further processed in loop filter, an update of estimate is performed in the digital integrator. While, the operation of this digital phase tracker can be expressed as:

$$\widehat{\Delta\theta}_{k+1} = \widehat{\Delta\theta}_k + C \times e_k \tag{2.13}$$

where, C is the coefficient of the digital integrator. This digital phase-lock-loop (DPLL) performs quite similar to that of the analog one and has been well studied [5,28]. For a modulated carrier both NDA-PLL and DD-PLL exist [7]. The major drawbacks of PLL algorithm in practice are long acquisition and hang-up problem. The latter means that a false estimate appears under certain circumstances and can last for a long time. We will study a DD-PLL circuit together with a NDA-FF phase estimator in Chapter 3.

- FF structure

The FF structure is remarkably useful for NDA application on MPSK [7]. NDA estimate usually results in great performance degradation as in QAM, but for MPSK signaling, the situation is quite different. There even exist NDA circuits which can be employed when no reliable data estimate exists, for example, at low SNR.

When fast NDA estimate for MPSK signaling is used, the data dependency at the MF output has to be removed. Consequently, r_k has to be taken to th M-th power. Replacing this non-linear transformation in (2.8), it becomes: $L(\Delta\theta) = \sum_{k=0}^{K-1} \Re\left\{r_k^M e^{-jM\Delta\theta}\right\}$ since $a^M = (e^{j2\pi m/M})^M = 1$. Taking the maximum of it for one shot, the estimate becomes:

$$e^{jM\widehat{\Delta\theta}} = e^{j\arg\Sigma_{k=0}^{K-1} r_k^M} \tag{2.14}$$

Note that this exponentiation operation causes an M-fold ambiguity. If $\widehat{\Delta\theta}$ is a solution to maximization, so is $\widehat{\Delta\theta} + \frac{2\pi m}{M}$ for $m = 0, 1, 2, ..., M-1$, since $e^{jM(\widehat{\Delta\theta}+\frac{2\pi m}{M})} = e^{jM\widehat{\Delta\theta}}$. It means that all NDA phase estimate systems suffer from an M-fold phase ambiguity problem, such that an ambiguity resolution method should be used.

If the noise is added, it is obvious that because of the M-th power operation for (1.2), there exist $r_k^i noise^{M-i}$ (for $i = 0, 1, 2, ..., M-1$) terms, which increase the effect of noise in the mean time. This causes the performance degradation which is called nonlinear loss. Such loss is not negligible for large M, consequently, this open-loop digital technique can not be used for all M. Even with small M, as for QPSK, although small, we can observe this nonlinear loss. To deal with this problem, Viterbi and Viterbi proposed a new estimator. Begin with (2.14), this algorithm is generalized to use $r_k^M = F(|r_k|)e^{jM\arg(r_k)}$ instead of $r_k^M = |r_k|^M e^{jM\arg(r_k)}$ directly [2].

The Viterbi and Viterbi (V&V) algorithm has been studied extensively [1,16]. Its significant advantage over the previous one is due to the fact that $F(|r_k|)$ can be chosen to minimize the variance of the estimate. In fact, it has been shown that the optimum $F(|r_k|)$ produces results that approach the CRLB closely. The performance of V&V algorithm for QPSK is shown in Figure 2.3. Where, $F(|r_k|) = |r_k|^i$ $i = 0, 2, 4$. We can observe that the M-th power operation degraded the variance performance of the system a lot, especially the original $F(|r_k|) = |r_k|^4$ operation is the worst case among all three.

In [3], the computer simulation results show that in a symbol-synchronous Multi-Frequency-TDMA system, with a properly chosen nonlinearity, the V&V algorithm can still offer excellent performance, so as to further verify the usefulness of the algorithm.

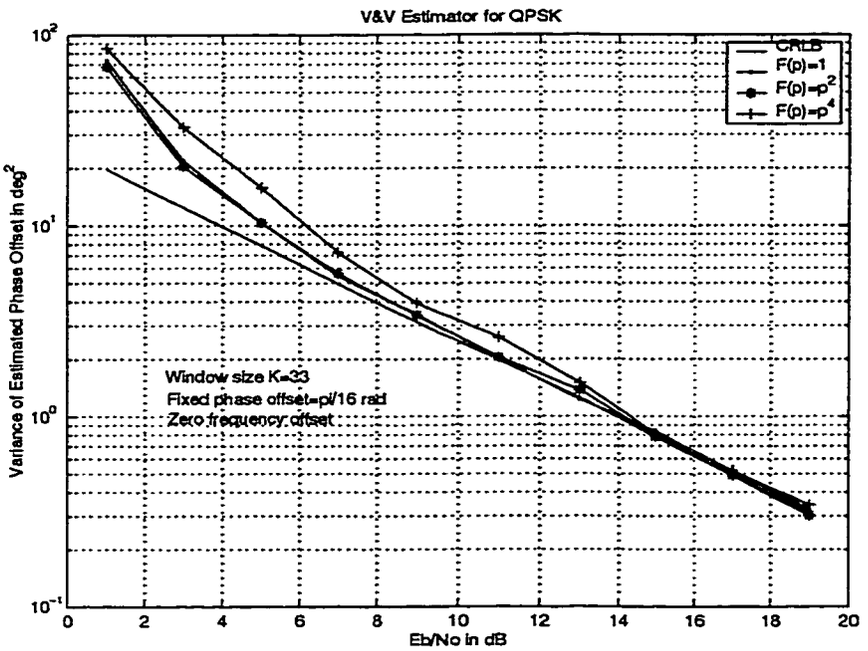

Figure 2.3: Graphic Example of the Effect of Non-Linear Factor on NDA Phase Estimator

2.3 Frequency Offset Estimation

For a large frequency offset, we must first compensate it before the other parameters, such as phase offset, can be estimated. This implies that frequency offset estimation algorithms must work independently of the values of the other parameters.

- FB structure

From the familiar way of maximizing the objective function by differentiating, the frequency error signal is obtained and the feedback algorithm is obtained in the same way as described for phase estimation [7]. Using the un-modulated received MPSK model (1.3) in the differentiated (2.8) by frequency offset, and maximizing it for one sample increment,

$$e(k) = \Re\left[r(k,\Delta f)\frac{\partial}{\partial \Delta f} r^*(k;\Delta f)\right]_{\Delta f=\widehat{\Delta f}_{k|k-1}} \tag{2.15}$$

There are many ways to obtain the final result of such a error signal $e(k)$. For example, passing the received signal through the frequency matched filter (FMF) [13], the differential part above can be realized as:

$$\frac{\partial}{\partial \Delta f} r(k;\Delta f) = r_{FMF}(k;\Delta f) - jkT_s r(k;\Delta f)$$

Using it to substitute into (2.15), the final error signal $e(k)$ can be obtained. Using the frequency signal in the feedback scheme, the estimated frequency offset can be adjusted to get an accurate estimation. In [14], such a algorithm is performed.

- FF structure

Feedforward frequency estimation can be performed via spectrum analysis or phase increment estimation [7]. To be simplified for illustration, the theoretical results are expressed with un-modulated signal model.

1. Phase increment estimation

We treat the frequency offset to be estimated as the argument of a rotating phaser. Starting for the objective function,

$$L(a,\Delta f,\Delta\theta) = \sum_{k=0}^{K-1} \Re\left\{r_k s_k^*\right\} = \sum_{k=0}^{K-1} \Re\left\{r_k e^{-j(2\pi\Delta f k+\Delta\theta)}\right\} \tag{2.16}$$

After passing through the channel, r_k can be generally expressed as $r_k = s(k;\Delta f,\Delta\theta) + n_k$. As we know $\vartheta_k = 2\pi\Delta f k + \Delta\theta$ is increased by an amount of $\Delta\vartheta_k = 2\pi\Delta f$ between sampling instants. A filtering of a phaser $e^{j\Delta\vartheta_k}$ yields an unbiased estimate of Δf.

Since, $s_k \approx e^{j2\pi\Delta f} s_{k-1}$,

Also for high SNR, $s_k \approx r_k$,

The objective function will then be expressed as,

$$\begin{aligned} L'(a,\Delta f) &= \sum_{k=1}^{K-1} \Re\left\{e^{-j2\pi\Delta f} r_k r_{k-1}^*\right\} \\ &= \sum_{k=1}^{K-1} \Re\left\{e^{-j2\pi\Delta f} \left|r_k r_{k-1}^*\right| e^{j\arg\left\{r_k r_{k-1}^*\right\}}\right\} \end{aligned} \tag{2.17}$$

The phase increment estimation will then be obtained as,

$$2\pi\widehat{\Delta f} = \frac{1}{K-1}\sum_{k=1}^{K-1}\arg\left\{r_k r_{k-1}^*\right\} \tag{2.18}$$

For the modulated case, the modulation has to be removed at first, then the same method can apply. This estimator is used in the initial estimate part of the DA-FB joint estimator. From the same approach, many variations of such kind of phase increment estimation have been proposed, such as [19],

$$2\pi\widehat{\Delta f}_{ML} = w_m\left(\arg\left\{\sum_{k=m}^{K} r_k r_{k-m}^*\right\}\right) \tag{2.19}$$

where, w_m is certain kind of estimator window function to get a good estimation when properly chosen.

2. Spectrum analysis

The Fourier transform of the signal is:

$$\begin{aligned}
F(\Delta f) &= \tfrac{1}{K}\textstyle\sum_{k=0}^{K-1} r_k e^{-j2\pi\Delta fk} \\
&= \tfrac{1}{K}\textstyle\sum_{k=0}^{K-1}\left\{(x_k+jy_k)\left[\cos(2\pi\Delta fk)-j\sin(2\pi\Delta fk)\right]\right\} \\
&= \tfrac{1}{K}\textstyle\sum_{k=0}^{K-1}\left\{\left[x_k\cos(2\pi\Delta fk)+y_k\sin(2\pi\Delta fk)\right]\right. \\
&\qquad \left.+j\left[y_k\cos(2\pi\Delta fk)-x_k\sin(2\pi\Delta fk)\right]\right\} \\
&= \tfrac{1}{K}\textstyle\sum_{k=0}^{K-1}(A_k+jB_k) \\
&= \tfrac{1}{K}\textstyle\sum_{k=0}^{K-1}A_k + j\tfrac{1}{K}\textstyle\sum_{k=0}^{K-1}B_k \\
&= F^I(\Delta f)+jF^Q(\Delta f)
\end{aligned} \tag{2.20}$$

We have defined a few temporary parameters A_k, B_k, $F^I(\Delta f)$, $F^Q(\Delta f)$ to simplify the expression, where,

$$A_k = \left[x_k\cos(2\pi\Delta fk)+y_k\sin(2\pi\Delta fk)\right]$$

$$B_k = \left[y_k\cos(2\pi\Delta fk)-x_k\sin(2\pi\Delta fk)\right]$$

$$F^I(\Delta f) = \frac{1}{K}\sum_{k=0}^{K-1} A_k = \frac{1}{K}\sum_{k=0}^{K-1}\left[x_k \cos(2\pi\Delta f k) + y_k \sin(2\pi\Delta f k)\right]$$

$$F^Q(\Delta f) = \frac{1}{K}\sum_{k=0}^{K-1} B_k = \frac{1}{K}\sum_{k=0}^{K-1}\left[y_k \cos(2\pi\Delta f k) - x_k \sin(2\pi\Delta f k)\right]$$

and are clearly defined from the derivation. Considering the objective function and the signal without modulation, a mathematically equivalent form leads to a different realization of the estimator from (2.8),

$$\begin{aligned}
\tfrac{1}{K}L(a,\Delta f,\Delta\theta) &= \tfrac{1}{K}\textstyle\sum_{k=0}^{K-1}\Re\left\{\left[r_k e^{-j2\pi\Delta f k}\right]e^{-j\Delta\theta}\right\} \\
&= \tfrac{1}{K}\textstyle\sum_{k=0}^{K-1}\Re\left\{[A_k + jB_k]\left[\cos(\Delta\theta) - j\sin(\Delta\theta)\right]\right\} \\
&= \tfrac{1}{K}\textstyle\sum_{k=0}^{K-1}\left\{A_k\cos(\Delta\theta) + B_k\sin(\Delta\theta)\right\} \\
&= \left(\tfrac{1}{K}\textstyle\sum_{k=0}^{K-1}A_k\right)\cos(\Delta\theta) + \left(\tfrac{1}{K}\textstyle\sum_{k=0}^{K-1}B_k\right)\sin(\Delta\theta) \\
&= F^I(\Delta f)\cos(\Delta\theta) + F^Q(\Delta f)\sin(\Delta\theta) \\
&= \Re\left\{F(\Delta f)e^{-j\Delta\theta}\right\}
\end{aligned} \tag{2.21}$$

Since, $L(a,\Delta f,\Delta\theta) \leq |F(\Delta f)|$, and discarding the coefficient K, the objective function is maximized by,

$$\widehat{\Delta f} = \arg\left(\max_{\widetilde{\Delta f}}|F(\Delta f)|\right) \tag{2.22}$$

where, $\widetilde{\Delta f}$ is the trial values of unknown frequency offset Δf.

In other words, the ML frequency estimate $\widehat{\Delta f}$, is obtained by locating the peak of the periodic $|F(\Delta f)|$. It corresponds to a maximum search process, and can be efficiently performed using Fast Fourier Transform (FFT). Such an FFT algorithm is merely a kind of implementation for use in practice. Since the signal amplitude response in frequency domain is related to the signal frequency power density distribution directly, another implementation method can be the analysis of the power spectral density function.

For phase-modulated carriers, the modulation has to be first canceled. When the M-th exponential function is used,

$$\widehat{\Delta f} = \frac{1}{M} \arg \max_{\widetilde{M\Delta f}} |F(M\Delta f)| \tag{2.23}$$

In fact, conventional approach for frequency estimation essentially assumes a single tone without data modulation usually. As in [9,10], a fast estimation scheme, which exploits knowledge of training bits embedded in the burst, is proposed. From the basic ML estimate function of Δf, this estimator finds a sample solution by exploiting the auto-correlation of the received sequences. However, to improve transmission efficiency, novel techniques try to estimate frequency offset using NDA approach. Paper [11] deals with the frequency estimation of phase-modulated carriers with known data pattern, and uses a spectrum analysis method. The estimator can be extended to be used as the joint estimator of timing/frequency/phase estimation. In [12], an NDA approach spectrum analysis technique is used to estimate the frequency offset directly from the received Minimum-Shift Keying (MSK) or Gaussian MSK (GMSK) modulation signals. Its performance is much better than that of other existing methods, but with higher computational complexity. A fully tutorial review of all existing FF frequency estimators can be found in [20].

2.4 Joint Phase/Frequency Offset Estimation

Many carrier phase/frequency synchronizers are realized by combining two separate estimators: one for frequency-offset estimation and another for phase-offset estimation [21]. The joint phase/frequency estimators, however, estimate frequency offset and phase offset together using ML method.

Originally, joint Least-Squares estimator (LSE) is drawn from the sample variance function of the estimation:

$$\overline{Var}(r_k, a_k|\Delta f, \Delta\theta) = \frac{1}{K} \sum_{k=0}^{K-1} (\varphi_k - 2\pi\Delta f k - \Delta\theta)^2 \tag{2.24}$$

if we express $r_k a_k^* = c_k e^{j\varphi_k}$, then $c_k = |r_k a_k^*|$, and

$$\varphi_k = \arg\{r_k a_k^*\} = 2\pi\Delta f k + \Delta\theta + \varepsilon_k$$

where,

ε_k stands for the phase noise, i.e., the phase due to the channel noise,

$\overline{Var}$ stands for the sample variance.

Here, if a_k is used directly, the DA algorithm is performed; if $\widehat{a}_k$ is used, then the DD algorithm is approached. The NDA algorithm can also be done by raising r_k to the M-th power first, and the DA algorithm then.

The estimator can be realized either by FF structure, or by FB structure if the estimated frequency offset $\widehat{\Delta f}$ and phase offset $\widehat{\Delta\theta}$ are used for the detection of ϑ_k.

Minimizing (2.24) by differentiating with respect to Δf and $\Delta\theta$ separately, we get,

$$\begin{array}{rcl} \sum_{k=0}^{K-1} k(\varphi_k - 2\pi\widehat{\Delta f}k - \widehat{\Delta\theta}) & = & 0 \\ \sum_{k=0}^{K-1} (\varphi_k - 2\pi\widehat{\Delta f}k - \widehat{\Delta\theta}) & = & 0 \end{array} \tag{2.25}$$

The estimation can be obtained by solving (2.25) as:

$$\begin{array}{rcl} 2\pi\widehat{\Delta f} & = & \frac{12}{K(K^2-1)} \sum_{k=0}^{K-1} k\varphi_k - \frac{6}{K(K-1)} \sum_{k=0}^{K-1} \varphi_k \\ \widehat{\Delta\theta} & = & \frac{2(2K+1)}{K(K-1)} \sum_{k=0}^{K-1} \varphi_k - \frac{6}{K(K-1)} \sum_{k=0}^{K-1} k\varphi_k \end{array} \tag{2.26}$$

This estimation can be shown to be a special case of another joint estimator derived from the linearized-ML function directly [22]. From (2.8), we get,

$$\begin{array}{rcl} \widehat{\Delta f}, \widehat{\Delta\theta} & = & \arg\left(\max_{\widetilde{\Delta f}, \widetilde{\Delta\theta}} \sum_{k=0}^{K-1} \Re\left\{r_k a_k^* e^{-j(2\pi\Delta f k + \Delta\theta)}\right\}\right) \\ & = & \arg\left(\max_{\widetilde{\Delta f}, \widetilde{\Delta\theta}} \sum_{k=0}^{K-1} c_k \cos\left(\varphi_k - 2\pi\Delta f k - \Delta\theta\right)\right) \end{array} \tag{2.27}$$

Maximizing (2.27) by differentiating for Δf and $\Delta\theta$ separately,

$$\begin{array}{rcl} \sum_{k=0}^{K-1} c_k \sin(\varphi_k - 2\pi\widehat{\Delta f}k - \widehat{\Delta\theta}) & = & 0 \\ \sum_{k=0}^{K-1} k c_k \sin(\varphi_k - 2\pi\widehat{\Delta f}k - \widehat{\Delta\theta}) & = & 0 \end{array} \tag{2.28}$$

Using Taylors series to expend the non-linear function in (2.28), and neglecting non-linear part, the function can be linearized,

$$\begin{aligned} \sum_{k=0}^{K-1} c_k \times (\varphi_k - 2\pi\widehat{\Delta f}k - \widehat{\Delta\theta}) &= 0 \\ \sum_{k=0}^{K-1} kc_k \times (\varphi_k - 2\pi\widehat{\Delta f}k - \widehat{\Delta\theta}) &= 0 \end{aligned} \tag{2.29}$$

the estimation can be obtained as:

$$\begin{aligned} 2\pi\widehat{\Delta f} &= \frac{\sum_{k=0}^{K-1} kc_k\varphi_k \sum_{k=0}^{K-1} c_k - \sum_{k=0}^{K-1} kc_k \sum_{k=0}^{K-1} c_k\varphi_k}{\sum_{k=0}^{K-1} k^2c_k \sum_{k=0}^{K-1} c_k - \left(\sum_{k=0}^{K-1} kc_k\right)^2} \\ \widehat{\Delta\theta} &= \frac{\sum_{k=0}^{K-1} c_k\varphi_k \sum_{k=0}^{K-1} k^2c_k - \sum_{k=0}^{K-1} kc_k\varphi_k \sum_{k=0}^{K-1} kc_k}{\sum_{k=0}^{K-1} k^2c_k \sum_{k=0}^{K-1} c_k - \left(\sum_{k=0}^{K-1} kc_k\right)^2} \end{aligned} \tag{2.30}$$

Approximating $c_k = 1$ if MPSK is used, (2.30) is approximated to be LSE in (2.26) exactly. Such joint estimators are supposed to be simple and fast, under the condition when phase jump can be controlled effectively and a properly chosen preamble.

2.5 Cramer-Rao Lower Bound (CRLB)

We have described various ML methods for estimating carrier parameters. During data transmission, the synchronizer provides estimate which most of the time exhibits small fluctuations about the true value. It means that the synchronizers are always in tracking mode. For such kind of estimate, moment analysis is important for evaluating the performance of the estimation system.

As what we discuss is ML estimate, it is known that ML estimate is efficient and consistent. This implies that the ML estimate converges, in probability, to the correct value of the unknown parameter, for large K. Such that

$$\lim_{K\to\infty} Pr\left\{\left|\widehat{\phi} - \phi\right| < \mu\right\} = 1$$

for some small constant μ such that it is unbiased. In the mean time, it has the minimum variance of the estimation.

Then, what is the ultimate accuracy that can be achieved in synchronization? Establishing bounds to this accuracy is an important goal as it provides benchmarks against which to compare the performance of actual synchronizers. Tools to approach this problem are available from parameter estimation theory in the form of Cramer-Rao bounds (CRBs) [25], which give the lower bounds for variance performance of the estimate so as to assess the implementation loss for different kind of synchronizers.

Since any modulation technique is expected to introduce degradation, the CRLB for the modulated case is higher than the CRLB for the un-modulated carrier. This fundamental lower limit on the variance of estimated parameters is equal to the diagonal elements of the inverse of Fisher's information matrix as shown in (2.31),

$$\begin{aligned} J &= \begin{bmatrix} J_{ff} & J_{f\theta} \\ J_{\theta f} & J_{\theta\theta} \end{bmatrix} \\ &= \frac{2E_s}{N_o} \begin{bmatrix} 4\pi^2 \sum_{k=l}^{l+K-1} k^2 & 2\pi \sum_{k=l}^{l+K-1} k \\ 2\pi \sum_{k=l}^{l+K-1} k & K \end{bmatrix} \end{aligned} \tag{2.31}$$

where,

l is the start point of the estimation in the burst,

$J_{\phi_i\phi_j} = \frac{\partial^2 \ln\{p(\overrightarrow{r}|\phi_i,\phi_j)\}}{\partial\phi_i\partial\phi_j}$ and $p(\overrightarrow{r}|\phi_i,\phi_j)$ is the ML function in (2.6) with the un-modulated signal form.

- CRLB for separate phase or frequency estimation

The CRLB for the separate phase or frequency estimation can be obtained directly from (2.31), where we have supposed that one of the parameters of Δf and $\Delta\theta$ has been known such that the terms $J_{\phi_i\phi_j}$ with $i \neq j$ are zero.

$$\begin{aligned} Var\left[\widehat{\Delta f}\right]_{separate} &\geq \frac{1}{J_{\Delta f\Delta f}} = \frac{3}{4\pi^2 K(K-1)(2K-1)\frac{E_s}{N_o}} \\ Var\left[\widehat{\Delta\theta}\right]_{separate} &\geq \frac{1}{J_{\Delta\theta\Delta\theta}} = \frac{6}{K^2(K^2-1)\frac{E_s}{N_o}} \sum_{k=l}^{l+K-1} k^2 \end{aligned} \tag{2.32}$$

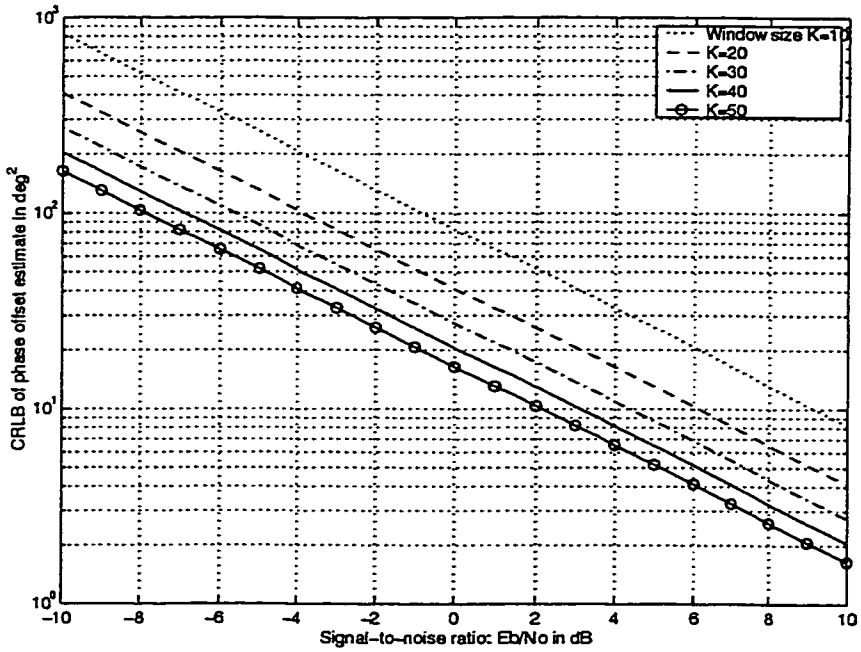

Figure 2.4: CRLB of Separated Phase Offset Estimate

In most cases, we cannot expect to know the phase information as what we have stated in the previous discussion for the frequency estimation. Therefore, we cannot take advantage of the preceding property of frequency estimate. Consequently, it is always assumed that the phase is unknown in the estimation of frequency, so that the CRLB for joint estimation of frequency offset is always used through the thesis.

We also want to mention the influence of symmetry characteristics of the observation window on the estimation. For example, from the derivation of (2.32), it is noticed that the bound on the variance of frequency offset is independent of the initial starting point of the samples. On the other hand, the bound for the variance of the phase offset is dependent on this initial starting point. In fact there is an optimum value of l which produces the lowest bound as shown in Figure 2.4,

$$Var\left[\widehat{\Delta\theta}\right]_{separate} \geq \frac{1}{2K\frac{E_s}{N_o}}$$

The minimization in the equation is obtain with

$$l = -\frac{K-1}{2} \tag{2.33}$$

This implies that a phase estimator employing discrete time observation will have minimum variance for the phase at the middle of the observation window. This optimum point is used later on.

For QPSK signaling, $\frac{E_s}{N_o} = 2\frac{E_b}{N_o}$ can be substituted directly in the formula directly.

- CRLB for joint phase/frequency estimation

For the joint phase/frequency estimation, the CRLB is obtained from the inverse of J,

$$\begin{aligned} J^{-1} &= \begin{bmatrix} J^{\Delta f \Delta f} & J^{\Delta f \Delta \theta} \\ J^{\Delta \theta \Delta f} & J^{\Delta \theta \Delta \theta} \end{bmatrix} \\ &= \frac{6N_o}{4\pi^2 E_s K^2 (K+1)(K-1)} \begin{bmatrix} K & -\pi K(K-1) \\ -\pi K(K-1) & \frac{2\pi^2 K(K-1)(2K-1)}{3} \end{bmatrix} \end{aligned} \tag{2.34}$$

From (2.34), the final expression for CRLB depends only on the signal-to-noise ratio and the observation window size K. It is expressed as:

$$\begin{aligned} Var\left[\widehat{\Delta f}\right]_{joint} &\geq J^{\Delta f \Delta f} = \frac{3}{2\pi^2 K(K^2-1)\frac{E_s}{N_o}} \\ Var\left[\widehat{\Delta \theta}\right]_{joint} &\geq J^{\Delta \theta \Delta \theta} = \frac{2K-1}{K(K+1)\frac{E_s}{N_o}} \end{aligned} \tag{2.35}$$

- CRLB for low SNR

CRLB for un-modulated carrier is a good approximation for higher SNR ratios but actual estimation techniques show significant departures for noisier modulated signals. With increased use of channel coding and packet transmission, tighter bounds at low SNR ratios are useful. Since in applications involving burst mode transmission or limited observation intervals, the estimation of synchronization parameters is often carried out over a block of PSK symbols, [18] derives new lower bounds for BPSK and QPSK.

$$CRLB_{new}\left(\widehat{\phi}\right) = \frac{CRLB}{F\left(\frac{N_o}{2E_s}\right)} \tag{2.36}$$

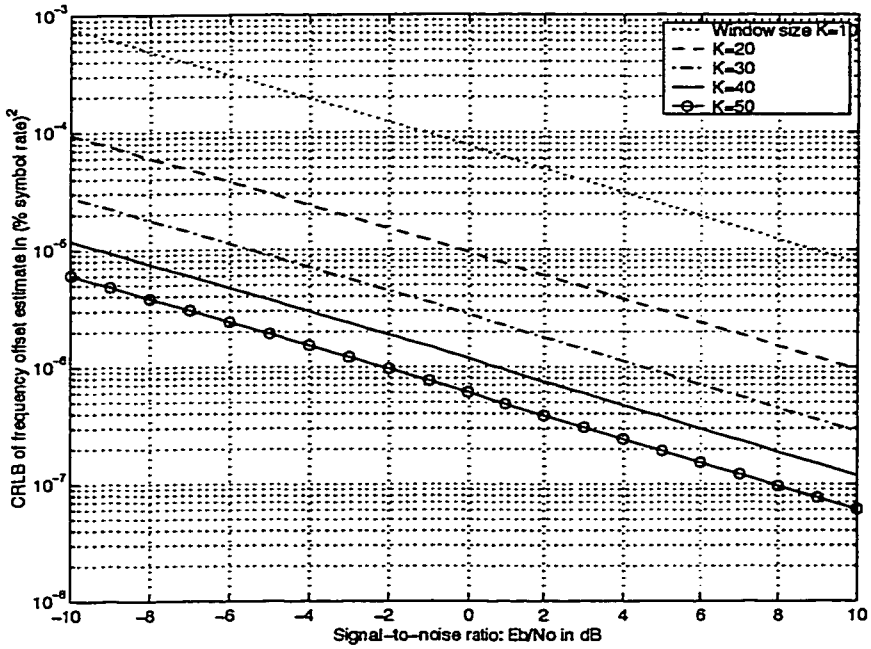

Figure 2.5: CRLB of Frequency Offset in Joint Estimate

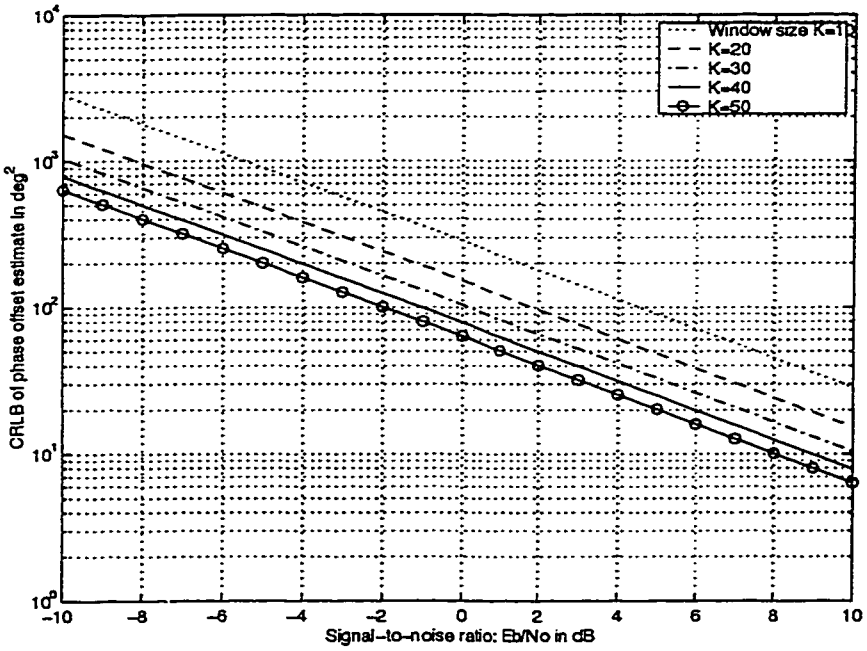

Figure 2.6: CRLB of Phase Offset in Joint Estimate

where,

CRLB stands for the lower bound for the un-modulated carrier case,

$F^{-1}\left(\frac{N_o}{2E_s}\right)$ is the ratio of the CRLB for random signal to the CRLB for an un-modulated carrier of the same power. This different is different for BPSK and QPSK signaling. Define $\varsigma^2 = \frac{N_o}{2E_s}$, then for BPSK,

$$F_B\left(\varsigma^2\right) = \int_{-\infty}^{\infty} \tanh^2\left(\frac{1+\widetilde{n}^I}{\varsigma^2}\right) \frac{e^{-\frac{\left(\widetilde{n}^I\right)^2}{2\varsigma^2}}}{\sqrt{2\pi}\varsigma} d\widetilde{n}^I$$

and for QPSK,

$$F_Q\left(\varsigma^2\right) = \int_{-\infty}^{\infty}\int_{-\infty}^{\infty} \frac{\sinh^2\left(\frac{1+\widetilde{n}^I}{\varsigma^2}\right)\frac{\left(\widetilde{n}^Q\right)^2}{\varsigma^2} + \sinh^2\left(\frac{\widetilde{n}^Q}{\varsigma^2}\right)\frac{\left(1+\widetilde{n}^I\right)^2}{\varsigma^2} - 2\sinh\left(\frac{1+\widetilde{n}^I}{\varsigma^2}\right)\sinh\left(\frac{\widetilde{n}^Q}{\varsigma^2}\right)\left(1+\widetilde{n}^I\right)\frac{\widetilde{n}^Q}{\varsigma^2}}{\left(\cosh\left(\frac{1+\widetilde{n}^I}{\varsigma^2}\right)+\cosh\left(\frac{\widetilde{n}^Q}{\varsigma^2}\right)^2\right)^2} \times \frac{e^{-\frac{\left(\left(\widetilde{n}^I\right)^2+\left(\widetilde{n}^Q\right)\right)^2}{2\varsigma^2}}}{2\pi\varsigma^2} d\widetilde{n}^I d\widetilde{n}^Q \tag{2.37}$$

where, $\widetilde{n} = ne^{-j\phi}$ and superscripts I and Q denote the real and imaginary parts respectively. In [6], it has been verified that the rotated noise $\widetilde{n}^I$ and $\widetilde{n}^Q$ are again independent variables with the same distribution as n^I and n^Q.

The difference between between BPSK and QPSK bounds and un-modulated case can be shown in Figure 2.7.

This result will be used in our performance evaluation in the combined NDA-FF synchronizer. As the NDA-FF frequency estimation can work under very low SNR, the traditional method of using CRLB for un-modulated carrier is not enough for the evaluation there.

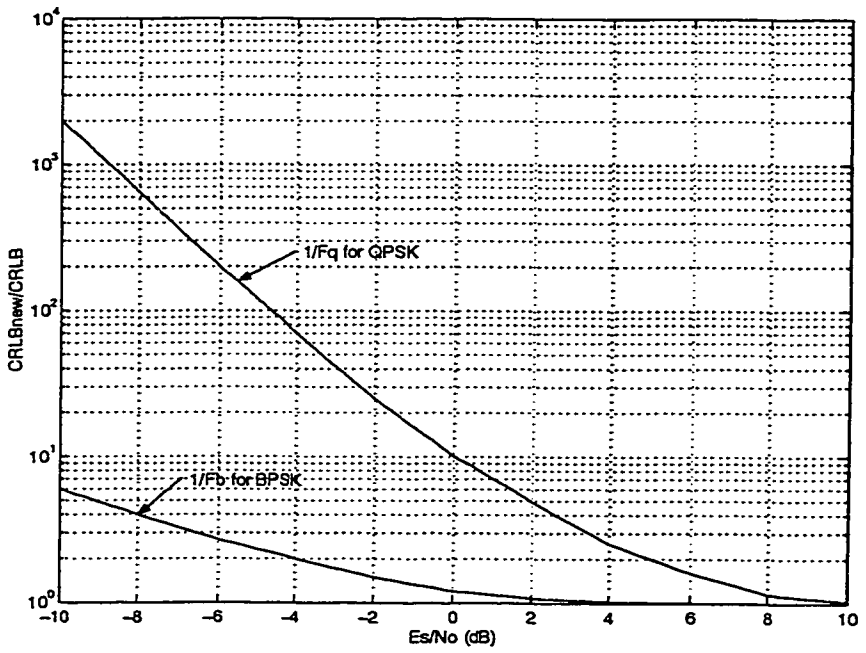

Figure 2.7: Ratio of the CRLB_{new} and CRLB with Un-Modulated Carrier

Chapter 3

Non-Data-Aided Feedforward Estimation Technique

From the discussion of last chapter, we know that both feedforward structure and feedback structure can realize carrier synchronization. In this chapter, a fully FF structure digital phase/frequency synchronizer is presented. It is realized by combining Rife and Boorstyn (R&B) [8] frequency estimator and Viterbi and Viterbi (V&V) phase estimator in cascade.

This FF algorithm is also NDA, which recovers the reference parameters form a block of the received symbol and has highest transmission efficiency. Such a NDA-FF algorithm suits coherent receivers operating in both burst-mode and continuous-mode environment. Since it can provide accurate synchronization and is free of hung-up problem of feedback schemes, it is the most preferred estimation method for fast and efficient estimation. Meanwhile, a DD-FB phase estimation technique is studied in this chapter to be compared with the NDA-FF one, so as to give numerical result for testing FB algorithm.

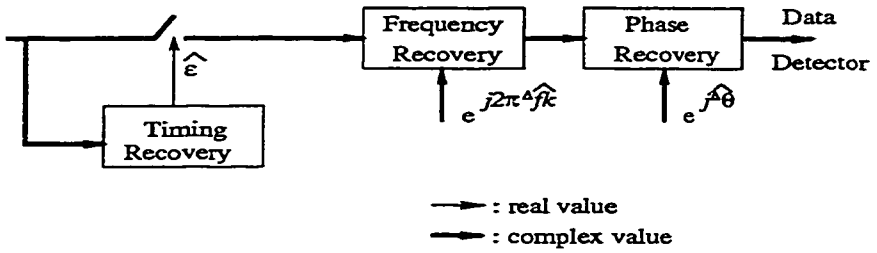

Figure 3.1: Simplified Block Diagram of the NDA-FF Synchronization Unit

3.1 Presentation of Techniques

As we have stated, this carrier phase/frequency estimation algorithm is a combined scheme. Both the phase offset estimation technique and frequency offset estimation technique fall under the category of feedforward estimators. They are appropriate for burst-mode TDMA systems. Its block diagram is shown in Figure 3.1.

The synchronization unit follows the procedure as follows:

1. Frequency estimator delays the whole length of a burst and uses the whole burst information to obtain the frequency-offset estimate $\widehat{\Delta f}$.

2. Frequency offset estimation is used to subtract the frequency offset in the received signals so as to reduce the frequency-offset to a small value which phase estimator can tolerate.

3. The phase offset estimator estimates the phase offset $\widehat{\Delta\theta}$ using the frequency adjusted received signals from step two.

We should notice that phase offset estimation with frequency offset exiting does not deal with pure $\Delta\theta$, but with phase offset having frequency influence inside, which requires that the phase estimator be tolerable to certain frequency error. In the following, we will present and analyze the phase offset estimator and frequency offset estimator separately, and describe their combined characteristics.

3.1.1 Phase Offset Estimator

In this section, we will study two phase estimators: one is V&V NDA-FF phase offset estimator, the other one is a DD-FB phase offset estimator. The former will be emphasized more in the following analysis.

3.1.1.1 Presentation of Techniques

- NDA-FF algorithm

Starting with the polar form of the received signal as shown in (1.3), after phase being multiplied by M to remove the dependence on the modulation and the magnitude being passed through some nonlinearity $F(|r_k|)$, the result is then re-converted back to rectangular form, yielding,

$$\begin{aligned} r_k' &= F(|r_k|)\, e^{j(M\psi_k)} \\ &= F(|r_k|)\, e^{j(2\pi\Delta f k M + M\Delta\theta + M\varepsilon_k + M\theta_k)} \\ &= F(|r_k|)\, e^{j(2\pi\Delta f k M + M\Delta\theta + M\varepsilon_k)} \\ &= F(|r_k|)\cos\left(2\pi\Delta f k M + M\Delta\theta + M\varepsilon_k\right) + jF(|r_k|)\sin\left(2\pi\Delta f k M + M\Delta\theta + M\varepsilon_k\right) \end{aligned} \tag{3.1}$$

To obtain the estimation which minimizes the estimation variance, we redefine the observation window to make it symmetric about the estimated point. Such that,

$$r_k' = F(|r_k|)\cos\left(2\pi\Delta f(k-l-N)M + M\Delta\theta' + M\varepsilon_k\right) + jF(|r_k|)\sin\left(2\pi\Delta f(k-l-N)M + M\Delta\theta' + M\varepsilon_k\right) \tag{3.2}$$

where,

$N = \frac{K-1}{2}$,

l is the start point of the observation window,

k is the estimation point in the observation window.

Because of the redefinition of the observation window, $\Delta\theta' = \Delta\theta + 2\pi\Delta f(l+N)$. The estimation $\widehat{M\Delta\theta'}$ for $M\Delta\theta'$ is then found by averaging the K complex samples

$r_k^{'}$, and determining the corresponding argument of this mean. If the noise were absent, $M\varepsilon_k = 0$ and $r_k^{'}$ would be given by

$$r_k^{'} = F\left(|r_k|\right) e^{j\left(2\pi\Delta f(k-l-N)M + M\Delta\theta^{'}\right)} \tag{3.3}$$

Therefore,

$$M\widehat{\Delta\theta^{'}} = \arg\left[\frac{1}{K}\sum_{k=l}^{l+K-1} r_k^{'}\right]$$

$$\begin{aligned} \widehat{\Delta\theta^{'}} &= \frac{1}{M}\arctan\left[\frac{\frac{1}{K}\sum_{k=l}^{l+K-1} F(|r_k|)\sin\left(2\pi\Delta f(k-l-N)M + M\Delta\theta^{'}\right)}{\frac{1}{K}\sum_{k=l}^{l+K-1} F(|r_k|)\cos\left(2\pi\Delta f(k-l-N)M + M\Delta\theta^{'}\right)}\right] \\ &= \frac{1}{M}\arctan\left[\frac{\Im\left\{\frac{1}{K}\sum_{k=l}^{l+K-1} r_k^{'}\right\}}{\Re\left\{\frac{1}{K}\sum_{k=l}^{l+K-1} r_k^{'}\right\}}\right] \end{aligned} \tag{3.4}$$

In the meanwhile, if we use the trigonometric identity,

$$\alpha + \arctan\left[\frac{y}{x}\right] = \arctan\left[\frac{x\sin(\alpha) + y\cos(\alpha)}{x\cos(\alpha) - y\sin(\alpha)}\right]$$

we can also reduce the above equation (3.4) to,

$$\begin{aligned} \widehat{\Delta\theta^{'}} &= \Delta\theta^{'} + \frac{1}{M}\arctan\left[\frac{\frac{1}{K}\sum_{k=l}^{l+K-1} F(|r_k|)\sin(2\pi\Delta f(k-l-N)M)}{\frac{1}{K}\sum_{k=l}^{l+K-1} F(|r_k|)\cos(2\pi\Delta f(k-l-N)M)}\right] \\ &= \Delta\theta^{'} \end{aligned}$$

The last equality is due to the fact that the numerator of the arctan function argument tends to zero if we set the estimation as the middle point of the observation window. Such property is attributed directly to the symmetry of the frequency error for samples at opposite ends of the observation window,

$$F\left(\sqrt{E_s}\right)\sin\left(2\pi f\left(k-N\right)M\right) = -F\left(\sqrt{E_s}\right)\sin\left(2\pi f\left(N-k\right)M\right) \tag{3.5}$$

For convenience, we always suppose K is an odd number. Such property also means that only the middle point of the estimation is unbiased in a observation window. In practice, if the accuracy is precise enough for the detection of the data symbol, we can still use one estimation for the whole burst, and neglect the bias problem for all the points.

According to (3.4), the block diagram is easily shown as in Figure 3.2.

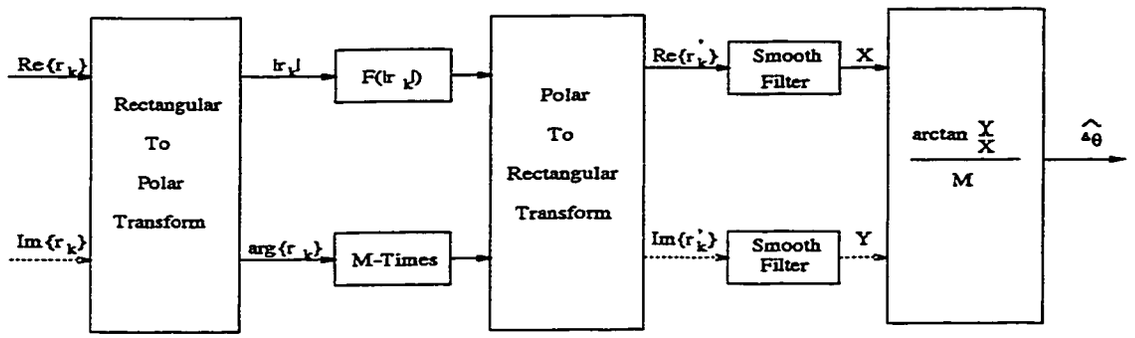

Figure 3.2: Block Diagram of V&V Phase Estimator

- DD-FB algorithm

The digital PLL circuit originates from the analog PLL, which remains an important algorithm in estimation area. We want to use it to show the general properties of decision-directed system, since the other DA-FB joint estimation algorithm in next chapter also involves the DD operation.

The general structure of PLL has been shown in Figure 2.2. We want to use the second approach (2.10) to realize the function [4]. A procedure to make the summation vanish is as follows.

1. a_k is replaced with the decision $\widehat{a}_k$ from the detector.

2. The generic term in the summation is computed setting $\Delta\theta$ equal to the current estimate $\widehat{\theta}_c$.

3. The result is used as an error signal to improve the phase estimate, as shown in (2.13) and the e_k is formally expressed as:

$$e_k = \Im\left\{\widehat{a}_k^* r_k e^{-j\widehat{\theta}_c}\right\} \tag{3.6}$$

Referring to (2.13), as $e_k \to 0$, $\widehat{\Delta\theta} = \Delta\theta$. The function diagram is shown in Figure 3.3. In implementation, to obtain a better error signal, the loop filter is drawn before the error generator, and the detail block diagram is shown in Figure 3.4.

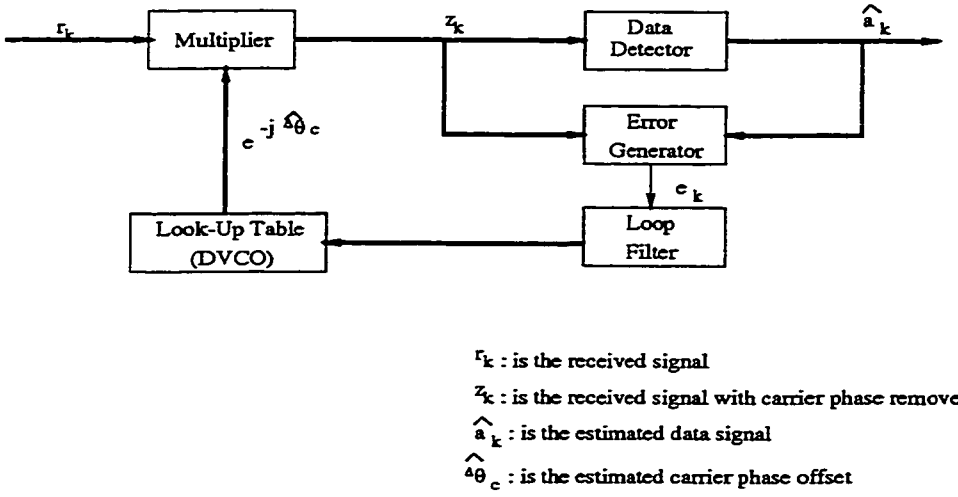

Figure 3.3: Function Diagram of DD-FB Phase Estimator

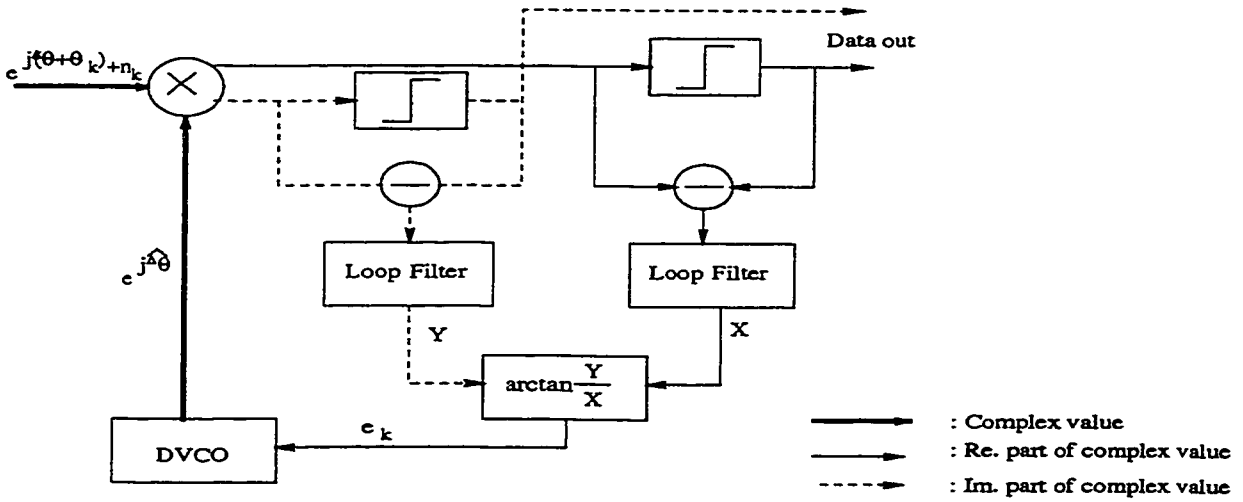

Figure 3.4: Block Diagram of DD-FB Phase Estimator

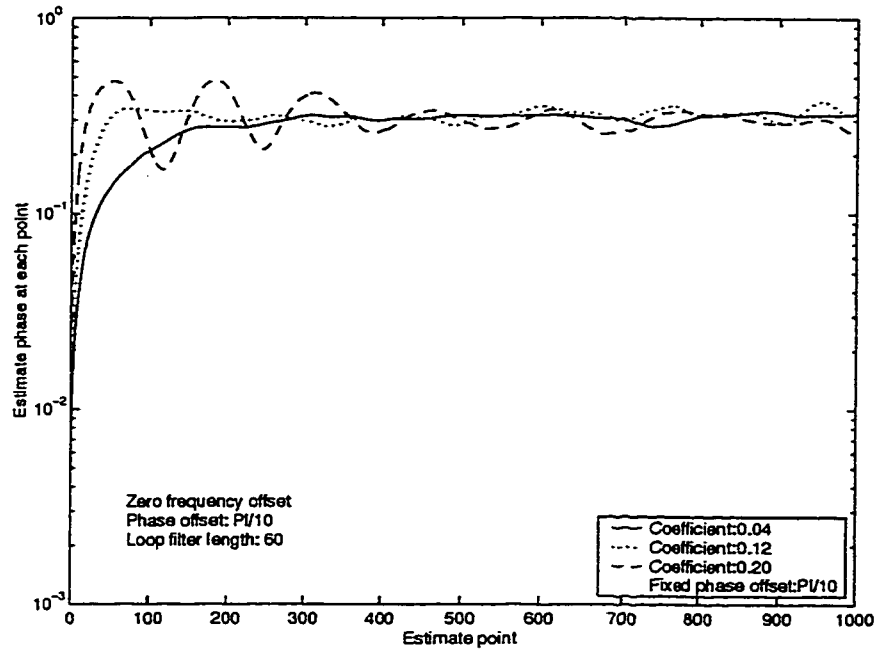

Figure 3.5: Effect of K_{VCO} on Acquisition Time of the DD-FB Phase Estimator

Unlike feedforward system, the feedback algorithm always requires acquisition time to bring the loop into lock. A proper chosen coefficient K_{VCO} can adjust the acquisition speed as well as the stability of the system. The influence of K_{VCO} is shown in Figure 3.5 and Figure 3.6, and the acquisition time in this system is about 60 symbols. It shows that the small K_{VCO} can give stable estimation but with long acquisition time, on the contrary, the larger K_{VCO} gives short acquisition time but with fluctuate estimation.

Without proper choice of K_{VCO}, the loop can easily loose lock, as shown in Figure 3.7. This phenomenon happens in both zero-frequency offset and nonzero-frequency offset circumstance. The reason for us to show the result in nonzero-frequency offset case is that we also want to show the influence of the frequency offset on the feedback structure phase estimator, which is different from that of the feedforward phase estimator, as we will see next.

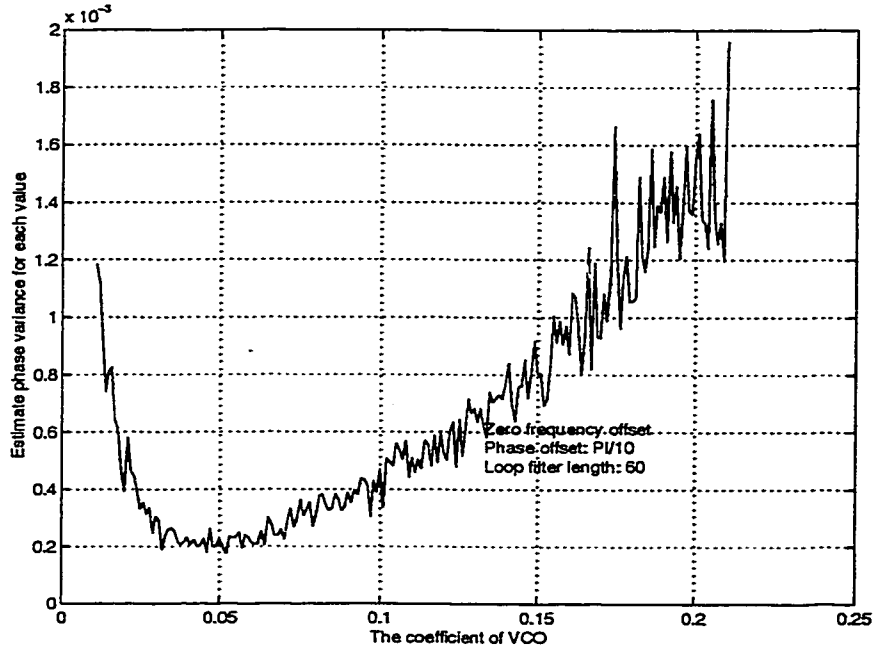

Figure 3.6: Effect of K_{VCO} on Variance Performance of the DD-FB Phase Estimator

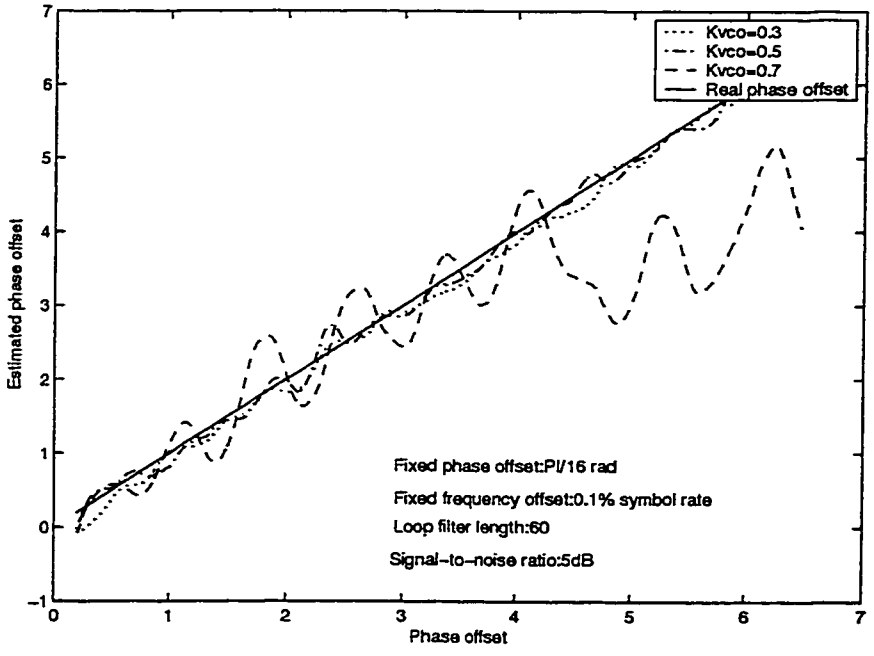

Figure 3.7: Hang-Up Phenomenon in DD Algorithm

3.1.1.2 Analysis of Techniques

In this section, we discuss the performance of the NDA-FF estimator and its properties. Meanwhile, we will show the difference between the characteristics of the NDA-FF and DD-FB phase estimators.

- Moment analysis of NDA-FF phase estimator

The algorithm has been derived in (3.4). In fact, as soon as the noise is considered,

$$F\left(\sqrt{E_s}\right)\sin\left(2\pi f\left(k-N\right)M+M\varepsilon_k\right)\neq -F\left(\sqrt{E_s}\right)\sin\left(2\pi f\left(N-k\right)M+M\varepsilon_k\right) \tag{3.7}$$

and as a result, the final estimate would be a function of both noise and frequency error.

$$\begin{aligned}\widehat{\Delta\theta'} &= \frac{1}{M}\arctan\left[\frac{\frac{1}{K}\sum_{k=l}^{l+K-1}F(|r_k|)\sin\left(2\pi f(k-l-N)M+M\Delta\theta'+M\epsilon_k\right)}{\frac{1}{K}\sum_{k=l}^{l+K-1}F(|r_k|)\cos\left(2\pi f(k-l-N)M+M\Delta\theta'+M\epsilon_k\right)}\right] \\ &= \Delta\theta'+\frac{1}{M}\arctan\left[\frac{\frac{1}{K}\sum_{k=l}^{l+K-1}F(|r_k|)\sin\left(2\pi f(k-l-N)M+M\epsilon_k\right)}{\frac{1}{K}\sum_{k=l}^{l+K-1}F(|r_k|)\cos\left(2\pi f(k-l-N)M+M\epsilon_k\right)}\right] \\ &= \Delta\theta'+degradtion(f,|r_k|,\varepsilon_k)\end{aligned} \tag{3.8}$$

Finding the variance of the degradation turns out to be equivalent to finding the pdf of the degradation part in the above equation. Define $degradtion(f,|r_k|,\varepsilon_k)=\delta$, where δ is a random variable. Its probability density function $f_\delta(\delta)$ can be derived as in Appendix. From $f_\delta(\delta)$, the mean and variance of the estimates can be obtained.

Since, $E\left[\widehat{\Delta\theta'}\right]=\Delta\theta'+E[\delta]$. Notice from the $f_\delta(\delta)$ that it is a nonlinear symmetric function. Since it is symmetrically distributed about $\delta=0$, $E[\delta]=0$. Consequently, $E\left[\widehat{\Delta\theta'}\right]=\Delta\theta'$. For such an unbiased estimate, we can find its variance as,

$$Var\left[\widehat{\Delta\theta'}\right]=E\left[\left(\widehat{\Delta\theta'}-\Delta\theta'\right)^2\right]=E\left[\delta^2\right] \tag{3.9}$$

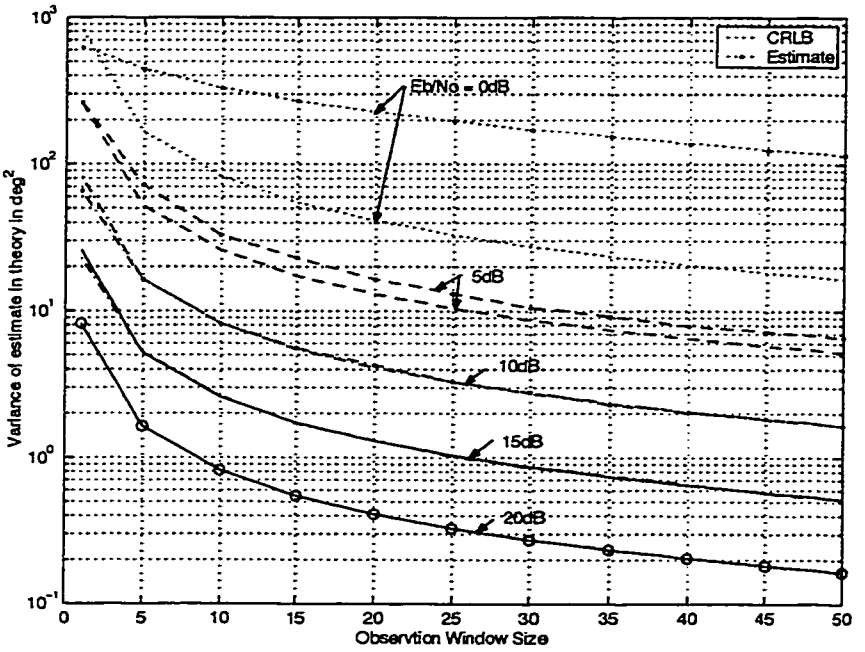

Figure 3.8: Theoretical Variance of NDA-FF Phase Estimator for Zero Frequency Offset

where, $E[\delta^2] = \int_{-\frac{\pi}{M}}^{\frac{\pi}{M}} \delta^2 f_\delta(\delta)\, d\delta$, and it can numerically integrated as in Figure 3.8. The simulation result can also be shown in Figure 3.9. The reason why we use N instead of $K = 2N + 1$ is that we want to emphasize that the estimate is unbiased only for the middle symbols. In the computer simulation, differential encoding technique is used to compensate the phase ambiguity problem. To compare all the phase estimators fairly, we use differential encoding technique for every estimator from now on.

We have already seen the effect of nonlinearity function in Figure 2.3. It is seen that $i = 0$ and $i = 2$ result in almost the same performance, such that $i = 0$ can be implemented in application in order to reduce the implementation complexity.

We can compare the variance performance of NDA-FF phase estimator with DD-FB phase estimator in Figure 3.10. Here, the sliding-window type NDA-FF estimator is used to obtain the unbiased phase estimation for all the points, and to compare with DD-FB algorithm easily. In practice, there is no need to do so and

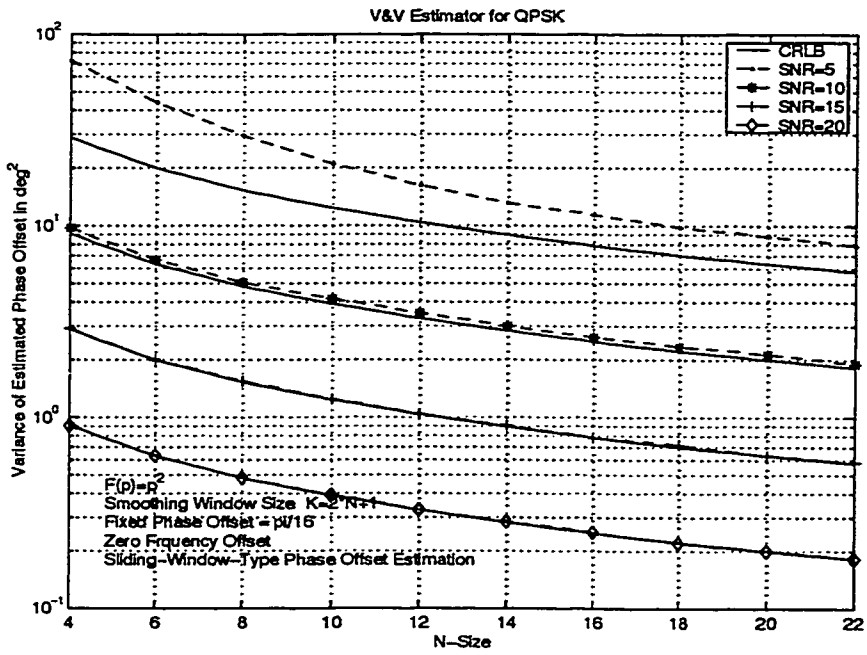

Figure 3.9: Simulation Result of Variance Performance of NDA-FF Phase Estimator for Zero Frequency Offset

one estimate from a block can be used for the whole block. This is called block-estimate in the thesis. The difference between the two estimators in Figure 3.10 can be contributed to two factors:

1. As stated in Chapter 2, NDA algorithm should be worse than data-aided case because of the scanty of the data information.

2. Although they are using the same length of smooth filter, the feedback structure uses the received signals' information recursively. Therefore, the observation window length is far larger than the symbol number used in the smoothing filter.

- Phase ambiguity for phase estimation algorithm

For MPSK, Gray Code is applied. If only Gray Code is used, its modulation can be shown as in Table 3.1. For such encoding scheme, since $s(k;\Delta\theta) = \sqrt{E_s}e^{j(\Delta\theta+\theta_k)}$, if

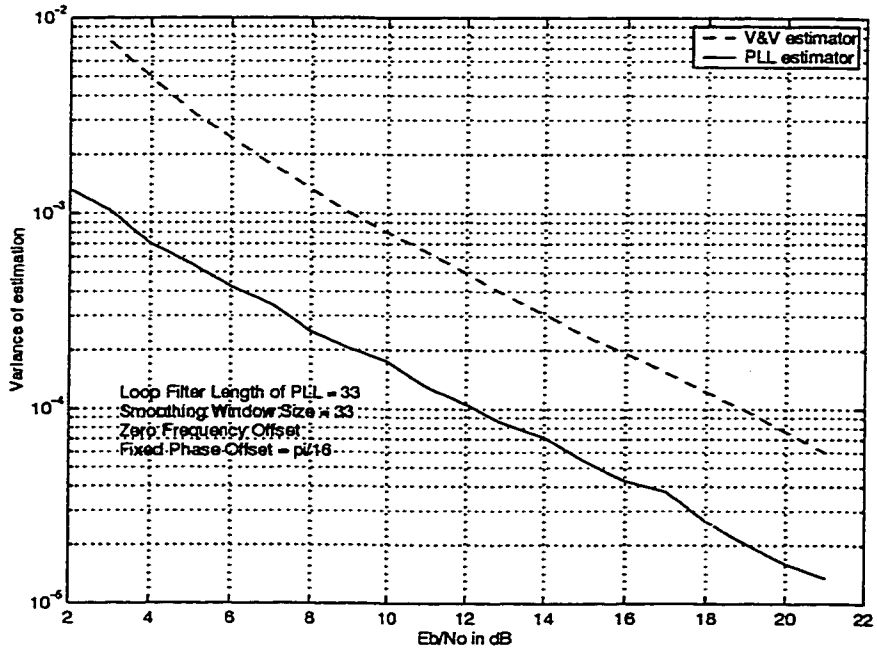

Figure 3.10: Variance Performance with Zero Frequency of NDA-FF and DD-FB Phase Estimator with Same Length Smooth Filter

Input data bits (DB) a_k	Gray coded symbol phase θ_k
00	$\pi/4$ or 0
01	$3\pi/4$ or $\pi/2$
11	$5\pi/4$ or π
10	$7\pi/4$ or $3\pi/2$

Table 3.1: General Gray Coding without Differential Encoding

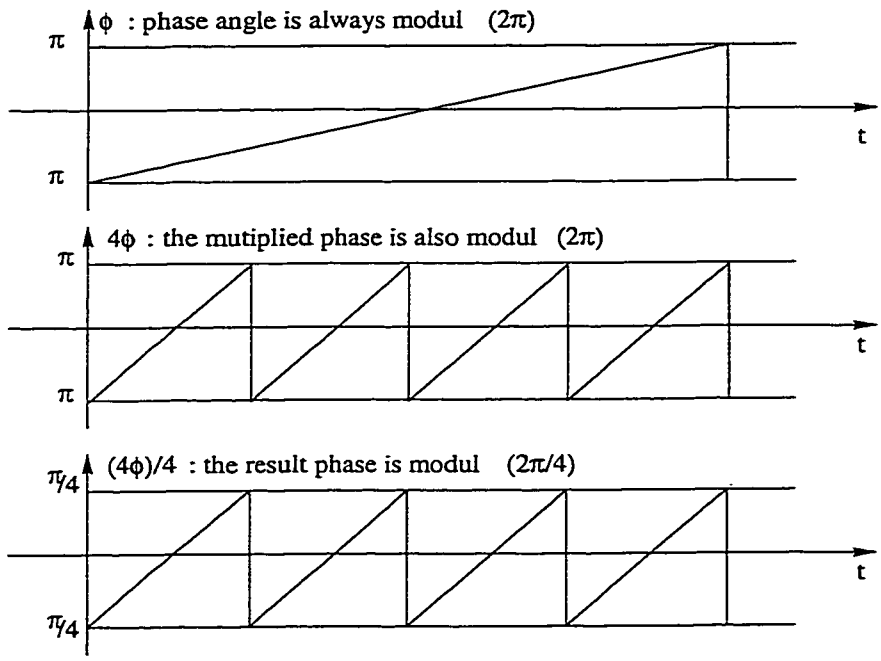

Figure 3.11: Cause of Phase Ambiguity

the estimate of $\Delta\theta$ is wrong, the data phase detection will be definitely wrong, and so does the data bits decoded.

As stated in Chapter 2, for the non-data-aided algorithms, since the modulation is removed by the nonlinear transform, phase ambiguity becomes their common problem. The nonlinear transform in fact multiplies the phase of received symbols by M. The influence of the multiplication process which causes the phase ambiguity can be shown graphically in Figure 3.11, where we use $M = 4$ for QPSK.

This phase ambiguity on phase estimation will then push the data phase detection by $\frac{2\pi m}{M}$ for $m = 0, 1, 2, 3$. Such that wrong decisions are directly made in the decoding procession of Gray Code. The probability of such wrong decision has been derived in detail [16]. According to [2,16], there are, generally, three kinds of method to solve phase ambiguity problem. First, is to use the forward error-correction coding and decoding through use of a transparent code. Second, is unique word preamble. The third is differential encoding method. Since we want to use a whole NDA algorithm, we choose differential encoding technique, and the corresponding decoding

Previous DB	Current DB	Difference of DB	Encoded symbol phase
00/01/11/10	00/01/11/10	00	$\frac{\pi}{4}$ or 0
00/01/11/10	01/11/10/11	01	$\frac{3\pi}{4}$ or $\frac{\pi}{2}$
00/01/11/10	11/10/00/01	11	$\frac{5\pi}{4}$ or π
00/01/11/10	10/11/01/00	10	$\frac{7\pi}{4}$ or $\frac{3\pi}{2}$

Table 3.2: Gray Code with Differential Encoding Technique

technique is used at the receiver end. The procedure of differential encoding is shown in Table 3.2.

By differential encoding, it can be seen that the decoding of data is independent of the phase ambiguity since the $\Delta\theta$ has been deleted by the differential operation when decoding. The drawback of such technique is approximately doubling of the bit error rate, since each symbol demodulation error gives rise to two successive transition errors upon differential decoding.

- Sensitivity to frequency offset

As stated in the frequency offset estimation part in Chapter 2, the frequency offset makes the whole phase offset a rising line instead of straight horizontal line as in zero frequency offset case. For the phase estimator, it is a increasing carrier phase $\vartheta_k = 2\pi\Delta f k + \Delta\theta$ instead of the constant $\Delta\theta$ to be estimated, along with a typical trajectory of the feedforward carrier phase estimate $\widehat{\Delta\theta}$ which is restricted to the interval $\left(-\frac{\pi}{M}, \frac{\pi}{M}\right)$. Cycle slips may occur in the successive blocks of phase estimation: obviously the estimation algorithm cannot handle a carrier frequency offset, as shown in Figure 3.12, where QPSK signaling is applied.

Cycle slipping is a highly nonlinear phenomenon. It particularly destructive to operations in which every cycle counts. Especially, when a cycle slip occurs, it will last for long time until the condition change and make the stable point for the whole circuit changed to another position. It implies that a single cycle will make a series long error, and course a big bit error. An exact theoretical analysis is not possible for many cases, so that one must resort to approximations. Computer

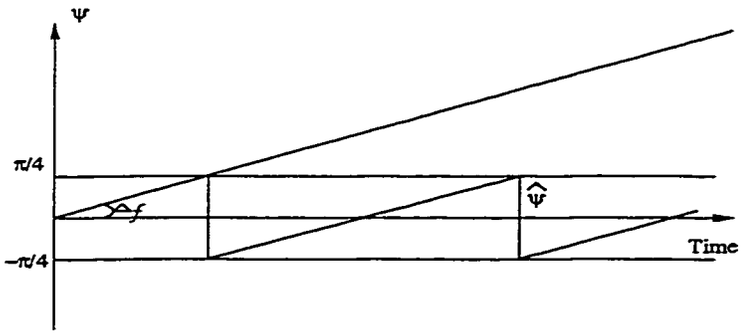

Figure 3.12: Trajectories of Feedforward Carrier Phase Estimate without Unwrapping

simulations provide an alternative to theoretical analysis; however, under normal operating conditions cycle slips should have a probability of occurrence which is at least a few orders of magnitude smaller than the decision error probability for perfect synchronization, which implies that computer simulations of cycle slips are extremely time consuming [7].

For the PLL circuits, many literatures have provided the characteristics of cycle slipping problem. Frequency of cycle slip is a steep function of signal-to-noise ratio [17, 36]. Its expected time to a skipped cycle can also be approximately calculated in theory and by experimental results [35].

Cycle slipping phenomenon is a problem not only for FF phase estimator [30], but also for all estimation schemes using angle measurements. Normally, the feedforward estimates resulting from the successive blocks are to be post-processed in order to obtain estimates that follow the dynamics of the synchronization parameter to be estimated. The task of the post-processing is to unwrap the estimate. For the NDA algorithm, we follow the following procedure: the newly estimated phase offset has to be compared with the previous estimated phase offset, an additional offset of $\pm\frac{\pi}{M}$ must be added whenever the phase difference is outside the range $\pm\frac{\pi}{M}$.

It sounds to be very reasonable, but in fact, it only works when the signal-to-noise ratio is high. When the SNR is low, with noise being too large, very frequently, such an unwrapping scheme can make successively wrong unwrapped estimates if

one estimate is wrong, as shown in Figure 3.13.

Such phenomenon can be shown directly in the simulation as shown in Figure 3.14. In the test, whenever the first cycle slip occurs, we say cycle slip happens in the estimation of that burst. The test repeats for 10^5 times to calculate the occurring rate of cycle slip. It shows that occurring rate for all the bursts is very high when the SNR is low. We also notice that cycle slips happen more frequently when frequency offset increases. [2] has verified that the NDA-FF estimator is in fact affected by the factor ΔfK because of the mixed phase offset $\vartheta_k = 2\pi\Delta fk + \Delta\theta$ changing too much in an estimation block. With this big frequency offset, the slowly varying condition for the phase estimator that what we assumed in Chapter 2 is no more valid. From the theoretical analysis and simulation results, it is shown that if $|\Delta fK| \geq 0.05$, this NDA-FF estimator cannot work even for high SNR. Such a fact is very different from the DD-FB phase estimator, which has a better tracking ability because of its feedback structure and can tolerate lager frequency offsets than the NDA-FF phase estimator. It is reflected on the bit-error rate (BER) clearly, as shown in Figure 3.15 and Figure 3.16.

- Bit-Error (BER) performance

For coherent detection for differentially encoded MPSK, [5] gives the complete derivation for the BER performance. The bit error probability for QPSK is,

$$P_E(M=4) = erfc\sqrt{\frac{E_b}{N_o}} - erfc^2\sqrt{\frac{E_b}{N_o}} + \frac{1}{2}erfc^3\sqrt{\frac{E_b}{N_o}} - \frac{1}{8}erfc^4\sqrt{\frac{E_b}{N_o}} \qquad (3.10)$$

which we call "Lower bound" in the simulation result figures later on.

The difference of the BER performance for the two estimators is due to the feedback and feedforward topology. For DD-FB phase estimator with nonzero frequency offset, at low SNR, the noise is the most important interference. Thus, the difference between the two curves in Figure 3.16 is very small. Meanwhile, at high SNR, when noise is very weak, frequency offset is the main cause of degradation,

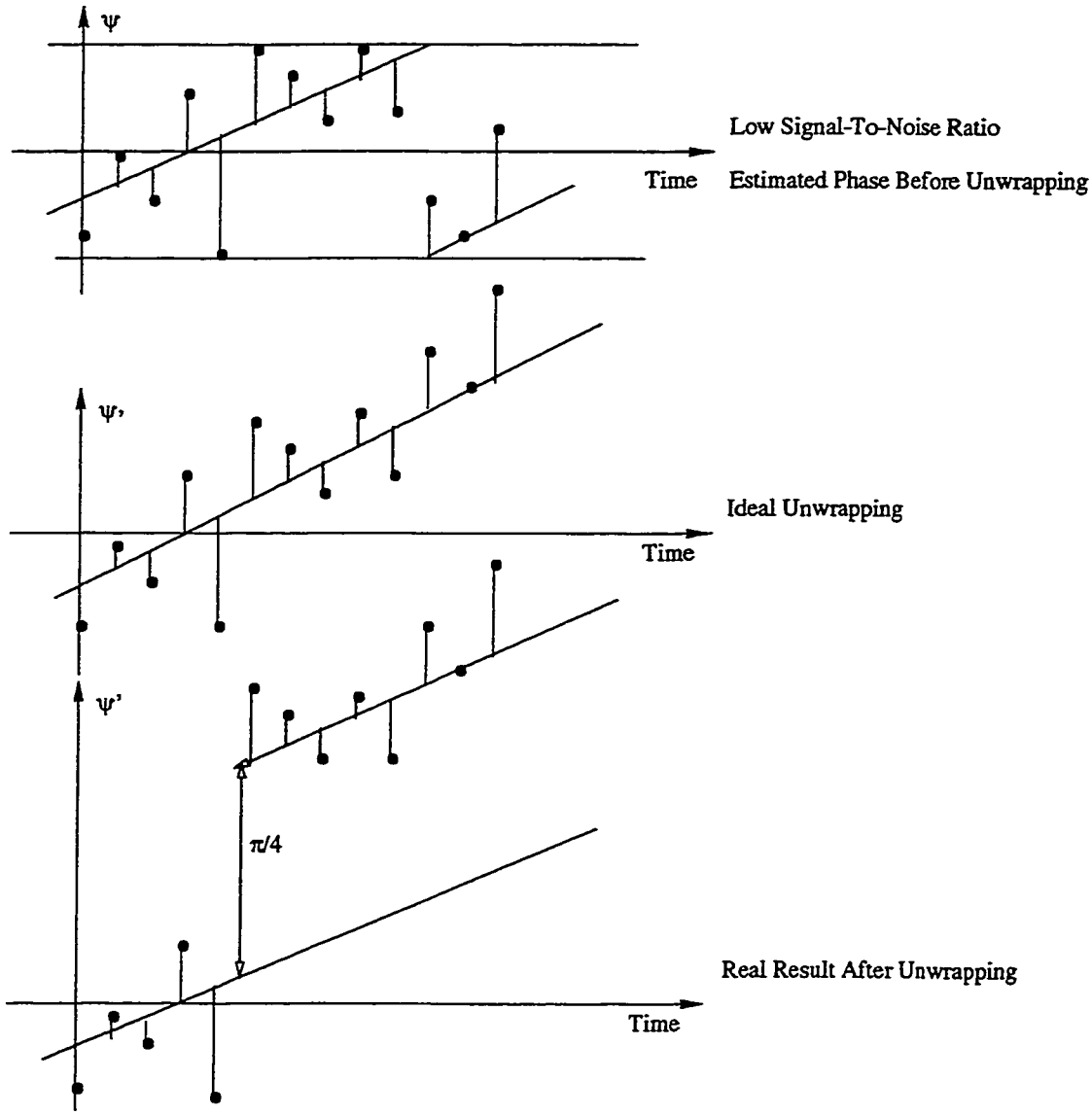

Figure 3.13: Function of Unwrapping Process

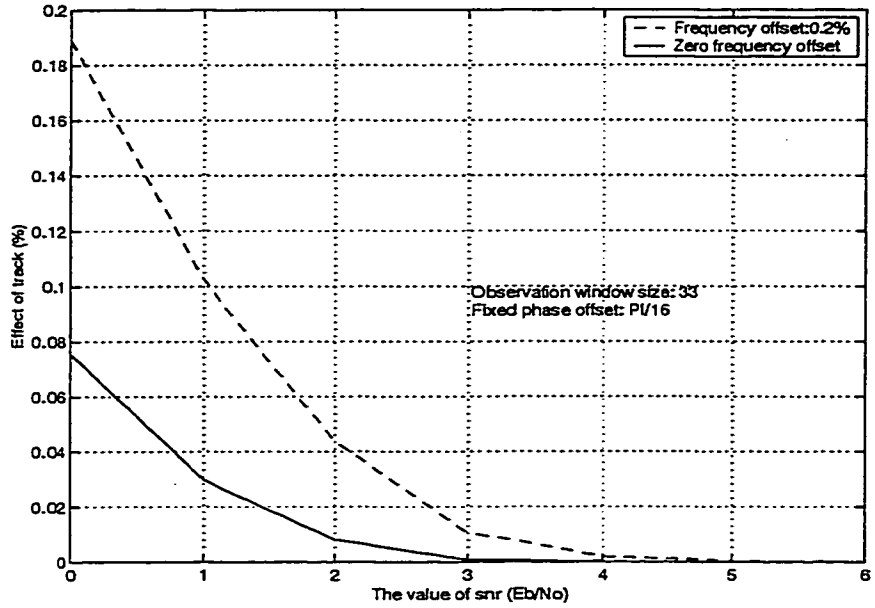

Figure 3.14: Tracking Effect of NDA-FF Phase Estimator for Different Frequency Offset

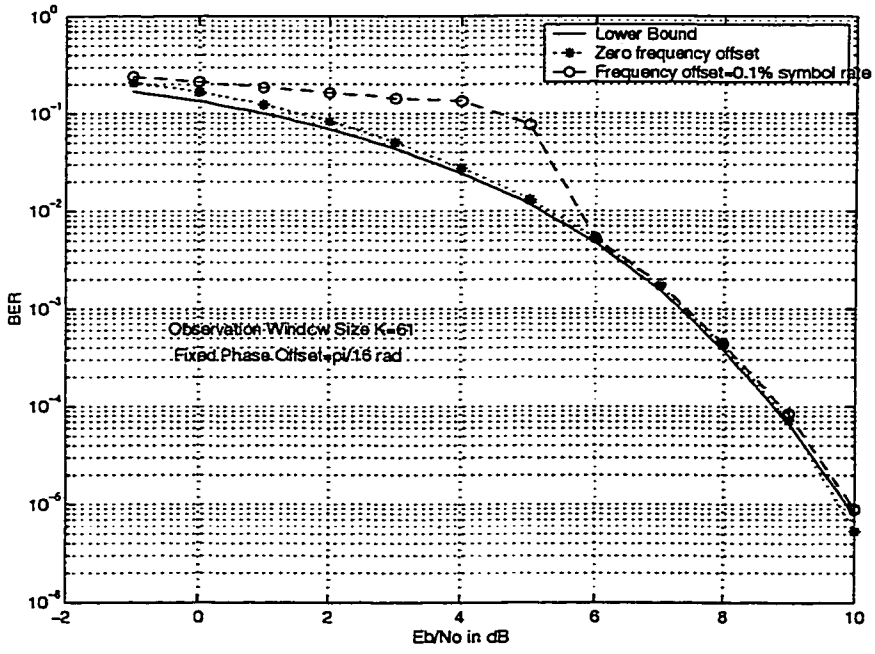

Figure 3.15: BER Performance of NDA-FF Phase Estimator

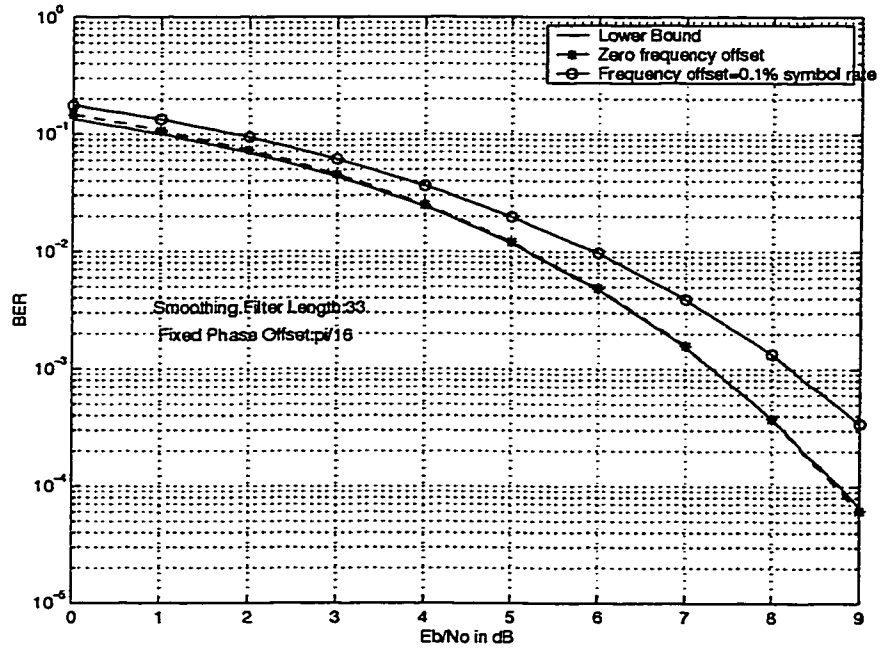

Figure 3.16: BER Performance of DD-FB Phase Estimator

which makes the difference between the two curves larger. On the other hand, for NDA-FF phase estimator, the feedforward structure is always calculating the phase estimate value, instead of trying to catch the slope as the feedback structure does. Therefore, with small frequency offset, the BER performance of the FF is better with high SNR. However, such advantage will diminish when the frequency offset is larger than what the FF structure can tolerate because of the effect of cycle slipping.

3.1.1.3 Summary

From the above analysis of the NDA-FF phase estimator. We can draw the following conclusion:

- the FF structure gives no acquisition problem, which permits the NDA-FF phase estimator perform fast and efficiently at both continuous-mode and burst-mode condition, and gives performance comparable to linear estimators
- the NDA-FF phase estimator is not only fast, but also simple, as shown in

	Register	Real Multi.	LU (or CORDIC)
DD-FB	$2K+2$	10	3
NDA-FF (Sliding-window)	$2K+4$	4	3
NDA-FF(Block-estimation)	4	4	3

Table 3.3: Complexity Comparison for NDA-FF and DD-FB Phase Estimator

Table 3.3 of the complexity comparison for their main functions, where the same size of registers, same precision of real multiplication(Multi.) and lookup table (LU) for both estimators are assumed

- despite all the above advantages of the NDA-FF algorithm, it has phase ambiguity problem, and thus, requires the addition of processing techniques; it is also very sensitive to frequency offset, which implies that some other processing must be done to restrict the frequency offset into a very small range

3.1.2 Frequency Offset Estimator

According to the current literatures, most of the phase estimators perform under certain restriction of frequency offset. Since frequency offset is unavoidable in the telecommunication system, considerable research has been done in the area of frequency offset estimation. [8] has proposed a estimation scheme that estimates the parameters of a single-frequency complex tone from a finite number of noisy discrete-time observation. Its frequency offset estimation has been compared with that of many other frequency estimators [20] and been proved to have the best performance in terms of minimum operating SNR-threshold. In this section, we modify this algorithm to make it suitable for the estimation of MPSK type format.

3.1.2.1 Presentation of the Technique

As derived in Chapter 2, it is known that the spectrum analysis provides a way to determine frequency offset. Rewrite (2.22) to study it closely,

$$\widehat{\Delta f} = \frac{1}{M} \arg \max_{\widetilde{M\Delta f}} |F(M\Delta f)|$$

Our goal is not only to estimate Δf in the absence of any information on the received phase-modulated symbols, which is NDA-FF, but also decrease the complexity for Fast Fourier Transform (FFT) calculation. To this end, four-step procedure are followed and is shown in Figure 3.17:

1. Passing the demodulated samples through the non-linear device,

$$r_k^{'} = F\left(|r_k|\right) e^{jM(2\pi\Delta fk+\Delta\theta+\theta_k)} = F\left(|r_k|\right) e^{jM(2\pi\Delta fk+\Delta\theta)} \tag{3.11}$$

   where, $F\left(|r_k|\right)$ is the stimulated suggestion from the NDA phase estimator to optimize the variance.

2. Passing $r_k^{'}$ through a D-step decimation filter (with Hamming window inside to restrict the frequency band in order to avoid aliasing [32]) to obtain fewer points t_k to use in the FFT calculation.

3. Comparing the amplitude in frequency domain for each decimated point to obtain a coarse frequency offset estimate

$$\widehat{\Delta f} = \frac{1}{MD} \arg \max_{\widetilde{MD\Delta f}} |F(MD\Delta f)| \tag{3.12}$$

4. Using a maximum search scheme around the coarse frequency offset value to obtain a accurate frequency offset estimate.

The fine search can be done by many methods, such as the interpolating procession and secant method [34].

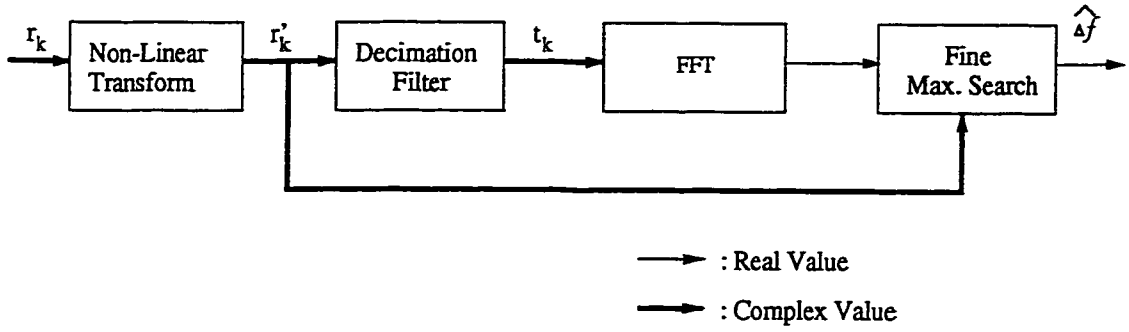

Figure 3.17: Block Diagram of Modified NDA-FF Frequency Estimator

This algorithm uses an estimation period equal to the burst length, and estimates the frequency offset for the whole burst. It requires estimating the carrier frequency offset from the complex data stream prior to phase correction and symbol detection, and the data has to be delayed by a burst length to find the estimation.

3.1.2.2 Analysis of Techniques

Frequency estimators have special characteristic, such as the threshold, outlier. In this section, the property of NDA-FF frequency estimator will be analyzed. Provided an unlimited resolution of the spectrum analyzer in the above structure, its performance should not be measured in terms of an the variance or estimation bias alone. An additional performance measure for a maximum seeking algorithm is whether or not and how often the estimation error exceeds a given threshold.

- Moment analysis

The non-linear transform gives the result as,

$$r'_k = F\left(|r_k|\right) e^{jM(2\pi\Delta fk+\Delta\theta+\theta_k)} + n'_k = F\left(|r_k|\right) e^{jM(2\pi\Delta fk+\Delta\theta)} + n'_k \qquad (3.13)$$

To analyze the frequency offset, we use $\Delta f'$ to stand for the modulation-removed frequency offset $M\Delta f$ (since decimation is used to decrease the complexity of the algorithm - it is optional in the application, we do not consider the D-factor in the

moment analysis). Use the polar form,

$$r_k' = F\left(|r_k|\right) e^{j\left(2\pi\Delta f' k + M\Delta\theta\right)} + v_k e^{j\varepsilon_k'} \tag{3.14}$$

where, we let $\{\varepsilon_k'\}$ be a set of independent random variable uniformly distributed over $[-\pi, \pi)$.

Thus,

$$F(f') = \frac{1}{K} e^{j(M\Delta\theta)} \sum_k \left[F\left(|r_k|\right) e^{-j2\pi k\beta} + v_k e^{-j(2\pi k\beta - \gamma_k)}\right] \tag{3.15}$$

where, $\beta = \left(f' - \Delta f'\right)$ and $\gamma_k = \varepsilon_k' - \Delta\theta - 2\pi\Delta f' k$. Since the ε_k's are independently, uniformly distributed, in effect so are γ_ks.

From the above formula, it is seen that $\left|F(f')\right|$ is not a function of the phase offset $M\Delta\theta$, which can also be observed in the simulation, such that the frequency estimation is independent of any given phase offset value. Thus, without loss of generality, let $\widehat{\beta}$ be the value of β in the range of $\left[-\frac{1}{2}, \frac{1}{2}\right)$ that maximize $\left|F\left(f'\right)\right|$. The ML estimate $\widehat{\Delta f'}$ will then be obtained:

$$\widehat{\Delta f'} = \Delta f' + p_f \widehat{\beta} \quad mod\, p_f \tag{3.16}$$

where, $p_f = 1$ is the period of $\Delta f'$. Observe that $\left|F(f')\right|$ is an even function of the pair (β, γ). The statistics of $-\gamma$ is the same as γ. Thus the statistics of $-\widehat{\beta}$ must be the same as that of $\widehat{\beta}$. Hence, $E\left\{\widehat{\beta}\right\} = 0$. Therefore, when SNR is high enough,

$$E\left\{\widehat{\Delta f'}\right\} = \Delta f' \tag{3.17}$$

However, when SNR is low, $\widehat{\Delta f'}$ may depart from $\Delta f'$ very far away and cause "bias" problem when evaluating its expect $E\left\{\widehat{\Delta f'}\right\}$, which we will discuss later on.

The variance performance above the SNR where large error may happen can approach the CRLB as closed as desired by increasing the number of search step. It means,

$$Var\left[\widehat{\Delta f'}\right] = CRLB \tag{3.18}$$

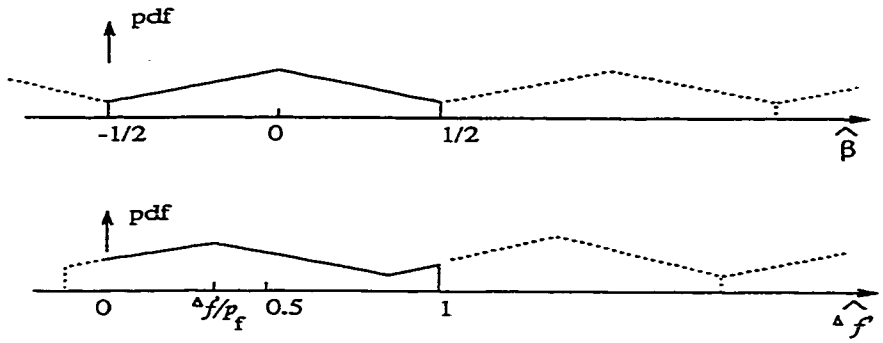

Figure 3.18: Relationship of pdf of $\widehat{\beta}$ and pdf of $\widehat{\Delta f'}$

However, with the estimator working under the SNR which large error may happen, the variance of the estimation is definitely very large because of the biased estimation.

- Threshold and outliers

At low SNR, there is usually a range of SNR where the mean-squared error (MSE) rises very rapidly as SNR decreases. The SNR at which this effect is first apparent is called the threshold. It is necessary for the estimator to work above this threshold so that no outliers, whose frequency offset estimation value is very far away form the real frequency offset estimation value, occurs.

If the estimator works below the threshold, outliers occur, and the outcome of the estimation is biased. It is because we choose $\widehat{\Delta f'}$ according to $\widehat{\beta}$, such that their pdf are related to each other, as illustrated in Figure 3.18.

This relative-ship creates the "bias" problem. The pdf of $\widehat{\beta}$ is even about zero itself. However, because of the shift of $\Delta f'$, the $\widehat{\Delta f'}$ is even about $\Delta f'$ except for the part from $2\Delta f'$ to p_f when $\Delta f' < \frac{p_f}{2}$ (or for the part from zero to $2\Delta f' - p_f$ when $\Delta f' > \frac{p_f}{2}$). Consider the situation when $\Delta f' < \frac{p_f}{2}$. If $Pr\left[2\Delta f' < \widehat{\Delta f'} < p_f\right]$ is small, which is the situation when the SNR is large enough, then the estimate is unbiased. If $Pr\left[2\Delta f' < \widehat{\Delta f'} < p_f\right]$ is significant then the estimate is biased in the direction of $\frac{p_f}{2}$. If $\Delta f' > \frac{p_f}{2}$, the preceding explanation reply with the corresponding modification according to Figure 3.18. That is, as outliers occur, the estimate can

$\Delta f'$	$E\left[\widehat{\Delta f'} - \Delta f\right]$
0	$\frac{p_f}{2}$
$\frac{p_f}{2}$	0
p_f	$-\frac{p_f}{2}$

Table 3.4: Frequency Estimate Value in Low SNR

easily have values in the following directions shown in Table 3.4, which gives the character value with $\Delta f' = 0, \frac{p_f}{2}, p_f$. Clearly, we expect to make large frequency estimation errors if $\Delta f'$ is closed to zero or p_f.

This phenomenon of this "bias" problem can be observed in the computer simulation, as shown in Figure 3.19 and Figure 3.20, where we did the simulation of estimation for 2×10^5 times. If the SNR is high enough for the frequency estimator to do estimation as in Figure 3.20, i.e., if the estimator operates above the threshold of the estimator, all the estimations are around the real frequency offset value, such as $\frac{1}{110}$ symbol rate in the figure, and its expect is unbias; however, if the SNR is too low as in Figure 3.19, i.e., if the estimator operates below the threshold, the large departure of outliers, such as the two outliers -10^{-3} symbol rate and -5×10^{-4} symbol rate in the figure, always go to the same direction and the expect of the outcome is bias.

Fortunately, the threshold has already been very low from our simulation results. Our operation later on, such as phase estimation, should be normally higher than that. Therefore, we care less about the frequency estimation below the threshold.

- Estimation range and precision

$|F(f')|$ is a periodic function of normalized frequency with period 1. Thus, its maximum lies in the interval $\pm\frac{1}{2}$. After the nonlinear transform and decimate process,

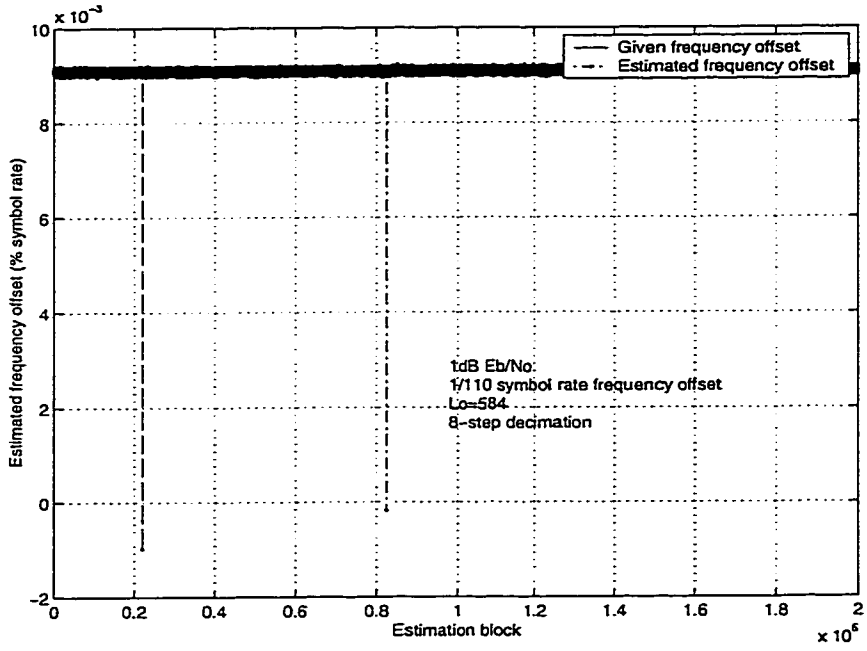

Figure 3.19: Threshold Effect of NDA-FF Frequency Estimator at 1dB Out of 2×10^5-Burst Runs

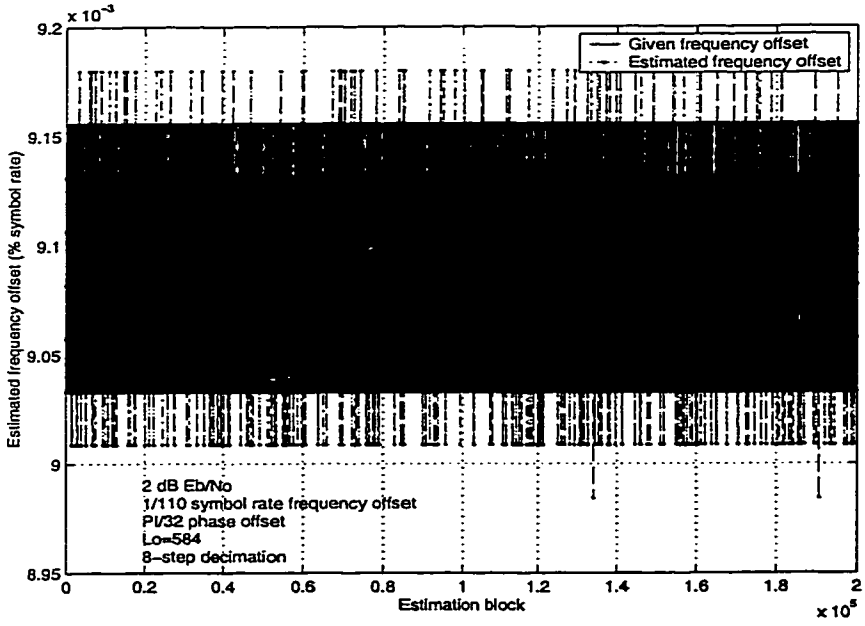

Figure 3.20: Threshold Effect of NDA-FF Frequency Estimator at 2dB Out of 2×10^5-Burst Runs

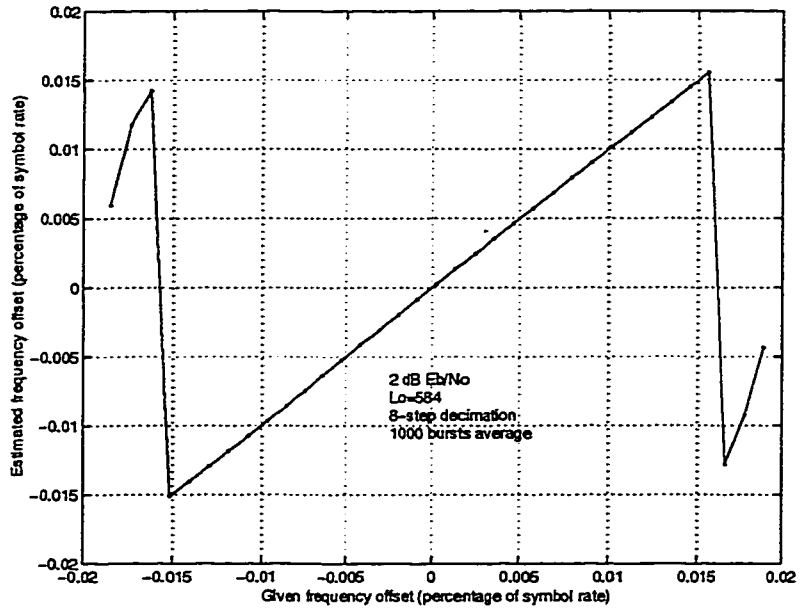

Figure 3.21: Linearity Characteristics of NDA-FF Frequency Estimator

the estimation range reduce to,

$$\begin{aligned} M|D\Delta f| &< \tfrac{1}{2} \\ |\Delta f| &< \tfrac{1}{2MD} \end{aligned} \tag{3.19}$$

For example, in our simulation for QPSK signaling and for 8-step decimation, the estimation range reduces to $(-\frac{1}{64}, \frac{1}{64})$, as shown in Figure 3.21.

As we can see, the estimation range has been greatly reduced. Therefore, in Chapter 5, we do effort to increase the estimation range while trying to keep the same estimation precision.

The precision of this estimator is very high depending on the precision of the maximum search scheme. With the scheme used in this thesis, after coarse search from 128-FFT, we divide each $\frac{1}{128}$ into 15 sections to do fine search. Therefore, the precision can reach $\frac{1}{1920}$. In the mean time, with such a 2-step search scheme, the complexity of maximum search is dramatically reduced. Its complexity is discussed in [20], where it has been throughly compared with all other present FF frequency estimators.

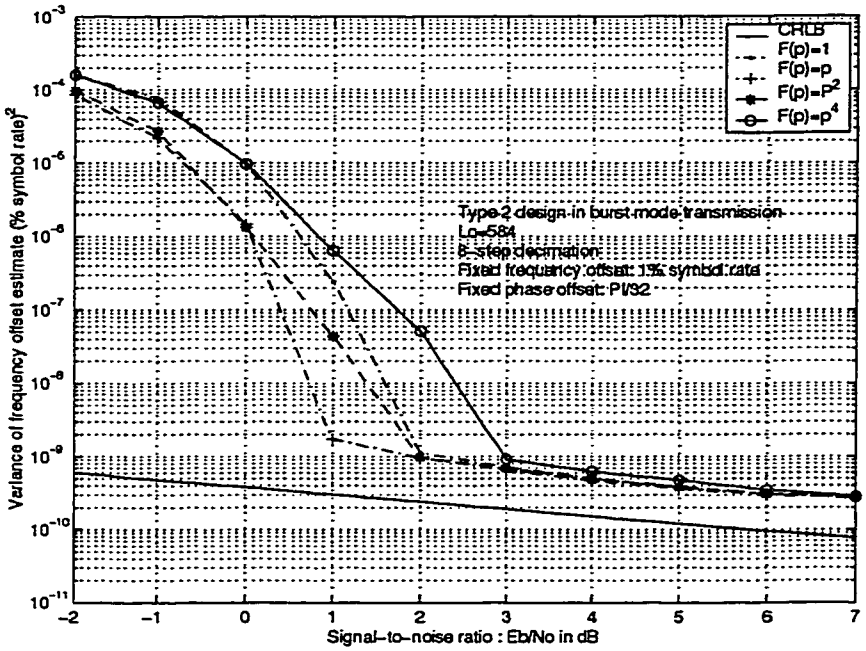

Figure 3.22: Effect of Non-Linear Factor on Frequency Estimator

- Other considerations

We have used $F(|r_k|)$ function in the processing of the received signal. In the simulation, we have tried to use

$$F(|r_k|) = (|r_k|)^i \quad where,\ i = 0, 1, 2, 4 \tag{3.20}$$

The effect of this factor can be shown in Figure 3.22, and Figure 3.23. With proper choice of the non-linearity, the threshold can be obtained with the possible lowest value. Studying Figure 3.22 more closely shows that for QPSK, $i = 1$ has the lowest variance, and the threshold is just 1.2dB. The reason for better performance of $i = 1$ is that it limits the noise most effectively and causes no loss of the received symbol information. On the other hand, $i = 0$ causes too much loss of information, and $i = 2$ and $i = 4$ enhance the noise effect too much. However, $i = 1$ will causes more implementation complexity than $i = 0$ and $i = 2$.

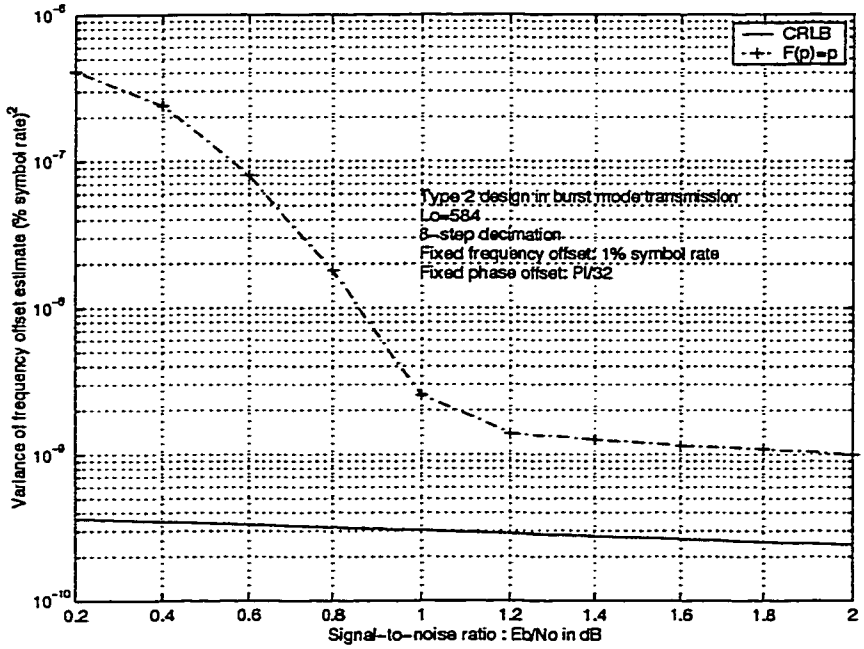

Figure 3.23: Close Look of Threshold with Properly Chosen Non-Linear Factor

Of course, we can also use as much as information in the FFT computation, where we can use fewer step-decimation than 8 as what we used in the above algorithm, or do not use decimation filter at all. In the meanwhile, the high frequency filter should also be used corresponding to the number of step in the decimation operation. It should be noticed that the complexity of the whole estimator will be also increased because of the larger number of FFT points operation.

3.1.2.3 Summary

From the analysis of last section, we draw the following conclusions about this NDA-FF frequency estimator:

- The FF structure is efficient and is very suitable for burst-mode transmission.
- The FFT analysis method gives the most accurate estimation with the lowest threshold compared with all other available FF frequency estimators.

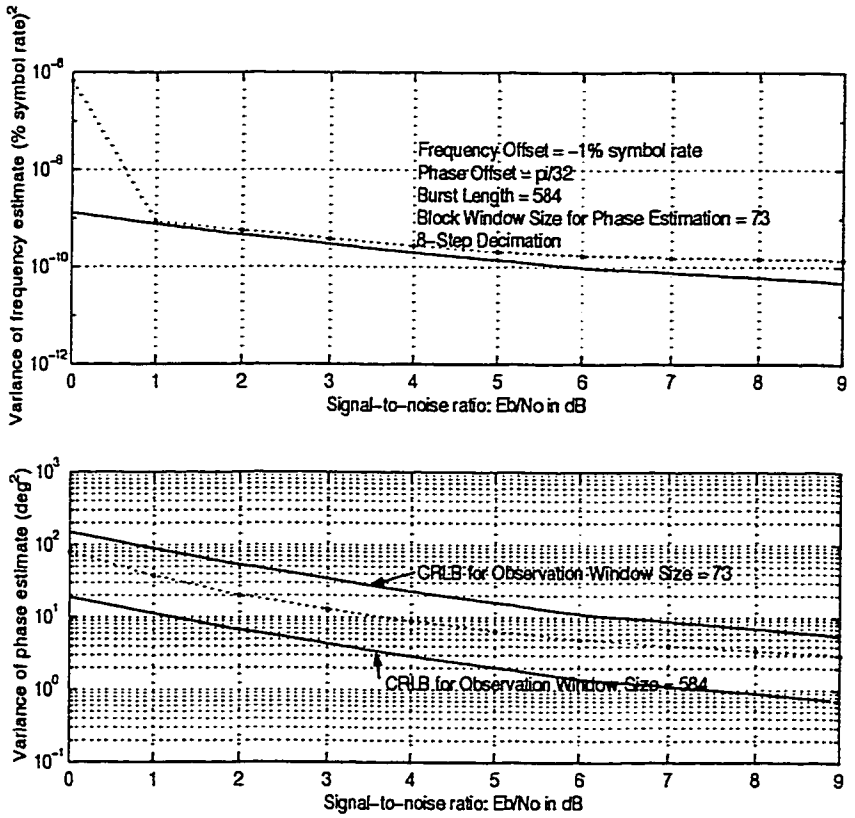

Figure 3.24: Variance Performance of the NDA-FF Carrier Synchronizer

- The drawback of it is its high complexity and long delay to get the estimate, but along with the highly advanced digital signal processing techniques and hardware, it can all be compensated.

3.2 Simulation Results

The simulation results for variance performance and bit error performance are presented in Figure 3.24 and Figure 3.25 to illustrate how the combined estimator performs.

We observe that the phase estimation variance performance is between the CRLB with observation window size of $K = 73$ and $K = 584$. It is because the simulation is done by a sequential scheme, where the whole burst symbol information

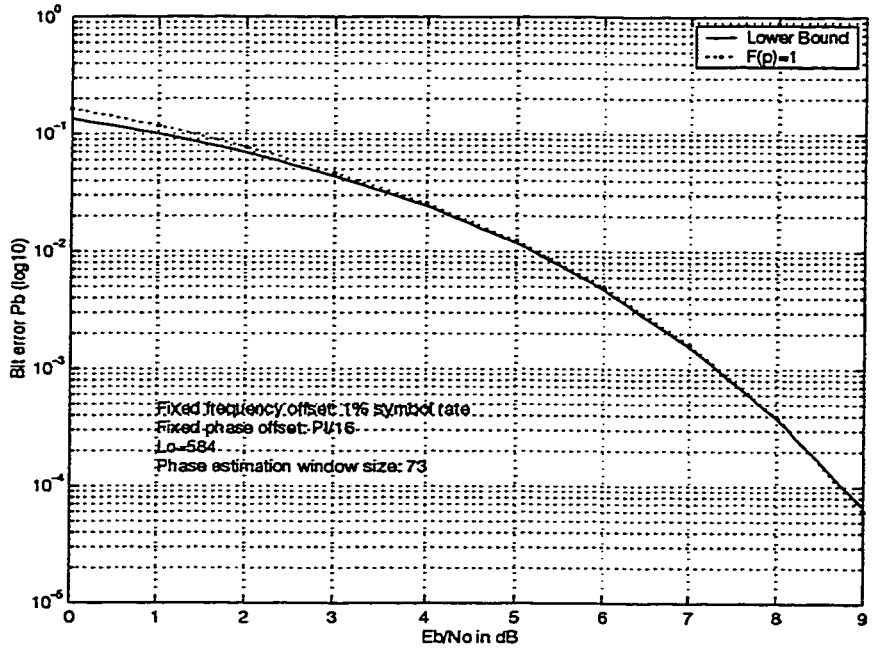

Figure 3.25: BER Performance of NDA-FF Carrier Synchronizer

is used to estimate the frequency offset at first, and then the whole burst is divided into 8 blocks and the phase offset is estimated for each block. Furthermore, in the variance performance figure, the CRLB for the low SNR is used. Otherwise, the CRLB of $K = 73$ and the estimation curve will cross.

The theoretical lower bound for BER performance is from equation (3.10).

3.3 Summary

As expected, it is shown from the performance figures that:

- With the two high-performance NDA-FF frequency estimator and NDA-FF phase estimator, the final NDA-FF estimator can work efficiently.
- With frequency offset being reduced to an extremely small value by the frequency estimator, the phase estimator can work as good as zero frequency offset case, such that the whole synchronizer can work accurately.

Chapter 4

Data-Aided Feedback Estimation Technique

In the last chapter, we propose a full non-data-aided carrier synchronizer with feed-forward topology. For either the NDA-FF phase estimator or NDA-FF frequency estimator part, there must be a certain kind of delay applied to obtain the estimation for the block, which is supposed to lower down the estimation speed and increase the system complexity. Although we prefer to have the highest transmission efficiency that non-data-aided algorithms can provide, their above disadvantages are the drawbacks for their use in certain applications. Therefore, we also want to analyze some other estimation principles as discussed in Chapter 2, which are also commonly used in practice because of their special features which are suitable for certain applications.

In this chapter, we analyze a joint phase/frequency estimation scheme, which is supposed to be fast and have a simple structure. It is data-aided estimator with feedback topology: it uses a preamble to draw the estimation into the estimated range quickly, and use decision-directed symbol information to help to further refine the estimation.

In practice, it is usual that a known preamble is inserted at the beginning of a

frame to aid the receiver in acquiring the carrier. The throughput and power penalty incurred by the preamble insertion can often be justified by an overall improvement in system performance and robustness.

4.1 Presentation of Technique

The derivation of the algorithm follows the procedure discussed in the joint phase/frequency estimate part in Chapter 2. We rewrite (2.28) here to derive it in depth,

$$\begin{array}{rcl} \sum_{k=0}^{K-1} c_k \sin(\varphi_k - 2\pi\widehat{\Delta f}k - \widehat{\Delta\theta}) & = & 0 \\ \sum_{k=0}^{K-1} kc_k \sin(\varphi_k - 2\pi\widehat{\Delta f}k - \widehat{\Delta\theta}) & = & 0 \end{array} \tag{4.1}$$

Instead of the simple linearized method as in (2.29), where we obtain the estimation at $(K-1)\,th$ sample, we use the full expression of the Taylor series and factor out the term $(\varphi_k - 2\pi\widehat{\Delta f}k - \widehat{\Delta\theta})$,

$$\begin{array}{rcl} \sum_{k=0}^{K-1} c_k(\varphi_k - 2\pi\widehat{\Delta f}k - \widehat{\Delta\theta})\left[1 - \frac{1}{3!}(\varphi_k - 2\pi\widehat{\Delta f}k - \widehat{\Delta\theta})^2 + \ldots\right] & = & 0 \\ \sum_{k=0}^{K-1} kc_k(\varphi_k - 2\pi\widehat{\Delta f}k - \widehat{\Delta\theta})\left[1 - \frac{1}{3!}(\varphi_k - 2\pi\widehat{\Delta f}k - \widehat{\Delta\theta})^2 + \ldots\right] & = & 0 \end{array} \tag{4.2}$$

Since the actual values of phase and frequency offset are unknown, a good approximation of (4.2) is to use the most up-to-date phase and frequency estimate $\Delta\theta_{K-1|K-1}$ and $\Delta f_{K-1|K-1}$, to compute the weights

$$\bar{c}_{k|K-1} = \{\bar{c}_k\}_{k=0}^{K} \; where, \; k \in [0, K]$$

here, we define $\bar{c}_{k|K-1}$, named that the weight at $k\,th$ sample is computed using the previous $0\,to\,(K-1)\,s'$ estimation of frequency offset and phase offset, as

$$\begin{array}{rcl} \bar{c}_{k|K-1} & = & c_k\left[1 - \frac{1}{3!}(\varphi_k - 2\pi\widehat{\Delta f}k - \widehat{\Delta\theta})^2 + \ldots\right] \\ & = & c_k sinc\left(\frac{\varphi_k - 2\pi k\Delta f_{K-1|K-1} - \Delta\theta_{K-1|K-1}}{\pi}\right) \end{array} \tag{4.3}$$

They are then used to estimate phase and frequency offset at the Kth sample.

The estimation is similar to (2.30) except the weights c_k are replaced by $\bar{c}_{k|K-1}$,

$$\begin{aligned} 2\pi\widehat{\Delta f}_{K|K-1} &= \frac{\sum_{k=0}^{K} k\bar{c}_{k|K-1}\varphi_k \sum_{k=0}^{K} \bar{c}_{k|K-1} - \sum_{k=0}^{K} k\bar{c}_{k|K-1} \sum_{k=0}^{K} \bar{c}_{k|K-1}\varphi_k}{\sum_{k=0}^{K} k^2\bar{c}_{k|K-1} \sum_{k=0}^{K} \bar{c}_{k|K-1} - \left(\sum_{k=0}^{K} k\bar{c}_{k|K-1}\right)^2} \\ \widehat{\Delta\theta}_{K|K-1} &= \frac{\sum_{k=0}^{K} \bar{c}_{k|K-1}\varphi_k \sum_{k=0}^{K} k^2\bar{c}_{k|K-1} - \sum_{k=0}^{K} k\bar{c}_{k|K-1}\varphi_k \sum_{k=0}^{K} k\bar{c}_{k|K-1}}{\sum_{k=0}^{K} k^2\bar{c}_{k|K-1} \sum_{k=0}^{K} \bar{c}_{k|K-1} - \left(\sum_{k=0}^{K} k\bar{c}_{k|K-1}\right)^2} \end{aligned} \tag{4.4}$$

This approximation is valid if the error, after appropriate phase unwrapping, is confined to within $\pm\pi$ to ensure $\bar{c}_{k|K-1}$ are nonnegative. This condition is intuitively satisfying because according to the feature of *sinc* function, signals with small amplitudes or large prediction errors, or both, will be weighted less, which lead to better performance.

According to [31], large phase error in the received symbol can seriously degrade the performance of the frequency estimation. In the formula derived above, the *sinc* function is used to reduce the influence of peak error in the received signal, since the *sinc* function is able to make the large error weighted less. To obtain good performance, we try to restrict the range of error to a certain value so that extremely large errors can be deleted. The function is realized by a peak-error detector. From the simulation results, we will verify whether *sinc* function and the peak-error detector are effective.

As analysis in the NDA-FF phase estimator, all estimation schemes using angle measurements with non-frequency offset, phase unwrapping is necessary to remove $\pm 2\pi$ phase jumps, which is difficult at low SNR. As for any unwrapping scheme, the current measurement has to compare certain previous value - for example the previous angle measurements in the unwrapping scheme for NDA-FF scheme described in Chapter 3. We believe that the approximated correct estimation of phase offset $\widehat{\Delta\theta}$ and frequency offset $\widehat{\Delta f}$ from the preamble are better than the measurements themselves. Therefore, we make the measurement compared with the updated estimation

$$\varphi_{k+1|k} = 2\pi\widehat{\Delta f}_{k|k}(k+1) + \widehat{\Delta\theta}_{k|k} \tag{4.5}$$

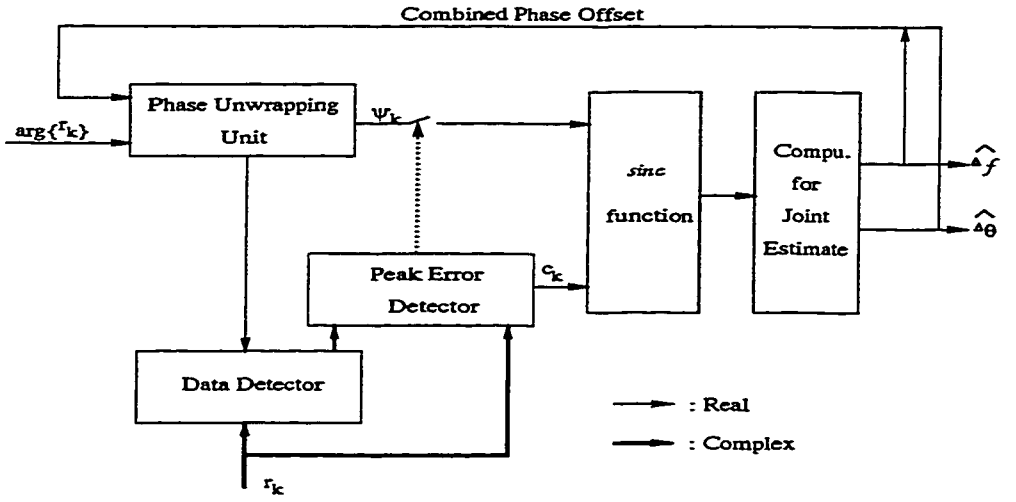

Figure 4.1: Block Diagram for DA-FB Joint Synchronizer

Taking consideration of all the features discussed above, according to (4.4), we can obtain a turbo-type joint phase/frequency estimation algorithm as shown in Figure 4.1.

The estimation is implemented as follows:

1. Use the preamble measurements on preamble of length K_P to compute the frequency offset for the initial unwrapping. The initial frequency offset estimation follows the phase increment estimation method (2.18) described as in Chapter 2,

$$2\pi\widehat{\Delta f} = \frac{1}{K-1}\sum_{k=1}^{K-1}\arg\left\{r_k r_{k-1}^*\right\}$$

Since the phase jumps can occur, there are $(K_P - 1)$ possible frequency estimate $\widehat{\Delta f_i}$, which are

$$2\pi\widehat{\Delta f}_i = \frac{1}{K_P-1}\left(\sum_{k=1}^{K_P-1}\arg\left\{r(k)r^*(k-1)\right\} + 2\pi i\right) \tag{4.6}$$

with $i = 0, 1, \cdots, K_P - 1$, or let it ranges from both sides of the middle point, which is $i = -\frac{K_P}{2}, \cdots, \frac{K_P}{2}$. These $\widehat{\Delta f_i}$s are used for phase unwrapping the K_P

measurement. For each set of measurement, (2.30) described in Chapter 2,

$$2\pi\widehat{\Delta f} = \frac{\sum_{k=0}^{K-1} kc_k\varphi_k \sum_{k=0}^{K-1} c_k - \sum_{k=0}^{K-1} kc_k \sum_{k=0}^{K-1} c_k\varphi_k}{\sum_{k=0}^{K-1} k^2c_k \sum_{k=0}^{K-1} c_k - \left(\sum_{k=0}^{K-1} kc_k\right)^2}$$

$$\widehat{\Delta\theta} = \frac{\sum_{k=0}^{K-1} c_k\varphi_k \sum_{k=0}^{K-1} k^2c_k - \sum_{k=0}^{K-1} kc_k\varphi_k \sum_{k=0}^{K-1} kc_k}{\sum_{k=0}^{K-1} k^2c_k \sum_{k=0}^{K-1} c_k - \left(\sum_{k=0}^{K-1} kc_k\right)^2}$$

is performed to compute the joint estimation results. These results are substituted into (2.27) to select the maximum likelihood pair, which is chosen as the initial unwrapping estimated $\widehat{\Delta f}$ and $\widehat{\Delta\theta}$ to do the further estimation.

2. Phase unwrap the next new measurement with the most up-to-date estimate of $\widehat{\Delta f}$ and $\widehat{\Delta\theta}$.

3. Detect the data phase from the unwrapped phase, make decision, and calculate the distance between the received symbol and the constellation point. Here, the peak error with large departure from the constellation point will be deleted and will not be counted into the computation of the new estimation.

4. Use (4.4) to compute the new estimated $\widehat{\Delta f}$ and $\widehat{\Delta\theta}$.

5. Repeat step 2 to 4 until the end of a burst.

4.2 Analysis of Technique

We have added the peak-error detector and *sinc* function in the estimator. From the simulation result shown in Figure 4.2, we cannot see significant improvement with either of them although there are a few difference in the simulation curves. However, if we observe the simulation curves closely, we find for different ranges of signal-to-noise ratio, the estimator with the added function performs differently.

It is obviously that the algorithm described in (4.4) is not as simple as what is in (2.30). Such as for the Kth estimation of frequency offset and phase offset, in (2.30), it is just a forward computation: the weight c_k is an additional computation with new measurement, where each new additional measurement is only used to

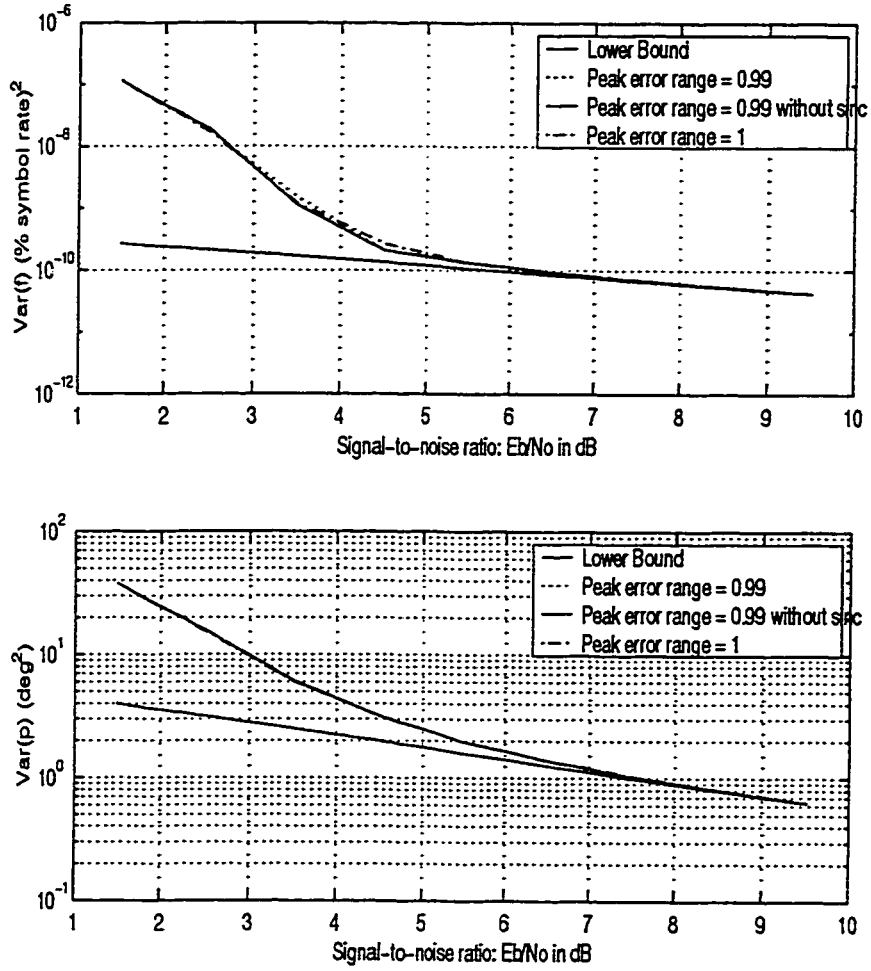

Figure 4.2: Comparison of Estimator with Different Functions

updated and store the cumulative sums $\sum_{k=0}^{K} c_k$, $\sum_{k=0}^{K} kc_k$, $\sum_{k=0}^{K} k^2 c_k$, $\sum_{k=0}^{K} c_k\varphi_k$, $\sum_{k=0}^{K} kc_k\varphi_k$. However, for (4.4), the updating of the weight $\bar{c}_{k|K-1}$ has to be recalculated, as a result, the cumulative sums $\sum_{k=0}^{K} \bar{c}_{k|K-1}$, $\sum_{k=0}^{K} k\bar{c}_{k|K-1}$, $\sum_{k=0}^{K} k^2\bar{c}_{k|K-1}$, $\sum_{k=0}^{K} \bar{c}_{k|K-1}\varphi_k$, $\sum_{k=0}^{K} k\bar{c}_{k|K-1}\varphi_k$ have to be updated for every estimation.Therefore, to obtain a simple implementation, we can only use the algorithm from (2.30) evaluate its performance.

- Moment analysis

As we know, phase measurement can be expressed as:

$$\varphi_k = (2\pi\Delta f k + \Delta\theta + \varepsilon_k) \tag{4.7}$$

Define $\Delta\omega = 2\pi\Delta f$ to simplify the notation. Substitute $\varphi_k = (\Delta\omega k + \Delta\theta + \varepsilon_k)$ into (2.30),

$$\begin{aligned}
\widehat{\Delta\omega} &= \frac{\sum_{k=0}^{K-1} kc_k(\Delta\omega k+\Delta\theta+\varepsilon_k)\sum_{k=0}^{K-1} c_k - \sum_{k=0}^{K-1} kc_k \sum_{k=0}^{K-1} c_k(\Delta\omega k+\Delta\theta+\varepsilon_k)}{\sum_{k=0}^{K-1} k^2c_k \sum_{k=0}^{K-1} c_k - \left(\sum_{k=0}^{K-1} kc_k\right)^2} \\
\widehat{\Delta\theta} &= \frac{\sum_{k=0}^{K-1} c_k(\Delta\omega k+\Delta\theta+\varepsilon_k)\sum_{k=0}^{K-1} k^2c_k - \sum_{k=0}^{K-1} kc_k(\Delta\omega k+\Delta\theta+\varepsilon_k)\sum_{k=0}^{K-1} kc_k}{\sum_{k=0}^{K-1} k^2c_k \sum_{k=0}^{K-1} c_k - \left(\sum_{k=0}^{K-1} kc_k\right)^2}
\end{aligned} \tag{4.8}$$

Use $\sum$ for $\sum_{k=0}^{K-1}$ for simplicity,

$$\begin{aligned}
\widehat{\Delta\omega} &= \frac{\left(\Delta\omega\sum k^2c_k+\Delta\theta\sum kc_k+\sum kc_k\varepsilon_k\right)\sum c_k - \sum kc_k(\Delta\omega\sum kc_k+\Delta\theta\sum c_k+\sum c_k\varepsilon_k)}{\sum k^2c_k\sum c_k-(\sum kc_k)^2} \\
\widehat{\Delta\theta} &= \frac{(\Delta\omega\sum kc_k+\Delta\theta\sum c_k+\sum c_k\varepsilon_k)\sum k^2c_k - \left(\Delta\omega\sum k^2c_k+\Delta\theta\sum kc_k+\sum kc_k\varepsilon_k\right)\sum kc_k}{\sum k^2c_k\sum c_k-(\sum kc_k)^2}
\end{aligned} \tag{4.9}$$

Define,

$$A = \sum c_k$$

$$B = \sum kc_k$$

$$C = \sum k^2c_k$$

$$D = \sum k^2c_k \sum c_k - \left(\sum kc_k\right)^2 = AC - B^2$$

$$E = \sum c_k\varepsilon_k$$

$$F = \sum kc_k\varepsilon_k$$

The above equation can be derived as,

$$\begin{aligned}
\widehat{\Delta\omega} &= \frac{(\Delta\omega C+\Delta\theta B+F)A - B(\Delta\omega B+\Delta\theta A+E)}{D} \\
\widehat{\Delta\theta} &= \frac{(\Delta\omega B+\Delta\theta A+E)C - (\Delta\omega C+\Delta\theta B+F)B}{D}
\end{aligned} \tag{4.10}$$

Therefore,

$$\begin{aligned} \widehat{\Delta\omega} &= \frac{\Delta\omega\left(AC-B^2\right)+(AF-BE)}{D} \\ \widehat{\Delta\theta} &= \frac{\Delta\theta\left(AC-B^2\right)+(EC-FB)}{D} \end{aligned} \tag{4.11}$$

Such that,

$$\begin{aligned} \widehat{\Delta\omega} &= \Delta\omega + \frac{A\sum kc_k\varepsilon_k - B\sum c_k\varepsilon_k}{D} \\ \widehat{\Delta\theta} &= \Delta\theta + \frac{C\sum c_k\varepsilon_k - B\sum kc_k\varepsilon_k}{D} \end{aligned} \tag{4.12}$$

It is easy for us to find the pdf of ε_k. Since the phase noise sequence ε_k is identically independent distributed, it has zero-mean with variance σ_ε^2, its pdf can be derived according to Appendix,

$$f\left(\varepsilon_k\right) = \int_0^\infty f_{|r_k|,\varepsilon_k}\left(|r_k|, \varepsilon_k\right) d\,|r_k| \tag{4.13}$$

Such that,

$$f\left(\varepsilon_k\right) = \frac{1}{2\pi} e^{-\frac{1}{2\sigma^2}} + \frac{1}{2\sqrt{2\pi\sigma^2}} \cos\left(\varepsilon\right) e^{-\frac{\sin^2(\varepsilon)}{2\sigma^2}} \left[1 + erf\left(\frac{1}{\sqrt{2\sigma^2}} \cos\left(\varepsilon\right)\right)\right] \tag{4.14}$$

Which means,

$$\begin{aligned} E\left\{\varepsilon_i\varepsilon_j\right\} &= \sigma_\varepsilon^2, \; for\; i = j \\ &= 0, \; otherwise \end{aligned}$$

but for the pdf of c_k part, we will find it is very complex involving some terms that unsolvable. Therefore, we turn to use computer simulation to see their results, as shown in Figure 4.3 and Figure 4.4. It shows that for the estimations above the threshold, both phase estimation and frequency estimation are unbiased. For the extreme case, as in the lest-square-estimation (LSE) case, where all c_k are supposed to be 1, it is easy to verify that it is unbiased, and the variance of the estimations can also be obtained.

The variances of the two estimation are:

$$\begin{aligned} Var\left\{\widehat{\Delta\omega}\right\} &= E\left\{\frac{A\sum kc_k\varepsilon_k - B\sum c_k\varepsilon_k}{D}\right\}^2 \\ Var\left\{\widehat{\Delta\theta}\right\} &= E\left\{\frac{C\sum c_k\varepsilon_k - B\sum kc_k\varepsilon_k}{D}\right\}^2 \end{aligned} \tag{4.15}$$

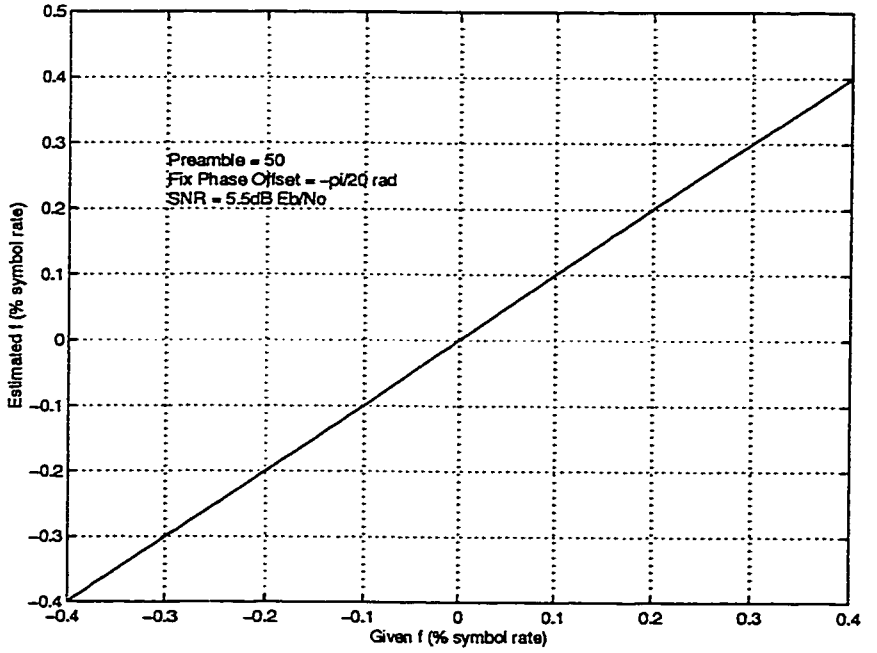

Figure 4.3: Mean of Estimated Frequency Offset

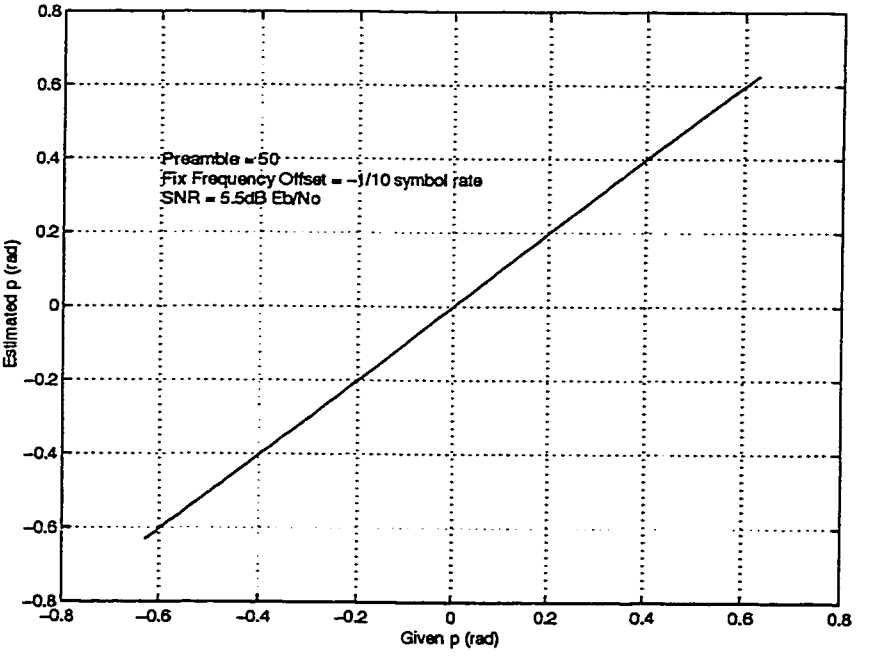

Figure 4.4: Mean of Estimated Phase Offset

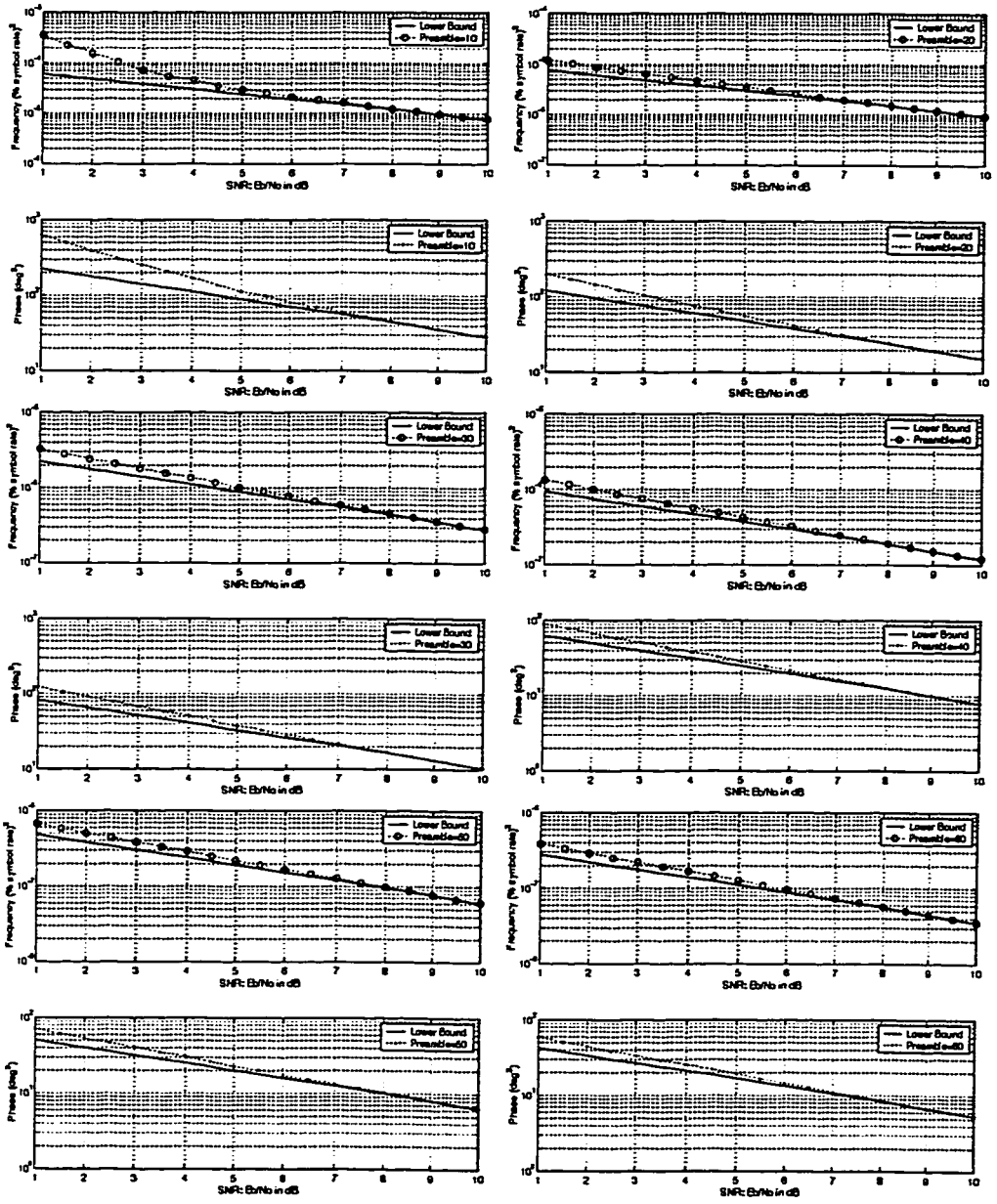

Figure 4.5: Variance Performance for the Joint Estimation in the Preamble

SNR $\left(\frac{E_b}{N_o}\ in\ dB\right)$	Preamble	No. of Outliers
6	50	0
6	40	0
6	30	12
5	60	0
5	50	0
5	40	2
4	70	0
4	60	0
4	50	4

Table 4.1: Outliers Number Changing with SNR and Preamble Length Out of 10^6-Burst Runs

- Preamble

The variance performance for the preamble is shown in Figure 4.5.

The simulation results show that the variance of estimate is very close to CRLB in the preamble part, so that the joint estimator can draw the initial unwrapping estimates to a rational range very quickly even with very few preamble bits and low signal-to-noise ratio. If the estimate from the initial part is accurate enough, it will enable the following phase unwrapping, and therefore, for the continuous estimate to be very accurate. The simulation result is summarized in Table 4.1, the statistic is obtained from 10^6-burst runs and each burst has 584 symbols. It shows that there is trade-off between preamble length and signal-to-noise ratio.

We can see although the estimation from the initial part is very close to CRLB from very low threshold, the whole estimation does not approach CRLB from very low threshold corresponding. The reason for that is because the initial estimate from the preamble is not accurate enough although it approaches CRLB. For a long enough burst, such as the 584-symbol burst in our simulation, a 0.05% symbol rate frequency offset can make the total phase offset over 2π at the end of the burst. Occasionally, when the initial estimate is not very accurate, and the noise happens to be large so as to make wrong data detection, the whole estimate for the burst

can be destroyed. Since such kind of phenomenon happens randomly, it is difficult to be compensated.

In the meanwhile, we should notice that the fewer measurement in the initial state requires for initialization at higher SNR to obtain an accurate enough initial value for the next stage of estimation. We find in the simulation that the initial estimation has significant influence on the estimation on information symbols later on. The penalty of the transmission power can be fully compensated for its fast and accurate joint estimation.

We should also remark that although a phase increment frequency offset algorithm has been used in the initial estimation, its performance has nothing to do with the performance of this DA-FB estimator. In the simulation, we notice that $\widehat{\Delta f}_i$ in the frequency estimation set given by the phase increment estimator differ from each other with big difference. It is with the DA-FB that draw the coarse initial unwrapping frequency offset to the approximately accurate value. This can be illustrated as in Table 4.2 from the computer simulation. In this table, it is seen that although the peak ML value in $i = 10$ computed from (2.27) using the corresponding estimation pair $(\widehat{\Delta f}_i, \widehat{\Delta\theta}_i)$, which is chosen as the start value for DA-FB estimation, is quite lager than the others, its frequency offset estimation value $\widehat{\Delta f}_{10} = 0.600766$ is still quite different from the estimation after the DA-FB estimated value $\widehat{\Delta f}_{10} = 0.095941$.

- Bit Error performance

To be consistent with the simulation result of NDA-FF estimator of last chapter, all the simulations are performed with differential encoding technique. The BER performance is shown in Figure 4.3.

It shows that with a sufficiently long preamble, the estimation can be accurate enough for the estimator to get good bit error performance which is very close to the theoretical lower bound as of (3.10). It is obvious that its threshold of frequency

i	$\widehat{\Delta f_i}$	$\widehat{\Delta f_i}$after DA-FB Estimate	ML Value
0	-2.706173	-0.418933	3.484550
1	-2.375480	-0.398032	-0.463417
2	-2.044786	-0.338166	1.978206
3	-1.714092	-0.280786	4.837123
4	-1.383398	-0.215830	0.059202
5	-1.052704	-0.158325	-0.873094
6	-0.722010	-0.124084	1.525104
7	-0.391316	-0.071701	4.040230
8	-0.060622	-0.022575	7.016372
9	0.270072	0.024329	6.736557
10	0.600766	0.095941	25.622028
11	0.931460	0.165117	5.150429
12	1.262154	0.212289	4.268384
13	1.592848	0.261351	4.324929
14	1.923542	0.320186	3.487827
15	2.254236	0.350207	-0.520309
16	2.584930	0.411618	-1.843230
17	2.915624	0.462576	2.808113
18	3.246318	0.527611	-2.525526

Table 4.2: DA-FB Function in the Initial State with Preamble=20 and Given Frequency Offset =10% Symbol Rate

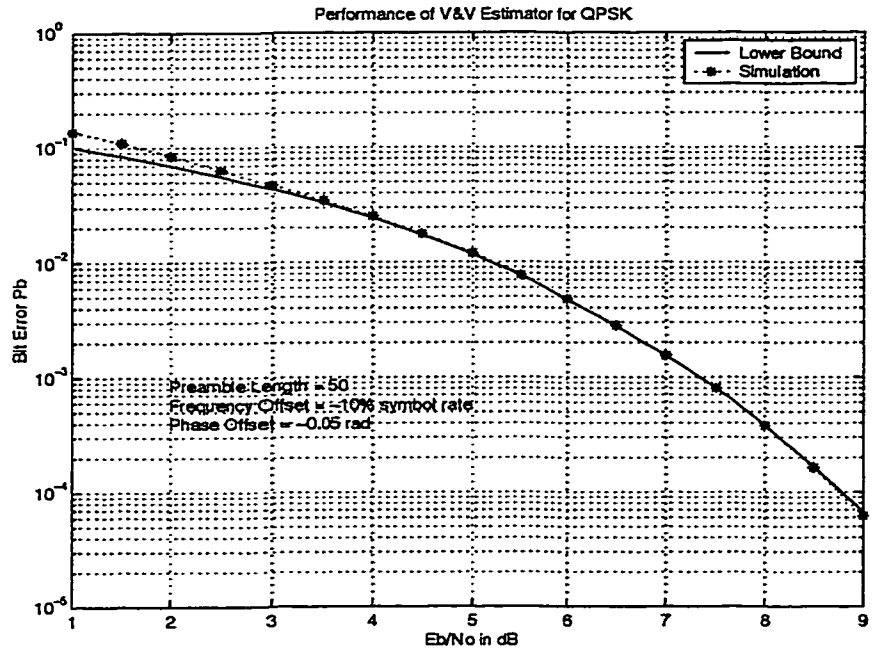

Figure 4.6: BER Performance of DA-FB Joint Estimator

offset estimation part with preamble less than 10% of burst length is higher than the NDA-FF frequency offset estimator.

- Other considerations

1. The estimation range of this joint estimator is very broad. For example, normally in the simulation, we limit the frequency estimate to ± 0.4 to avoid phase ambiguity. It implies that the estimation range can almost reach $(-\frac{1}{2}, \frac{1}{2})$, which is the whole repeat period of the normalized frequency Δf.

2. The complexity of this estimator is low. For the main part of the estimation, the computation required for the evaluation of (2.28) is ten multiplications and eight additions.

4.3 Summary

From the analysis of the DA-FB joint estimator in this chapter, we conclude:

- Although the use of preamble reduces the transmission efficiency, it can give fast estimation at low complexity.

- The estimation range of the frequency offset is almost across the whole period of Δf. Such a dramatically large estimation range is fascinating, so that in next chapter, we try to make use of this advantage .

Chapter 5

Further Improvement of Techniques

In Chapter 3 and Chapter 4, we studied two carrier phase/frequency offset estimators. In this chapter, we want to take advantages of both of the two synchronizers to obtain a better estimation scheme. Our work will be mainly on the frequency offset part. Two kinds of improvements will be made in the following,

- The spectrum analysis method NDA-FF frequency estimator is combined with the DA-FB frequency estimator to obtain both larger estimation range and lower threshold, after the frequency correction, either NDA-FF phase offset estimator or DD-FB phase offset estimator can be used for the phase estimation.
- Effort will be made to decrease the number of outliers of the NDA-FF frequency estimator.

At first, we should have a close look at the two carrier synchronizers to study the advantages and disadvantages between them for separated frequency offset estimation and phase offset estimation. Then, the improved schemes can be obtained.

5.1 Comparison of Proposed Techniques

The comparisons are in terms of implementation complexity, transmission efficiency, estimation range, threshold for frequency estimator, and acquisition time for phase estimator.

5.1.1 Frequency Offset Estimator

- Complexity

Compared with all the FF frequency offset estimators, NDA-FF frequency estimator has the highest complexity and longest estimation delay. According to the characteristics of the FFT computation, we need more points to obtain more accurate estimation in the coarse frequency estimation part, which is in conflict with the complexity consideration. On the contrary, the DA-FB has a very simple implementation structure and low computation complexity.

- Transmission efficiency

NDA structure gives the highest transmission efficiency. On the other hard, the low complexity DA-FB estimator has the drawback of its low transmission efficiency, and power and bandwidth waste. Although it is proved that such penalties can be compensated by its fast estimation, we still want to have as high as possible transmission efficiency.

- Estimation range

It has been throughly discussed that the NDA-FF frequency estimator has very limited estimation range because of the non-linear operation to remove modulation and the decimation operation to reduce the computational complexity, which is

$$|\Delta f| < \frac{1}{2MD}$$

where, M is the modulation factor and D is the decimation factor.

While the DA-FB estimator can almost reach the whole range of the frequency offset itself, which is

$$|\Delta f| < \frac{1}{2}$$

- Threshold

Among all the FF frequency estimators, the NDA-FF frequency estimator has the lowest threshold. We have also shown from the simulation, that the DA-FB algorithm also has a higher threshold than the NDA-FF one.

We also notice the initial estimation part in the DA-FB algorithm has variance performance that approaches the CRLB closely even with very short preamble. However, with further estimation with this initial estimate, it was shown that the initial estimation is still not accurate enough to gain a low threshold for the whole estimation.

5.1.2 Phase Offset Estimator

- Complexity

From Table 3.3 and explanation of last chapter, we conclude that the DA-FB algorithm has lower complexity, while the DD-FB has higher complexity.

- Transmission efficiency

Still, it is the NDA-FF has the highest transmission efficiency. If we do not use any additional preamble to help the DD-FB algorithm to get short acquisition time, DD-FB algorithm also has the same efficiency as the NDA-FF algorithm does. While, the DA-FB algorithm always has lower efficiency.

- Acquisition

As the feedforward structure, the NDA-FF algorithm never meet acquisition time problem because its estimation is always obtained by direct calculation. Meanwhile, DD-FB and DA-FB algorithm all have acquisition time problem because of their feedback structure. The advantage of the DA algorithm is that its acquisition time has been shortened by the additional preamble information. If a few preamble bits can be added to the DD algorithm, its acquisition performance can be improved.

5.2 Further Improvement of Techniques

As stated at the beginning of this chapter, the further improvement of the techniques is mainly on the frequency offset estimation.

5.2.1 Scheme 1: Combination of NDA-FF and DA-FB

- Presentation of the scheme

The combined scheme is shown in Figure 5.1. The combination scheme works as the following steps:

1. use certain preambles and follow the procedure as in the initial part of the DA-FB scheme stated in part **4.1** to give a coarse frequency offset estimation $\widehat{\Delta f_1}$,
2. use $\widehat{\Delta f_1}$ to reduce the frequency offset in the received signal samples, after which there is still a small frequency offset Δf_2 left,
3. use NDA-FF scheme stated in part **3.1.2.1** to estimate $\widehat{\Delta f_2}$,
4. the result of the addition of $\widehat{\Delta f_1}$ and $\widehat{\Delta f_2}$ is the final frequency offset estimation value.

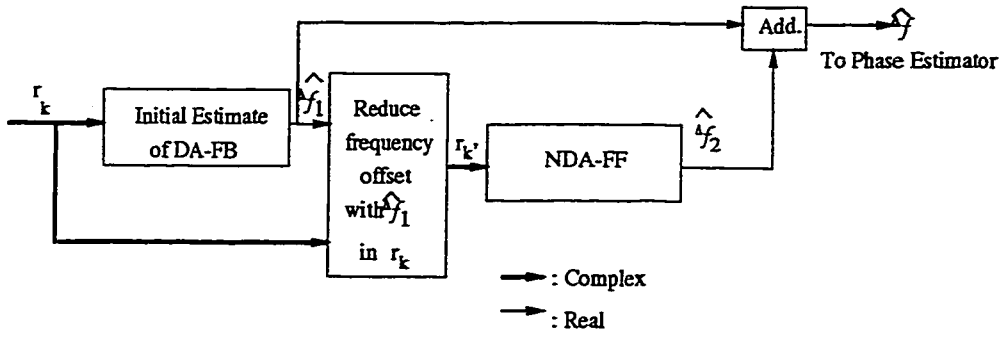

Figure 5.1: Block Diagram of the Combination Scheme of NDA-FF and DA-FB

In fact, when we combine these two algorithms together, the transmission must have preamble so we cannot call NDA-FF as NDA-FF. Meanwhile, since we just want to use the initial estimation part of the DA-FB algorithm, where there is no necessary for us to estimate data phase and there is no more DD function in this part of the algorithm.

- Analysis of the combined scheme

We have analyzed in detail the performance of the estimators separately in the last two chapters. So, now we concentrate only on their threshold value. We want to see whether the estimate range has been increased with a low threshold, and how long the preamble needs to be to reach this estimate. The reason for us to use the frequency offset equal to -10% symbol rate is just for the purpose of being consistent reason as what we used in Chapter 4, as well as a given large value to be estimated. If other given frequency offsets are used, the result will be the same. The corresponding simulation figures are shown in Figure 5.2 - Figure 5.5. Table 5.1 concludes the result of the simulation from the figures.

A few conclusions can be drawn as follows:

1. For a properly chosen preamble length, the estimated range has been greatly increased with a low threshold for both the NDA-FF frequency offset estimator and DA-FB frequency offset estimator. However, we find that the DA-FB

Preamble	SNR$\left(\frac{E_b}{N_o}\ in\ dB\right)$	Estimated Value (% symbol rate)	No. of Outliers
20	2	-10%	3
20	3	-10%	0
15	4	-10%	1
15	5	-10%	0

Table 5.1: Threshold Effect of the Combined Estimator

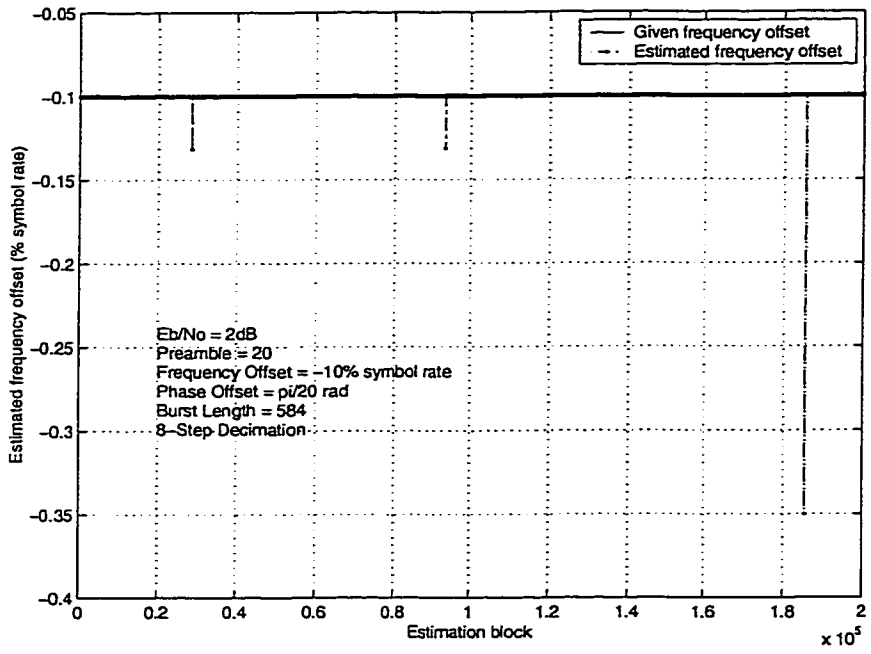

Figure 5.2: Threshold Effect of the Combined Estimator with Preamble=20, and SNR=2dB Out of 2×10^5-Burst Runs

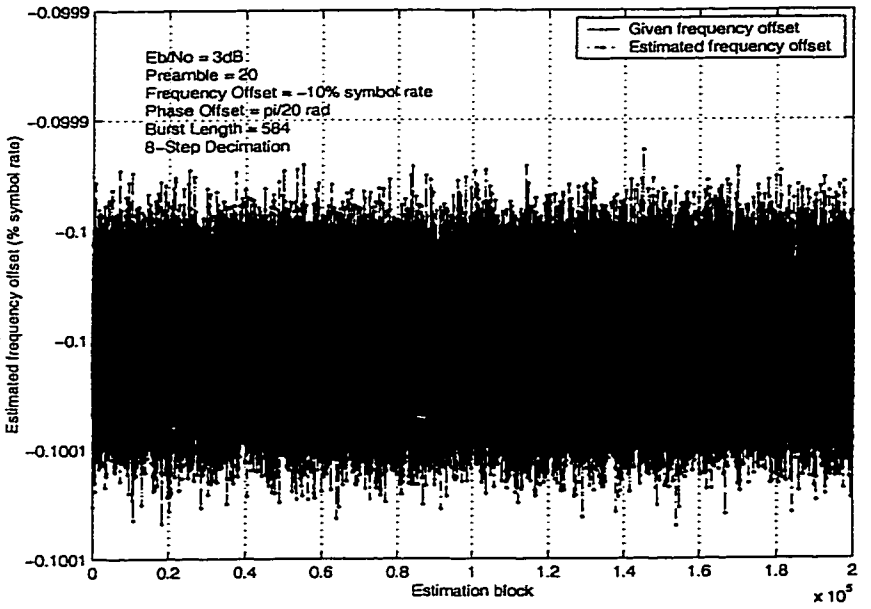

Figure 5.3: Threshold Effect of the Combined Estimator with Preamble=20, and SNR=3dB Out of 2×10^5-Burst Runs

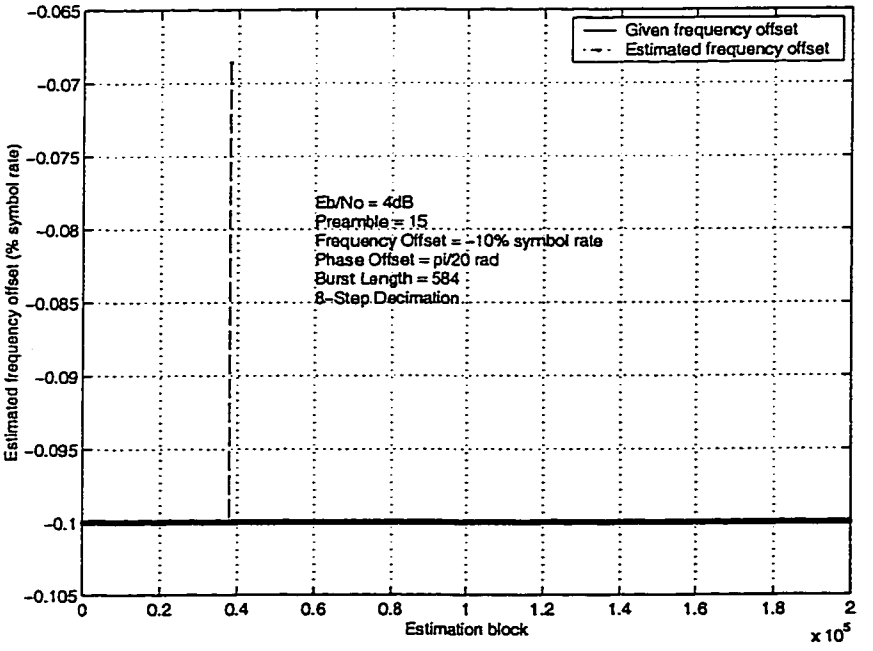

Figure 5.4: Threshold Effect of the Combined Estimator with Preamble=15, and SNR=4dB Out of 2×10^5-Burst Runs

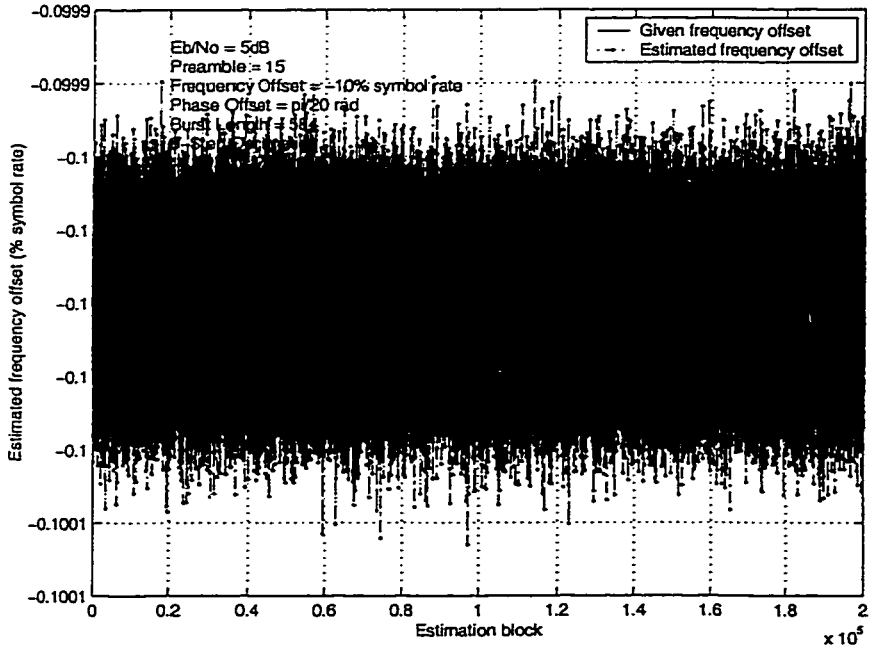

Figure 5.5: Threshold Effect of the Combined Estimator with Preamble=15, and SNR=5dB Out of 2×10^5-Burst Runs

algorithm works properly above the threshold of the NDA-FF algorithm which is just 1.2dB. Therefore, the threshold is only decided by the DA-FB estimator. Whenever the DA-FB estimator can give estimation which leaves residual frequency offset

$$\Delta f_2 < \left| \frac{1}{2MD} \right|$$

which is in the estimation range of the NDA-FF algorithm, the whole estimator can work accurately. It is seen from Table 5.1 that the threshold of the combined scheme is higher than the separate NDA-FF scheme, but greatly lower than the separate DA-FB scheme with short preamble. For preamble length of 20, the threshold is only 3dB, but the estimation frequency offset range has been increased to ± 0.4.

2. As was discussed in Chapter 3, because the maximum search method has been used for the NDA-FF frequency estimator, its variance performance can be as

close as possible to CRLB. Since it is always with the maximum search method to estimate the remaining small frequency offset part, the estimation of this part can be as accurate as possible. It means that the whole estimation can approach the real value as close as possible, such that its variance performance can approach CRLB as close as possible after the SNR larger than threshold.

3. The subsequent phase offset estimator can either use the NDA-FF one or the DD-FB one since there is already preamble in the transmitted signal. The known received symbol can help the DD-FB estimator to shorten the acquisition time and get into lock quickly. As we stated, the DD-FB algorithm has a "better" variance performance than that of the NDA-FF algorithm, but also with a little more complexity than the block-estimation method in the latter estimator.

4. The complexity of the combined estimator has increased compared with the separated DA-FB algorithm. As we have discussed in Chapter 4, the complexity of the DA-FB algorithm is not high, especially we just use the initial part of its estimation scheme. The main part which gives high complexity is still the NDA-FF estimation part. Therefore, compared with the NDA-FF frequency estimator, the complexity of the combined one is almost the same as that of the NDA-FF one.

5.2.2 Scheme 2: Improvement of NDA-FF

NDA-FF frequency estimator can give very low threshold. When the estimator works under the threshold, outliers may occur. The reason for us to say "may" is that it really occurs very occasionally when the working SNR approaches the threshold. If certain error-detection coding technique, such as CRC, is used, the receiver can ask for retransmission of the burst which has encountered outliers. Such kind of technique is very efficient if the outliers are really few. Our objective here is to

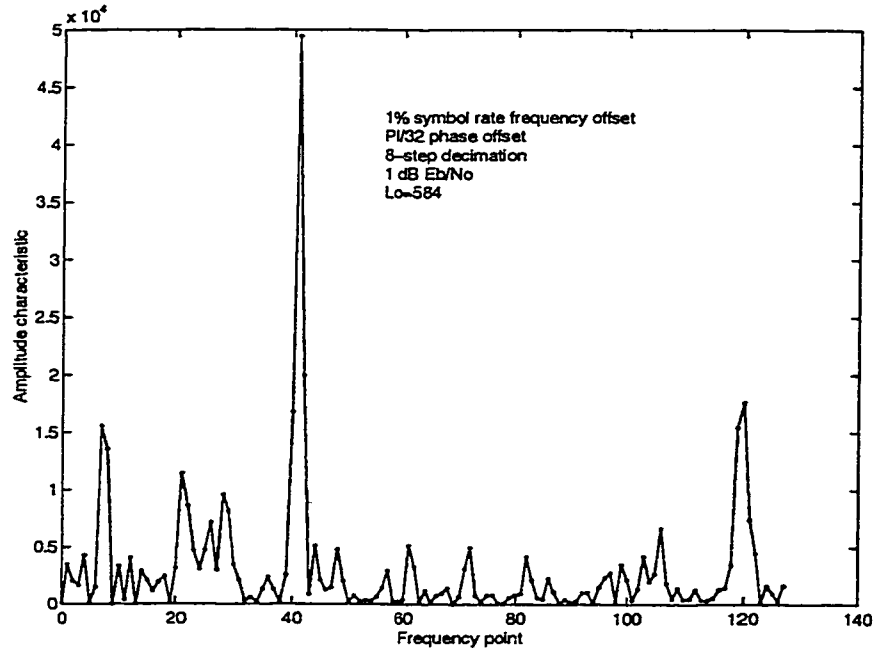

Figure 5.6: Amplitude Response of the Signal

propose a scheme which can provide as few outliers as possible when the estimator working under threshold occasionally.

- Presentation of the algorithm

Let us see the amplitude response of the non-linear transformed signal after the decimation filter closely as in Figure 5.6. We find the peak amplitude which correspond to the given frequency offset is greatly higher than the other points nearby, even for the ones right besides it. However, in the occasional cases when the outlier happens, this obvious difference disappears. The peak amplitude appears randomly with large departure to the biased direction.

However, we notice that in our algorithm in Chapter 3, we just used one set of 8-step decimated signals in the coarse search part. These signals can represent partly the received information, such that there is still information loss. In the simulation, we found that when the outlier occurs, there are such estimation results from the eight sets of decimated signals as shown in Table 5.2, which are selected

	Set 0	Set 1	Set 2	Set 3	Set 4	Set 5	Set 6	Set 7
All correct	-37	-37	-37	-37	-37	-37	-37	-37
All wrong	-1	-1	-1	-1	-1	-1	-1	-1
Half correct, half wrong	-8	-37	-37	-37	-8	-8	-37	-8
More correct, few wrong	1	-1	-37	-37	-37	-37	1	-37
Few correct, more wrong	-37	-8	-8	-8	-8	-8	-1	-8

Table 5.2: Close Look to Outliers ($\Delta\theta = -\frac{\pi}{32}$, $\Delta f = -\frac{1}{110}$symbol rate, $\Delta f' = 4\Delta f$ for QPSK)

from the printed simulation result directly. Where,

$$-\frac{1}{110} symbol\ rate \approx \frac{-37}{128 \times 4 \times 8}$$

because of 128-FFT calculation, QPSK signal model, and 8-step decimation. -1 and -8 are happened to be certain kind of random outlier value that always go to one direction according to the real frequency offset value.

From the Table, we find there are five kinds of possible results from the eight sets' simulations, as stated in the first column. Such phenomenon suggests that we can correct the estimation from the "more correct, few wrong" situation. We can use a selector to select the "more correct" value. The selector deletes the values that depart far away from the average of eight sets, and use the remaining average value as the coarse search result. Therefore, an improved algorithm is proposed as shown in Figure 5.7, where we try to use all 8 sets of information. However, for all the other situations with wrong search result, the selector cannot correct it.

- Analysis of the scheme

Running the program for a few times, we can find that the outliers can be decreased. For example, at $\frac{E_b}{N_o} = 1dB$, where we used to have 2-8 outliers during 10^6 burst estimation, the outliers are normally smaller than 5 with the newly improved scheme. The improvement of this scheme is small.

We also noticed that the complexity of the algorithm has been greatly increased because of the eight sets of FFT computation.

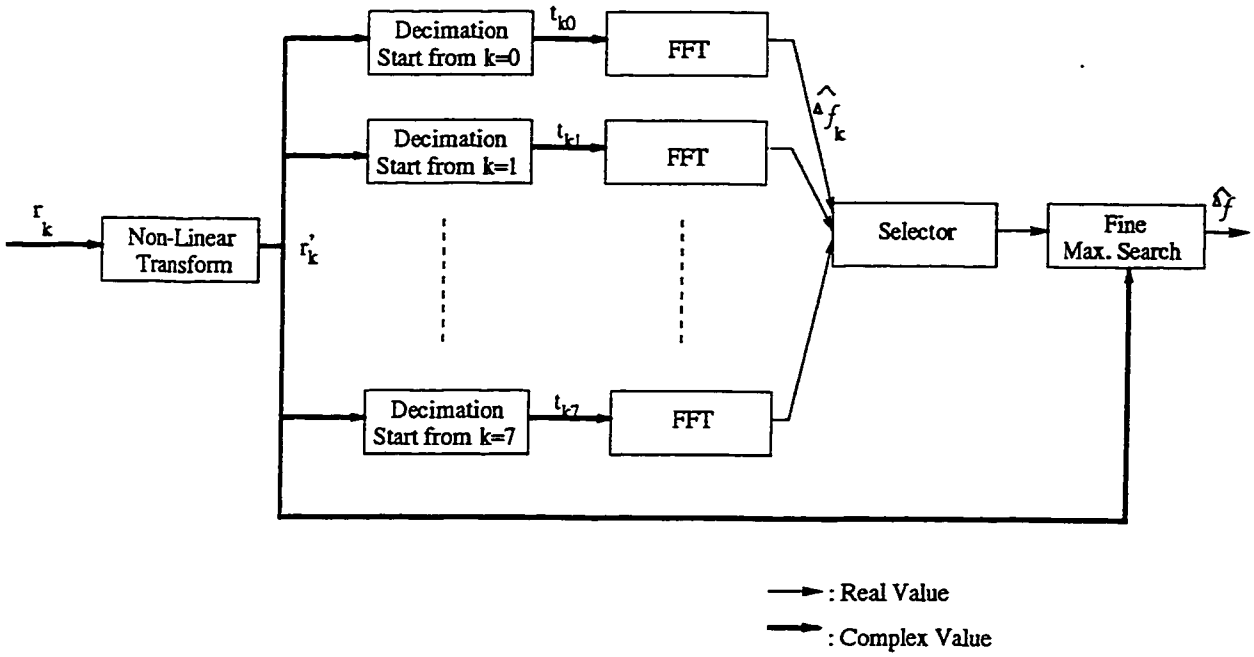

Figure 5.7: Block Diagram of Improved NDA-FF Frequency Estimator

Chapter 6

Conclusions and Suggestions for Further Research

6.1 Conclusions

The major objective of this research was to develop fast and efficient phase error and frequency error estimation techniques. To do so, we studied the Maximum Likelihood estimator class, analyzed and simulated various estimation scheme from non-data-aided to data-aided and decision-directed, from feedforward structure to feedback structure, and from the combination phase/frequency synchronizer to joint phase/frequency synchronizer. We have made effort to study closely all the various schemes, and to improve them not only individually, but also when they are used combined with one another so as to exploit all of their advantages to compensate their drawback characteristics.

For the phase estimator, we mainly studied the NDA-FF and DD-FB algorithms. The NDA-FF has the highest transmission efficiency, approximate good performance of the FB estimator, and can get fast estimation. These make it very

suitable for the burst-mode transmission as well as continuous transmission. However, its special phenomenon of phase ambiguity asks for addition processing techniques, such as phase unwrapping and differential encoding, which is supposed to degrade its performance. On the contrary to this disadvantage of NDA-FF algorithm, the DD-FB estimator is free of such drawback and also has the same high transmission efficiency for continuous transmission methods. The main drawback for DD-FB algorithm is its feedback topology which asks for long acquisition time. The acquisition time can be too long (such as 60 bits in the simulation result in Chapter 3) to be acceptable for many short burst TDMA systems. Therefore, in the circumstances where the burst length is long enough, the DD-FB algorithm can be a good choice for the phase estimation algorithm. Meanwhile, if we do not care about the highest transmission estimation efficiency, a few preamble can be added to help the acquisition. This makes it more suitable for the burst-mode transmission.

For the frequency estimator, we mainly studied the NDA-FF and DA-FB algorithms. As all the FF estimators, although with the highest transmission efficiency, this algorithm has limited estimation range because of the modulation removal process and high implementation complexity. The main advantage is its low threshold. On the other hand, the DA-FB algorithm has a simple implementation structure and very broad estimation range, but with low transmission efficiency and high threshold. These advantage and disadvantage factors are studied, and an improved algorithm is obtained to get a broad estimation range estimator with the threshold a little higher than the NDA-FF frequency estimator subject to proper choice of preamble.

For the phase/frequency estimator, the combined NDA-FF algorithm has been proven to have accurate estimation for both phase estimate and frequency estimate, but with long delay for getting the estimation. While the joint DA-FB estimator is much simple and fast, and can give accurate estimate with properly chosen preamble. With sufficient long preamble, the joint DA-FB estimator can get the estimate as

NDA-FF estimator can reach, where we say this in terms of both the accuracy and the lowest working SNR.

With all the above analysis and studies, we see that there is always trade-off factors between various algorithms. The choice in practice will be done according to different necessity in the implementation.

6.2 Suggestions for Further Research

The performance of the combined NDA-FF and DA-FB phase/frequency offset synchronizer have received the bulk of attention in this thesis. The aspects which remain to be studied further are categorized into three major headings:

- Channel model

The results presented in this thesis are applicable to linear channels with no ISI. First, since band limitation can introduce ISI, the effects of this form of interference should be studied. This ISI will invalidate the assumption of Gaussian noise (n_k^I and n_k^Q) in some circumstance. The ISI would further introduce dependence between the successive samples of received signal, and making the simulation and analysis results quite different from what we have now. As consequence, further work should be done under the condition of band-limited channel. Second, the nonlinear channel model can also be the subject of further investigation.

- Implementation

The thesis contains a trade-off among the complexity and computing burden on one hand and the effect of quantization on the performance of the algorithms on the other hand. For all of the comparisons we have made in this thesis, there are just for the core part of the estimation algorithm. The detail of the complexity will be proved by the implementation itself. It should be studied for the totality of the estimation algorithms considered, using detailed design and synthesis.

- Signaling format

The study in this thesis is centered around the MPSK signaling format. However, some of the ideas can be transplanted to other signaling formats, such as for offset-PSK, which is also a popular format in the telecommunication systems. It is expected that with a minor change of the algorithm, the estimator can perform equally good for certain other signaling formats.

Bibliography

[1] Ferdinand Classen, Heinrich Meyr, and Philippe Sehier, *An All Feed-Forward Synchronization Unit for Digital Radio*, IEEE, pp.738-741, 1993

[2] A. J. Viterbi and A. M. Viterbi, *Nonlinear Estimation of PSK-Modulated Carrier Phase with Application to Burst Digital Transmission*, IEEE Transactions on Information Theory, Vol. IT-29, No. 4, pp.543-551, July 1983

[3] R. A. Hrris and M. Yarwood, *Carrier Recovery and Inter-Burst Interference in a Symbol-Synchronous TDMA System*, International Journal of Satellite Communications, Vol. 9, pp.197-208, 1991

[4] Fumio Takahata et al, *A PSK Group Modem for Satellite Communications*, IEEE Journal on Selected Areas in Communications, Vol. SAC-5, No. 4, pp.648-661, May 1987

[5] William C. Lindesy, and Chak Ming Chie, *A Survey of Digital Phase-Locked Loops*, Proceeding of the IEEE, Vol. 69, No. 4, pp.410-431, April 1981

[6] John G. Proakis, *Digital Communications*, McGraw-Hill, U.S.A., 1995

[7] Heinrich Meyr, Marc Moeneclaey, and Stefan A. Fechtel, *Digital Communication Receivers, Synchronization, Channel Estimation, and Signal Processing*, John Wiley & Sons, U.S.A., 1997

[8] David C. Rife and Robert R. Boorstyn, *Single-Tone Parameter Estimation from Discrete-Time Observations*, IEEE Transaction on Information Theory, Vol. IT-20, No. 5, pp.591-598, September 1974

[9] Marco Luise and Reggero Reggiannini, *A Fast Carrier Frequency Recovery in All-Digital Modems for Burst-Mode Transmissions*, IEEE Transaction on Communications, Vol. 43, No. 2/3/4, pp.1168-1178, February/March/April 1995

[10] Michael P. Fitz, *Further Results in the Fast Estimation of a Single Frequency*, IEEE Transaction on Communications, Vol. 42, No. 2/3/4, pp.862-864, February/March/April 1994

[11] Yu Teh Su and Ru-Chwen We, *Frequency Estimation of Phase-Modulated Carriers*, IEICE Transaction on Communications, Vol. E81-B, No. 12, pp.2303-2310, December 1998

[12] M. Morelli and U. Mengali, *Feedforward Carrier Frequency Estimation with MSK-Type Signals*, IEEE Communications Letters, Vol. 2, No. 8, pp.235-237, August 1998

[13] F. M. Gardner, *Frequency Detectors for Digital Demodulators Via Maximum Likelihood Derivation*, ESA-ESTEC Final Report: Part 2, ESTEC contract No. 8022-88-NL-DG, March 1990

[14] Myung Sup Kim et al, *Design and Analysis of Decision-Directed Carrier Recovery for High-Speed Satellite Communications*, IEICE Transactions on Communications, Vol. E81-B, No. 12, pp.2567-2575, December 1998

[15] Willam G. Cowley, *Phase and Frequency Estimation for PSK Packets: Bounds and Algorithms*, IEEE transactions on Communications, Vol. 44, No. 1, pp.26-28, January 1996

[16] Rocco Di Girolamo, *Fast and Efficient Carrier Synchronization for Burst-Mode Communications*, master of Applied Science thesis, Concordia University, 1993

[17] F. M. Gardner, *Phaselock Techniques*, John Wiley and Sons, 1979

[18] Marc Moeneclaey, *On the True and the Modified Cramer-Rao bounds for the Estimation of a Scalar Parameter in the presence of Nuisance Parameters*, IEEE Transactions on Communications, Vol. 46, No. 11, pp.1536-1544, November 1998

[19] S. Kay, *A Fast and Accurate Single Frequency Estimator*, IEEE Trans. Acoust., Speech, Signal Processing, Vol. ASSP-37, pp.1987-1990, December 1989

[20] Michele Morelli and Umberto Mengali, *Feedforward Frequency Estimation for PSK: A Tutorial Review*, ETT, Vol. 9, No. 2, pp.103-116, March-April 1998

[21] Takeshi Onizawa, Kiyoshi Kobayashi, Masahiro Morikura, and Toshiaki Tanaka, *A Novel Coherent Preambleless Demodulator Employing Sequential Processing for PSK Packet Signals - AFC and Carrier Recovery Circuits* -, IEICE Transactions on Communications, Vol. E82-B, No. 3, pp.542-550, March 1999

[22] W. Shaw Yuan and Costas N. Georghiades, *Rapid Carrier Acquisition from Baud-Rate Samples*, IEEE Transactions on communications, Vol. 47, No. 4, pp.631-641, April 1999

[23] L. E. Franks, *Carrier and Bit Synchronization in Data Communication - A Tutorial Review*, IEEE Transactions on Communications, COM-28, 1107-1121,August 1980

[24] F. M. Gardner, *Demodulator Reference Recovery Techniques Suited for Digital Implementation*, European Space Agency, Final Report, ESTEC Contract No. 6847/86/NL/DG, August 1988

[25] M.D. Srinath, P. K. Rajasekaran and R. Viswanathan, *Introduction to Statistical Signal Processing with Applications*, Prentice-Hall Inc., 1996

[26] Rocco Di Girolamo and Tho Le-Ngoc, *Frequency Independent Nonlinear Feedforward Phase Estimator*, Wireless Personal Communications 5: 19-50, 1997

[27] G. Ascheid, M. Oerder, J. Stahl, and H. Meyr, *An All Digital Receiver Architecture for Bandwidth Efficient Transmission at High Data Rates*, IEEE Transaction on Communications, Vol. COM-37, No. 8, pp.804-813, October 1993

[28] Floyd M. Gardner, *Hangup in Phase-Lock Loops*, IEEE Transactions on Communications, Vol. COM-25, No. 10, October 1993

[29] M. Andronico, S. Casale, and Aurelio La Corte, *A feed-forward Technique for Initial Reference Parameter Estimation in Burst Mode PSK Demodulation (1)*, Telecommunication Transmissions, Vol. 9, No. 6, November-December 1998

[30] Geert De Jonghe and Marc Moeneclacy, *Cycle-slip Analysis of the Mth-Power NDA Feedforward Carrier Synchronizer for MPSK*, IEEE Transactions on Communications, Vol. 46, No. 8, pp. 1000-1002, August 1998

[31] Hyoung Kyu Song, *Frequency Offset Estimation Using the Peak Phase Error Detection for Burst Data Transmission*, IEICE Transactions on Communications, Vol. E82-B, No. 4, pp. 660-663, April 1999

[32] Boaz Porat, *A Course in Digital Signal Processing*, John Wiley & Sons Inc., U.S.A, 1997

[33] A. Papoulis, *Probability, Random Variables, and Stochastic Processes*, McGraw-Hill Book Inc., New York, U.S.A, 1991

[34] F. S. Acton, *Numerical Methods That Work*, Harper & Row Inc., New York, U.S.A, 1970

[35] J. J. Spilker, Digital Communications by Satellite, Prentice-Hall Inc., New Jersey, U.S.A, 1977

[36] William C. Lindsey, Marvin K. Simon, Phase-Locked Loops & Their Application, IEEE Press, The Institute of Electrical and Electronics Engineers Inc., New York, U.S.A, 1977

Appendix: Probability Density Function of the Degradation for NDA-FF Phase Estimator

We have known the characteristics as follows:

$$\begin{aligned} r_k &= \sqrt{E_k} e^{j(2\pi\Delta f k + \Delta\theta + \theta_k)} + n_k \\ &= a_k e^{j(2\pi\Delta f k + \Delta\theta)} + n_k \\ &= s(k; \Delta f, \Delta\theta) + n_k \\ &= s_k + n_k \end{aligned}$$

and

$$\begin{aligned} r_k &= s_k^I + j s_k^Q + n_k^I + j n_k^Q \\ &= x_k + j y_k \\ &= |r_k| e^{-j\psi_k} \\ &= |r_k| \exp\left[-j\left(2\pi\Delta f k + \Delta\theta + \theta_k + \varepsilon_k\right)\right] \end{aligned}$$

To find the $f_\delta(\delta)$, we must find $f_{X_k,Y_k}(x_k, y_k)$ at first.

We first note that the random variable n_k^I and n_k^Q are Gaussian. Their mean and variance are determined by using properties of $n(t)$. That is, $E[n(t)] = 0$ and

$E[n(t_1)\,n(t_2)] = \frac{N_o}{2}\delta(t_1 - t_2)$, where $\delta(t)$ is the Dirac delta function. Therefore,

$$\begin{aligned} E\left[n_k^I\right] = E\left[n_k^Q\right] &= 0 \\ E\left[n_k^I n_j^I\right] = E\left[n_k^Q n_j^Q\right] &= \begin{cases} 0 & k \neq j \\ \frac{N_o}{2} & k = j \end{cases} \\ E\left[n_k^I n_k^Q\right] &= 0 \end{aligned}$$

Given the transmitted symbols $\{a_k\}$, s_k^I and s_k^Q are constant. As a result, X_k and Y_k are Gaussian, with moments

$$\begin{aligned} E[X_k|\{a_k\}] &= s_k^I \\ Var[X_k|\{a_k\}] &= \frac{N_o}{2} \\ E[Y_k|\{a_k\}] &= s_k^Q \\ Var[Y_k|\{a_k\}] &= \frac{N_o}{2} \\ E[X_k Y_k|\{a_k\}] &= s_k^I s_k^Q \\ Cov[X_k Y_k|\{a_k\}] &= 0 \end{aligned}$$

Since X_k and Y_k are Gaussian and uncorrelated, they are also independent. This ensures that their joint pdf can be written as:

$$\begin{aligned} f_{X_k,Y_k}(x_k, y_k|\{a_k\}) &= f_{X_k}(x_k|\{a_k\})\, f_{Y_k}(y_k|\{a_k\}) \\ &= \frac{1}{\pi N_o} e^{\left[-\frac{(x_k)^2+(y_k)^2}{N_o} + \frac{s_k^I x_k + s_k^Q y_k}{\frac{N_o}{2}} - \frac{\left(s_k^I\right)^2+\left(s_k^Q\right)^2}{N_o}\right]} \\ &= \frac{1}{\pi N_o} e^{\left[-\frac{(x_k)^2+(y_k)^2}{N_o} + \frac{s_k^I x_k + s_k^Q y_k}{\frac{N_o}{2}} - \frac{E_s}{N_o}\right]} \\ & \qquad -\infty < x_k, y_k < \infty \end{aligned}$$

Since the samples are independent for different k, the joint pdf of all random X_k and Y_k denoted by vector X and Y respectively, is given by,

$$\begin{aligned} f_{X,Y}(x, y|\{a_k\}) &= \prod_{k=l}^{l+K-1} f_{X_k,Y_k}(x_k, y_k|\{a_k\}) \\ &= \frac{1}{\pi N_o} e^{\left[-\frac{(x_k)^2+(y_k)^2}{N_o} + \frac{s_k^I x_k + s_k^Q y_k}{\frac{N_o}{2}} - \frac{E_s}{N_o}\right]} \\ & \qquad -\infty < \forall x_k, y_k < \infty \end{aligned}$$

Using the polar form and substitute ε_k inside,

$$x_k = |r_k| \cos(\varepsilon_k)$$
$$y_k = |r_k| \sin(\varepsilon_k)$$

also with the use of Jacobian transformation, which is

$$f_{|r|,\varepsilon}(|r|, \varepsilon) = \frac{f_{X,Y}(x(|r|, \varepsilon), y(|r|, \varepsilon))}{J(x, y)}$$

where,

$$J(x, y) = \begin{bmatrix} \frac{\partial |r|}{\partial x} & \frac{\partial |r|}{\partial y} \\ \frac{\partial \varepsilon}{\partial x} & \frac{\partial \varepsilon}{\partial y} \end{bmatrix}$$

the final result of the transformation is,

$$f_{|r_k|,\varepsilon_k}(|r_k|, \varepsilon_k | \{a_k\}) = \frac{|r_k|}{\pi N_o} e^{\left[-\frac{(|r_k|)^2}{N_o} + \frac{\sqrt{E_s}|r_k|\cos(\varepsilon_k)}{\frac{N_o}{2}} - \frac{E_s}{N_o}\right]}$$
$$0 \leq |r_k| < \infty$$
$$-\pi \leq \varepsilon_k < \infty$$

Notice that the above is not explicitly dependent on the modulation. Furthermore, the same pdf is obtained for all the symbols in the observation window. Therefore, we may rewrite the pdf without the modulation condition, and without the $k'th$ sample subscript. That is:

$$f_{|r|,\varepsilon}(|r|, \varepsilon | \{a_k\}) = \frac{|r|}{\pi N_o} e^{\left[-\frac{(|r|)^2}{N_o} + \frac{\sqrt{\gamma}|r|\cos(\epsilon)}{\sqrt{\frac{N_o}{2}}} - \frac{\gamma}{2}\right]} \quad 0 \leq |r| < \infty, \quad -\pi \leq \varepsilon < \infty$$

with the substitution $\gamma = \frac{2E_s}{N_o}$ was made.

From the definition of δ, which is,

$$\delta = \frac{1}{M} \arctan\left[\frac{\frac{1}{K}\sum_{k=l}^{l+K-1} F(|r_k|) \sin\left(2\pi\Delta f(k-l-N)M + M\varepsilon_k\right)}{\frac{1}{K}\sum_{k=l}^{l+K-1} F(|r_k|) \cos\left(2\pi\Delta f(k-l-N)M + M\varepsilon_k\right)}\right]$$

Since $|r_k|$ and ε_k are independent from $|r_j|$ and ε_j for $(k \neq j)$, both numerator and denominator of the arctan function are sums of independent random variables. By

the central limit theorem (CLT), these sums, denoted as ξ and η, can be assumed to have Gaussian distribution. That is,

$$\begin{aligned}
\delta &= \frac{1}{M}\arctan\left[\frac{\eta}{\xi}\right] \\
\xi &= \frac{1}{K}\sum_{k=l}^{l+K-1} F\left(|r_k|\right)\sin\left(2\pi\Delta f(k-l-N)M+M\varepsilon_k\right) = \frac{1}{K}\sum_{k=l}^{l+K-1} A\left(k\right) \\
\eta &= \frac{1}{K}\sum_{k=l}^{l+K-1} F\left(|r_k|\right)\cos\left(2\pi\Delta f(k-l-N)M+M\varepsilon_k\right) = \frac{1}{K}\sum_{k=l}^{l+K-1} B\left(k\right)
\end{aligned}$$

The moments of $A\left(k\right)$ and $B\left(k\right)$ are shown below,

$$\begin{aligned}
E\left[A\left(k\right)\right] &= E\left[F\left(|r_k|\right)\sin\left(2\pi\Delta f(k-l-N)M+M\varepsilon_k\right)\right] \\
&= \sin\left(2\pi\Delta f\left(k-l-N\right)M\right)E\left[F\left(|r_k|\right)\cos\left(M\varepsilon_k\right)\right] \\
&\quad +\cos\left(2\pi\Delta f\left(k-l-N\right)M\right)E\left[F\left(|r_k|\right)\sin\left(M\varepsilon_k\right)\right]
\end{aligned}$$

Owing to the independence of the random variables, we can drop the subscript in the expectations. In addition, $E\left[F\left(|r_k|\right)\sin\left(M\varepsilon_k\right)\right]$ tends to zero. In fact, for general nonlinearity $g\left(|r|\right)$ and even R,

$$E\left[g\left(|r|\right)\sin\left(R\varepsilon\right)\right] = \int_0^{\infty}\int_{-\pi}^{\pi} g\left(|r|\right)\sin\left(R\varepsilon\right) f_{|r|,\varepsilon}\left(|r|,\varepsilon\right) d_{|r|}d_{\varepsilon} = 0$$

Using this result in the last equality yields

$$E\left[A\left(k\right)\right] = \sin\left(2\pi\Delta f\left(k-l-N\right)M\right)E\left[F\left(|r|\right)\cos\left(M\varepsilon\right)\right]$$

Similarly,

$$\begin{aligned}
Var\left[A\left(k\right)\right] &= \frac{E\left[F^2(|r|)\right]}{2} \\
&\quad -\frac{E\left[F^2(|r|)\cos(2M\varepsilon)\right]\cos(4\pi\Delta f(k-l-N)M)}{2} \\
&\quad -\sin^2\left(2\pi\Delta f\left(k-l-N\right)M\right)E^2\left[F\left(|r|\right)\cos\left(M\varepsilon\right)\right]
\end{aligned}$$

$$E\left[B\left(k\right)\right] = \cos\left(2\pi\Delta f\left(k-l-N\right)M\right)E\left[F\left(|r|\right)\cos\left(M\varepsilon\right)\right]$$

$$\begin{aligned}
Var\left[B\left(k\right)\right] &= \frac{E\left[F^2(|r|)\right]}{2} \\
&\quad -\frac{E\left[F^2(|r|)\cos(2M\varepsilon)\right]\cos(4\pi\Delta f(k-l-N)M)}{2} \\
&\quad -\cos^2\left(2\pi\Delta f\left(k-l-N\right)M\right)E^2\left[F\left(|r|\right)\cos\left(M\varepsilon\right)\right]
\end{aligned}$$

$$E\left[A\left(k\right),B\left(k\right)\right]=\frac{E\left[F^{2}\left(\left|r\right|\right)\cos\left(2M\varepsilon\right)\right]\sin\left(4\pi\Delta f\left(k-l-N\right)M\right)}{2}$$

If we note that all samples are independent, then the moments of ξ and η can be easily determined.

$$E\left[\xi\right]=0$$

$$\begin{aligned}Var\left[\xi\right] &= \frac{E\left[F^{2}\left(\left|r\right|\right)\right]}{2K} \\ &\quad -\frac{E\left[F^{2}\left(\left|r\right|\right)\cos\left(2M\varepsilon\right)\right]}{2K}S_{K}\left(2M\varepsilon\right) \\ &\quad -\frac{E^{2}\left[F\left(\left|r\right|\right)\cos\left(2M\varepsilon\right)\right]}{2K}\left[1-S_{K}\left(2M\varepsilon\right)\right]\end{aligned}$$

$$E\left[\eta\right]=E\left[F\left(\left|r\right|\right)\cos\left(M\varepsilon\right)S_{K}\left(M\varepsilon\right)\right]$$

$$Cov\left[\xi,\eta\right]=0$$

where, $S_{K}\left(2M\varepsilon\right)=\frac{\sin\left(2K\pi fM\right)}{K\sin\left(2\pi fM\right)}$.

Such that ξ and η are independent Gaussian random variables with moments $\mu_{\eta}=E\left[\eta\right]$, $\sigma_{\eta}^{2}=Var\left[\eta\right]$, $\mu_{\xi}=E\left[\xi\right]$, and $\sigma_{\xi}^{2}=Var\left[\xi\right]$. Their joint pdf can be written as,

$$f_{\eta,\xi}\left(\eta,\xi\right)=\frac{1}{2\pi\sigma_{\eta}\sigma_{\xi}}e^{\left[-\frac{\left(\eta-\mu_{\eta}\right)^{2}}{2\sigma_{\eta}^{2}}-\frac{\xi^{2}}{2\sigma_{\xi}^{2}}\right]}$$

We can now apply the following transformation,

$$\begin{aligned}Z_{1} &= \frac{1}{M}\arctan\left[\frac{\xi}{\eta}\right] \\ Z_{2} &= \xi^{2}+\eta^{2}\end{aligned}$$

therefore,

$$\begin{aligned}\xi &= z_{2}\sin\left(Mz_{1}\right) \\ \eta &= z_{2}\cos\left(Mz_{1}\right)\end{aligned}$$

The pdf of Z_1 and Z_2 is given by [33], such that the final result of $f_\delta(\delta)$ is given by:

$$
\begin{aligned}
f_\delta(\delta) \quad = \quad & \frac{Me^{-\mu_\eta^2/\mu_\xi^2}}{2\pi} \frac{\sigma_\eta \sigma_\xi}{\sigma_\eta^2 \sin^2(M\delta) + \sigma_\xi^2 \cos^2(M\delta)} \\
& \left\{ 1 + \frac{\mu_\eta}{\sqrt{2}\sigma_\eta} \sqrt{\pi} \sqrt{\frac{\sigma_\xi^2 \cos^2(M\delta)}{\sigma_\eta^2 \sin^2(M\delta) + \sigma_\xi^2 \cos^2(M\delta)}} \right. \\
& \exp\left[\frac{\mu_\eta^2}{2\sigma_\eta^2} \frac{\sigma_\xi^2 \cos^2(M\delta)}{\sigma_\eta^2 \sin^2(M\delta) + \sigma_\xi^2 \cos^2(M\delta)} \right] \\
& \left. \left[1 + erf\left(\frac{\mu_\eta}{\sqrt{2}\sigma_\eta} \sqrt{\frac{\sigma_\xi^2 \cos^2(M\delta)}{\sigma_\eta^2 \sin^2(M\delta) + \sigma_\xi^2 \cos^2(M\delta)}} \right) \right] \right\}
\end{aligned}
$$

for $-\frac{\pi}{M} \leq \delta < \frac{\pi}{M}$.